CONTACT BETWEEN MODELS OF ROUGH SURFACES CONTAINING SPHERICAL ASPERITIES

by

Wesley O. McCready

Thesis submitted to the Graduate Faculty of the
Virginia Polytechnic Institute and State University
in partial fulfillment of the requirement for the degree of

MASTER OF SCIENCE

in

Mechanical Engineering

APPROVED:

M. J. Furey, Chairman

N. S. Eiss

H. L. Wood

June, 1974

Blacksburg, Virginia

ACKNOWLEDGEMENTS

The author wishes to acknowledge the aid of Dr. M. J. Furey for his guidance during the course of the project. Appreciation is also extended to Dr. N. S. Eiss and Dr. H. L. Wood for serving on the Graduate Committee and providing helpful advice.

Thanks is also extended to other faculty and staff members who have provided technical advice and assistance and to Jennie Carroll for typing the thesis.

Appreciation is extended to the National Science Foundation for supporting the research.

Finally, I would like to thank my wife, Clemencia, for preparing the figures and for her support and understanding during the final phases of this work.

TABLE OF CONTENTS

		PAGE
Acknowledgements		ii
List of Figures		v
List of Tables		vii
I.	THE PROBLEM	1
II.	LITERATURE REVIEW	3
	A. Introduction	3
	B. Surface Topography	3
	C. Experimental Methods for Determining Contact Area	5
	1. Indirect Methods	6
	2. Direct Methods	13
	D. Theoretical Approaches to the Contact Area Problem	21
	1. Plastic Deformation	24
	2. Elastic Deformation	28
	3. Elasto-Plastic Deformation	34
	4. Effect of Tangential Loads	36
III.	APPROACH TO PROBLEM	40
	A. Introduction	40
	B. Model Design	42
	C. Model Fabrication	48
	D. Mold Fabrication	62
	E. Experimental Apparatus	65
	F. Description of Computer Program for Multiple Elastic Contact	70

TABLE OF CONTENTS (continued) PAGE

G. Criterion for the Limit of Elastic Behavior 73

IV. RESULTS 80

V. CONCLUSIONS 93

VI. RECOMMENDATIONS 96

VII. APPENDIX 100

1. An Investigation of the Friction in the Loading System of the Experimental Apparatus 101

2. Operation of Experimental Apparatus 108

3. Suggested Improvements to the Experimental Apparatus. . 120

4. Computer Program for Multiple Elastic Contact Between Rough Surfaces 122

5. Equations Used in Computer Program 141

6. Contact Data 150

VIII. REFERENCES 161

IX. VITA 165

LIST OF FIGURES

Figure	Title	Page
1.	Mechau Method of Contact Area Determination	15
2.	Modified Mechau Method of Contact Area Determination	16
3.	Extinction of Parallel Light	19
4.	Transmittance of Parallel Light	20
5.	Opaque Fluid Technique	22
6A.	Small Surface Model	53
6B.	Large Surface Model	54
7A.	View of Asperities on Small Model	55
7B.	View of Asperities on Large Model	56
8.	View of Experimental Apparatus	67
9.	Top View of Upper Model Support Plate	68
10.	Computer-Generated Curve for Number of Contacting Asperities vs. Load	86
11.	Computer-Generated Decrease in Approach vs. Load Curve	87
12.	Computer-Generated Contact Area vs. Load Curve	89
13.	Recommended Mold Design	97
14.	Schematic Diagram of the Pulley Loading System	102
15.	Input-Output Curves for a Loading System With and Without Friction	104
16.	Strain Bar Assembly for Determining Friction Force in the Loading System	106
17.	Mounting Models to Experimental Apparatus	109
18.	View of Models Mounted in Experimental Apparatus	110
19.	Establishing a Point of Reference Between Alignment Pins	112

LIST OF FIGURES (continued)

Figure	Title	Page
20.	Alignment of x-Reference Surfaces of the Models	115
21.	Alignment of y-Reference Surfaces of the Models	117
22.	Alignment of Single Asperity Models	119
23.	Determination of Maximum Asperity Misalignment for Contact	142
24.	Determination of Vertical Separation	144
25.	Free Body Diagram of Contact Between Misaligned Asperities	145
26.	Enlarged View of Intersection of Asperities	147
27.	Determination of Observed Contact Area	149
28.	Location of Contact Areas for One Case of Multiple Elastic Contact Between Models	91

LIST OF TABLES

		PAGE
I.	Surface Parameters for Bead-Blasted Surfaces	44
II.	Effect of Changing the Size of Two Contacting Hemispherical Asperities on Elastic Contact Behavior	45 45
III.	Asperity Locations and Heights	49
IV.	Average Properties of Polymethyl Methacrylate	81
V.	Input Data	82
VI.	Variance of Contact Parameters for Positions Tested	84
VII.	Contact Data	150

I. THE PROBLEM

There are many engineering situations in which the contact between two solid surfaces is of fundamental importance. The contact may be idealized by assuming contact over the entire surface between two contacting solids, but in reality this does not occur. The smoothest known surfaces, those produced by mica cleavage, contain irregularities on the order of 20 Angstroms in height. Because the surfaces of real solids are rough, contact between solid surfaces is not continuous, but occurs at discreet points. Thus the real area of contact between two surfaces is considerably less than the apparent area of contact.

A knowledge of the size and locations of these discreet areas of contact is useful in determining the contact strength and electric resistance in the contact zone of switches, in the study of contact corrosion, in determining the sealing capabilities of metal to metal seals, in the study of contact stresses, and in the study of resistance welding.

However, the most obvious discipline wherein a knowledge of the true contact area is of fundamental importance is tribology, a discipline which is almost exclusively concerned with two interacting solid surfaces. It is interesting to note that the most significant early investigator in the study of friction, A. Coulomb, failed to realize that contact occurred at discreet points. Based on his observations of a brick sliding on its side, end and top faces, Coulomb concluded that friction is independent of the area of contact between

sliding surfaces. If Coulomb had been aware of the discreet nature of contact between surfaces, the study of friction might have been advanced by 150 years.

"The main difficulty in tribology is that we still do not know enough about the detailed conditions existing at the solid-solid interface. Of course there are several problems in studying this interface, and these problems multiply when relative motion occurs. One of the most important unknowns concerns the nature of 'contact' itself. Knowledge of the size, number, and distribution of individual areas of contact would be of enormous fundamental value. For example, the information could be used in estimating intermolecular forces, assessing the sources of friction and wear, understanding mechanisms of lubrication, and calculating surface temperatures generated by friction. The key unknown in most of these problems is the area of contact and how it is distributed."(1)

II. LITERATURE REVIEW

A. Introduction

The following section provides a brief introduction to surface topography and reviews some of the experimental and theoretical approaches to the contact area problem.

B. Surface Topography

No real surface is perfectly smooth; all real surfaces contain asperities. The smoothest known surface, produced by mica cleavage, contains irregularities on the order of 20 Angstrom units in height. The topography of real surfaces is not dissimilar to the topography of the earth's surface; both can range from relatively smooth to very rough. Indeed, in both topographies similar criteria for surface measurement are encountered, i.e., local detail and long range coherence (2).

Various techniques for studying the geometry of solid surfaces have been reviewed by El-Refaie and Halling (3) and by Williamson (2). With these techniques it is possible to obtain not only photographs of microtopographical surface features, but also quantitative information and contour maps.

A number of articles which deal with the geometry of real surfaces have been published (4-9). From the evidence presented, it is obvious that surface asperities may have any shape and any height distribution. Some surfaces may have a geometry which is strongly

directional, whereas other surfaces may be completely random and exhibit no directional properties. However, it has been observed that most engineering surfaces contain asperities with rounded peaks and that the height distribution of these asperities (at least of the higher asperities) is approximately Gaussian (22).

For a reasonably comprehensive statement of surface characteristics, El-Refaie and Halling list the following as essential:

1. The geometric shape and size of the asperities.
2. The nature of the asperity height distribution, which could be taken along two directions in the plane of the surface in order to take directional properties into account.
3. The nature of the distribution of the asperities in the plane of the surface. This information should also be given for two directions in the plane of the surface.

Of course, three-dimensional surfaces and their geometric characterization has been the subject of investigation for a number of years and the study is by no means complete. These brief comments certainly do not review all that has been done in the area. However, the essential points are these:

1. Real surfaces are "rough" and their geometry is generally rather complex.
2. Surface roughness has been simulated by using conveniently shaped asperities.

3. The surface characteristics proposed by El-Refaie and Halling are essential in mathematically characterizing the geometry of rough surfaces.

C. Experimental Methods for Determining Contact Area

A number of methods for determining the true contact area have been developed over the years. D'yachenko (8) divides these methods into two groups: direct and indirect methods. Indirect methods are those which seek to determine the true contact area by first determining a parameter, such as contact resistance, which can be related to the true area of contact. Other indirect methods employ the use of photographs, surface profile charts, and microtopographical maps of surfaces to make inferences regarding the true area of contact. Direct methods are those which employ some optical technique of directly observing and recording the area of contact as contact occurs. These various methods have been applied before, during, or after contact in four types of systems:

1. Both surfaces engineering surfaces (i.e., surfaces commonly encountered in engineering practice)
   a. One surface "rough" and the other "flat" (i.e., ground and polished)
   b. Both surfaces rough
2. One engineering surface and the other a transparent surface (often an optical flat)

3. Both surfaces transparent replicas of real surfaces
4. One scaled-up model surface employing single or multiple asperities against a flat surface
   a. Both surfaces transparent
   b. One surface transparent
   c. Both surfaces opaque

1. Indirect Methods

Transfer of material

Probably the most straightforward method of contact area measurement is to coat one surface with a thin film of paint, luminous paint or carbon black and to note the amount of material transferred by examining the uncoated surface after contact (8). This assumes that transfer of material takes place during contact, and that the area occupied by the transferred material is equal to the true contact area. The contact areas may be measured by an ocular-micrometeric microscope, or the number of contact spots counted by eye. High contrast photographs can be obtained when luminous paints are employed and the contact areas illuminated with ultraviolet light. Tarasenko developed a method of using a microphotometer to measure the intensity of the radiation from transferred luminous paint and relating this to the contact area. The accuracy of the transfer of material method depends upon obtaining a layer of material on the surface which is sufficiently thin and uniform to prevent alteration

of the surface features. One disadvantage of this method is that it may be used only for static contact measurements.

It is interesting to note that Hertz used this method with soot covered lenses and glass plates to experimentally verify his classic equations of elastic contact (10).

Radioactive Method

Another method which could also be considered as a variation of transfer of material is the radioactive method (8). The procedure is to activate one surface and to measure the amount of radioactivity transferred to the other surface. Activation is achieved by neutron activation or by coating with a thin film of a radioactive substance. Although the transfer of material may be detected with a Geiger counter, radiographs are used to determine the distribution of the contacts. Radioactive sodium sulfate has been used for the surface coating because it is easily removed with water. A second coating of silver chloride may be used to increase the sensitivity.

There are several disadvantages associated with the use of this method. First it is difficult to obtain a uniform surface layer which is essential for accurate results. Measuring the contact area directly from the radiograph is difficult since the radioactive areas on the radiograph tend to be larger than the actual source. Furthermore, long periods of time may be required for exposing the radiographs (45 hours in one case). Finally, this method is good only

for static measurements.

Electric Contact Resistance

One of the early methods used to determine contact areas was that of electric contact resistance measurements (11). In 1912, Binder showed that electric contacts exhibited a smaller conductance than if the whole area was in contact. In 1939, Bowden and Tabor used electrical conductance measurements of crossed metal cylinders to determine the area of contact. These results compared favorably with values obtained from direct observation under a microscope. However, at light loads it was necessary to vibrate specimens with a tuning fork in order to obtain consistant results. Also there were 10-20% variations in the conductance at high loads.

Several factors complicate the use of this method. The total electrical resistance between two surfaces is a function of the conductivity of the material, the size of the contacts and the number of contacts. In order to use electric resistance to determine the contact area, it is necessary to know the size or number of individual contacts. Furthermore, when the separation distance between two contacts is small, the same material must carry current for both junctions. This interaction increases the contact resistance. Surface films also contribute to the resistance of the junction and the conductivity of the material may vary slightly with the load. In

order to avoid violating Ohm's law, there must be low heat emission (12).

Although there are a number of difficulties associated with the electrical resistance method, it is an important technique since it may be used for studying both static and sliding contact (12).

Thermal Resistance Techniques

Thermal resistance techniques, analogous to electrical resistance techniques, have also been used to determine the area of contact. Although this method is less affected by surface films than the method of electrical resistance, the loss of heat through air gaps must be taken into account. As cited by Rabinowicz (12), Newcomb (13) predicted plausible junction sizes using this technique.

Electron Probe Analysis of Interdiffused Surfaces

When two different metals contact, interdiffusion can take place. If this interdiffusion produces no new phases (i.e., only a solid solution), then exposure to the electron beam of an electron probe micro analyzer will produce a characteristic x-ray radiation. An x-ray count may be taken to obtain a quantitative measure of the area of contact between the two surfaces or photographs made to determine the distribution of contacts (14).

Since diffusion is a slow process, it is necessary to take mea-

sures which speed up diffusion. In an experiment with copper and nickel, loads were maintained for three hours at a temperature of 850°C and under a vacuum of more than 7.0×10^{-5} torr. Obviously this technique may be used only for static contact.

Surface Profilometry

One important method of determining the texture of real surfaces employs a surface profilometer to obtain height profiles of a given surface. Descriptions of the use of profilometers in surface measurement have been published by a number of authors (2, 6, 15 and others). Basically, the surface profilometer employs a sharply pointed stylus which traces along surface contours (6). An electric signal, which is the analog of the surface contour, is obtained. The resolution of the device is limited by the minimum tip radius of the stylus. Furthermore, there is a tendency for the stylus to trace around the side of a hill rather than across the summit and the sharp stylus penetrates soft surfaces. Nevertheless, the profilometer is an important tool in studying surfaces.

There are several ways to use the profilometer to determine contact areas. Profile charts may be used directly to determine the area of contact when the deformations involved are plastic. When asperities are deformed plastically, their peaks become flattened. By measuring the widths of the flattened peaks from the profilometer traces, determinations of the plastic contact area can be made.

Data from a surface profile chart can be processed by computer (or by laborious hand calculations) and the results displayed as a bearing area curve. This is simply a plot of the percentage of surface heights which are below a particular height level. This curve may also be interpreted to obtain the percentage of the total surface bearing the load when the asperities are deformed to various levels. Thus, if the approach of the two surfaces is known, bearing area curves may be used to estimate the contact area. However, in so doing, the effects of deformed material at the summits are neglected.

Still another profilometric technique involves the use of a computer to produce microtopographical maps from correlated adjacent profile traces. By analyzing microtopographical maps made before and after contact, information regarding the size and distribution of contacts may be obtained (4).

Parallel Sections

In this technique, a replica of the surface is made by covering the cleaned surface with Araldite, an epoxy resin. After it has hardened, the replica is ground on a plane parallel to the original surface and the area of the surface exposed at different levels of grinding is measured. The area of contact is determined from the separation of the two surfaces. For example, the contact area between a flat and a rough surface of 60 microns center line average (cla) when the flat has penetrated to a depth of 40 microns may be deter-

mined by grinding the replica to that level and measuring the bearing area.

Since this is a time-consuming technique, in practice only one grind is made at an angle of approximately 0.02° to the surface. If the grinding path is sufficiently long, the low heights are exposed at the low end and the higher asperities at the upper end. By considering a sufficiently wide band width at each height, estimates of the area at that level can be made. As with the bearing area curves, this method ignores the increase in the contact area (at a given penetration depth) due to the plastic flow of material from the asperity summits (9).

Taper Sections

This metallographic technique involves cutting a section from the surface at a very small angle to the surface. For a sectioning angle of 2° the resulting magnification of the profile is approximately 28. By taking these sections after contact has occurred, some estimate of the contact area may be obtained (9).

Etching

One unusual method of determining true contact area is to force an etching solution into the gaps between two contacting surfaces (16, 17). The contact areas are less affected by the etching pro-

cess and may be viewed under a microscope. The exact size of the unetched areas will depend upon whether the etching solution was forced from the surfaces or allowed to etch the periphery of the contact areas.

2. Direct Methods (Optical Techniques)

Technique used by Parker and Hatch

In this technique the specimen is loaded against a glass flat. The contact areas may be observed and measured from the opposite side of the glass by means of a microscope (18).

Phase Contrast

In this method the top surface of a polished glass plate is coated with silver. When a specimen is pressed against the top surface, both the silver film and the top surface are deformed. These deformations are observed through the glass using a microscope and the phase contrast method. Deformations appear bright against a dark background. It is claimed that deformations as small as a few Angstroms may be observed. Dyson and Hirst (19) used this method to measure contact areas which were within 10% of calculated values. This method also indicated that individual contact areas were much smaller than previously supposed. This method is limited to static applications and cannot be used after the surface becomes severely

damaged.

Mechau Method

This method has been described as the perturbation of internal reflection. The basic operating principle is that a beam of light is reflected or refracted as it passes from one medium to another of a different index of refraction.

Referring to Figure 1, the transparent specimen is loaded against one side of a truncated prism (20). Normally the light entering the prism from the left side is reflected between the two parallel surfaces until it emerges from the right side. However, wherever a ray of light strikes a part of the prism which is in contact with the model, it passes out of the prism through the interface. Because there is only a small difference in the index of refraction of glass and that of polymethyl methacrylate, the light passes through the interface as though it were not there. However, when there is an air gap between the two mediums, the difference in the indices of refraction of air and glass is great enough to cause the reflection and refraction phenomena. Thus the areas of contact show up as dark spots in a field of light. The area of contact may be determined from enlarged photographs.

Kragelskii (21) describes an interesting modification of this method in which photocells are used to measure the contact area. The apparatus is shown in Figure 2. Light from the source takes

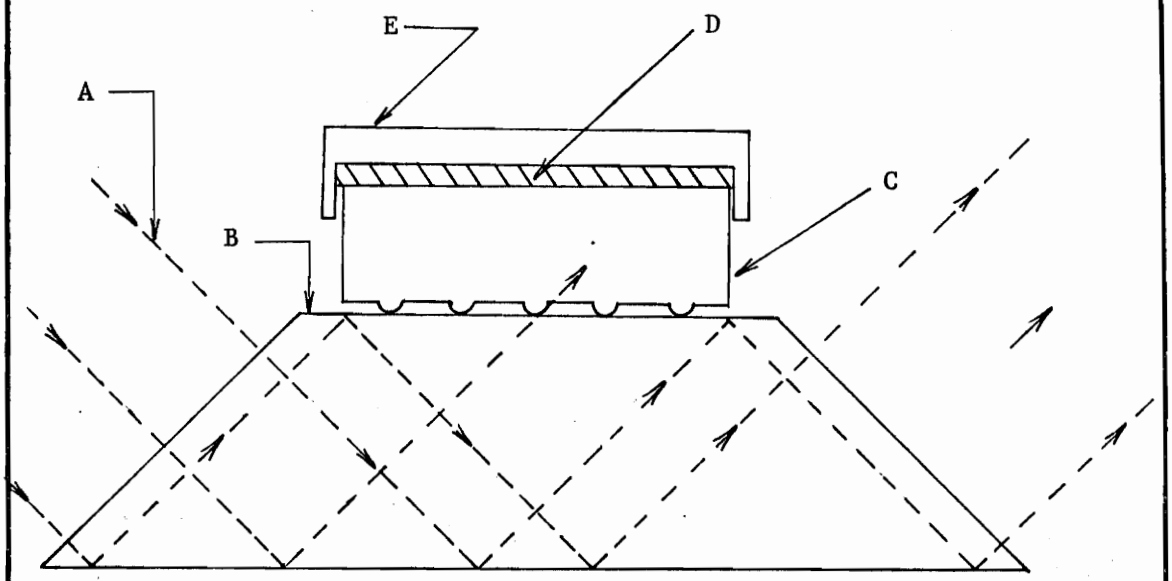

Figure 1. Mechau Method of Contact Area Determination

A. Incident light rays
B. Truncated Prism
C. Model Surface
D. Rubber Pad
E. Loading Device

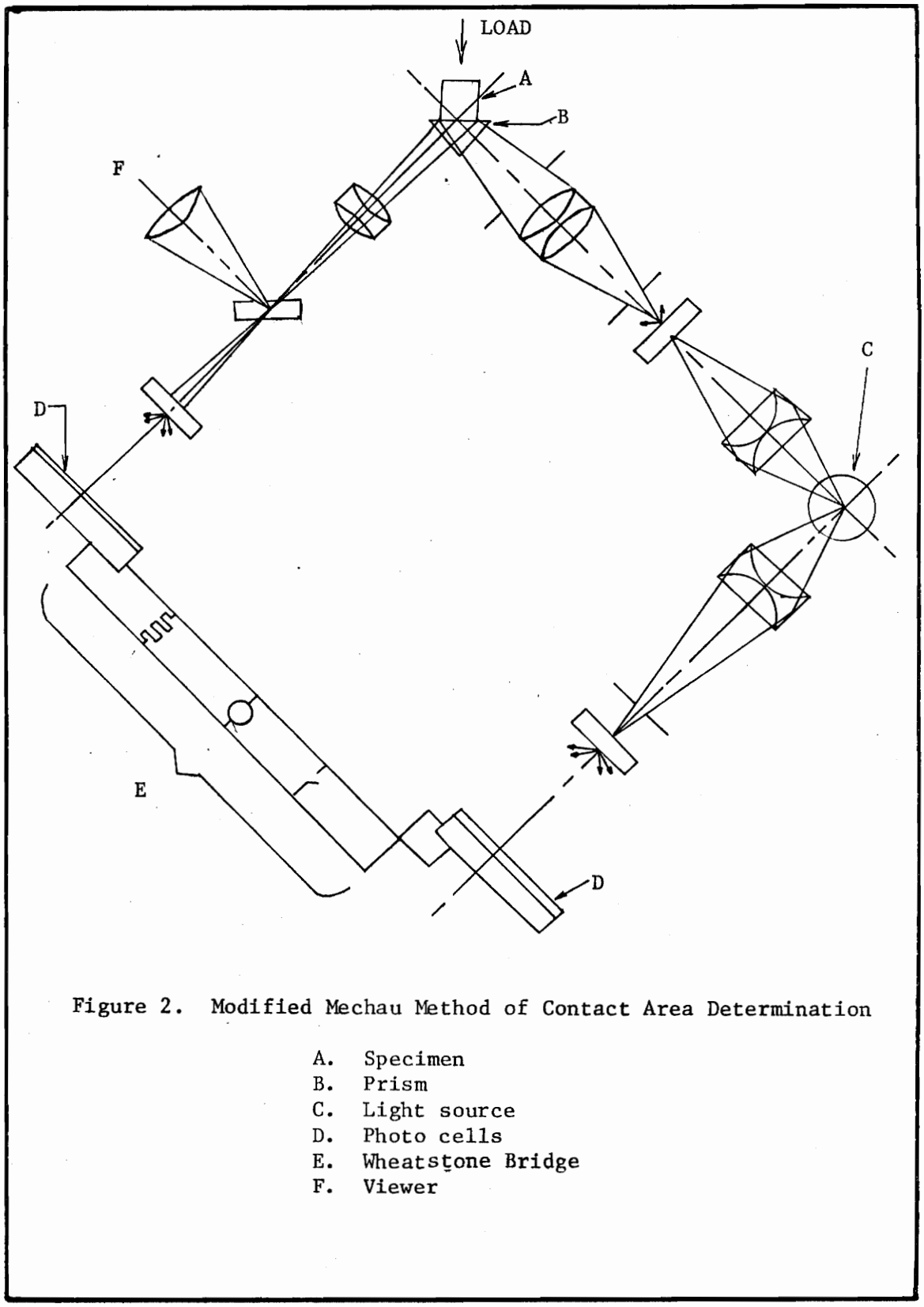

Figure 2. Modified Mechau Method of Contact Area Determination

A. Specimen
B. Prism
C. Light source
D. Photo cells
E. Wheatstone Bridge
F. Viewer

two separate paths to the photocells. The first path goes directly from the source through a lens system to a photocell. The second path goes through the truncated prism, a beam splitter, and finally to a second photocell. The photocells are connected to a resistance bridge in such a manner as to allow the output voltages to be balanced at zero contact area. When a transparent specimen is loaded against the prism, less light is reflected and the balance of the photocell bridge is disrupted. The voltage output may be calibrated in terms of the contact area by using a specimen which will deform plastically to produce a known contact area. The output of the photocells may also be calibrated by means of photographs.

The stability of the system was checked by using a steel ball loaded with a constant load. Successive readings were found to vary less than 1%. It was also found that there was a 2-3% variation in readings from the center and sides of the prism. Distortion due to bending of the light beam also introduced an error of 2-3% but readings could be corrected to account for this error. This technique is not suitable for use with smooth surfaces because the light rays may penetrate very small air gaps to introduce errors into the results. Kragelskii (21) states that for surfaces with asperity slopes greater than 7°, the error is approximately 3%. However, with smoother surfaces with slopes of 2-3°, the error may be as much as 15%. Areas as small as 5×10^{-4} cm^2 have been measured using this method. Dynamic measurements may also be obtained.

Extinction of Parallel Light

A technique which also employs the principle of reflection and refraction of light at the interface of two mediums with different indices of refraction is that of the extinction of parallel light. The technique has been employed by Furey (23) as shown in Figure 3. A spherical specimen is loaded against the lower surface of an optical flat and the contact area is viewed and illuminated from above as shown in the figure. For transparent specimens, when the light strikes the interface between the sphere and the flat (i.e., the area of contact) the light passes through the interface as though it were not there. At other locations, where there is no contact, part of the light is reflected to the camera. Thus the contact areas appear as dark spots in a light background. For the case of opaque materials, light striking the area of contact is reflected back to the camera. Thus, contact areas appear as bright spots. This method has been used for both static and dynamic measurements.

Transmittance of Parallel Light

Another method described by Kragelskii (21, 22) involves the transmittance of parallel light to determine the contact area between two transparent specimens. Referring to Figure 4, parallel light strikes the interface between the two specimens. At areas where there is no contact, the light is reflected or refracted. However,

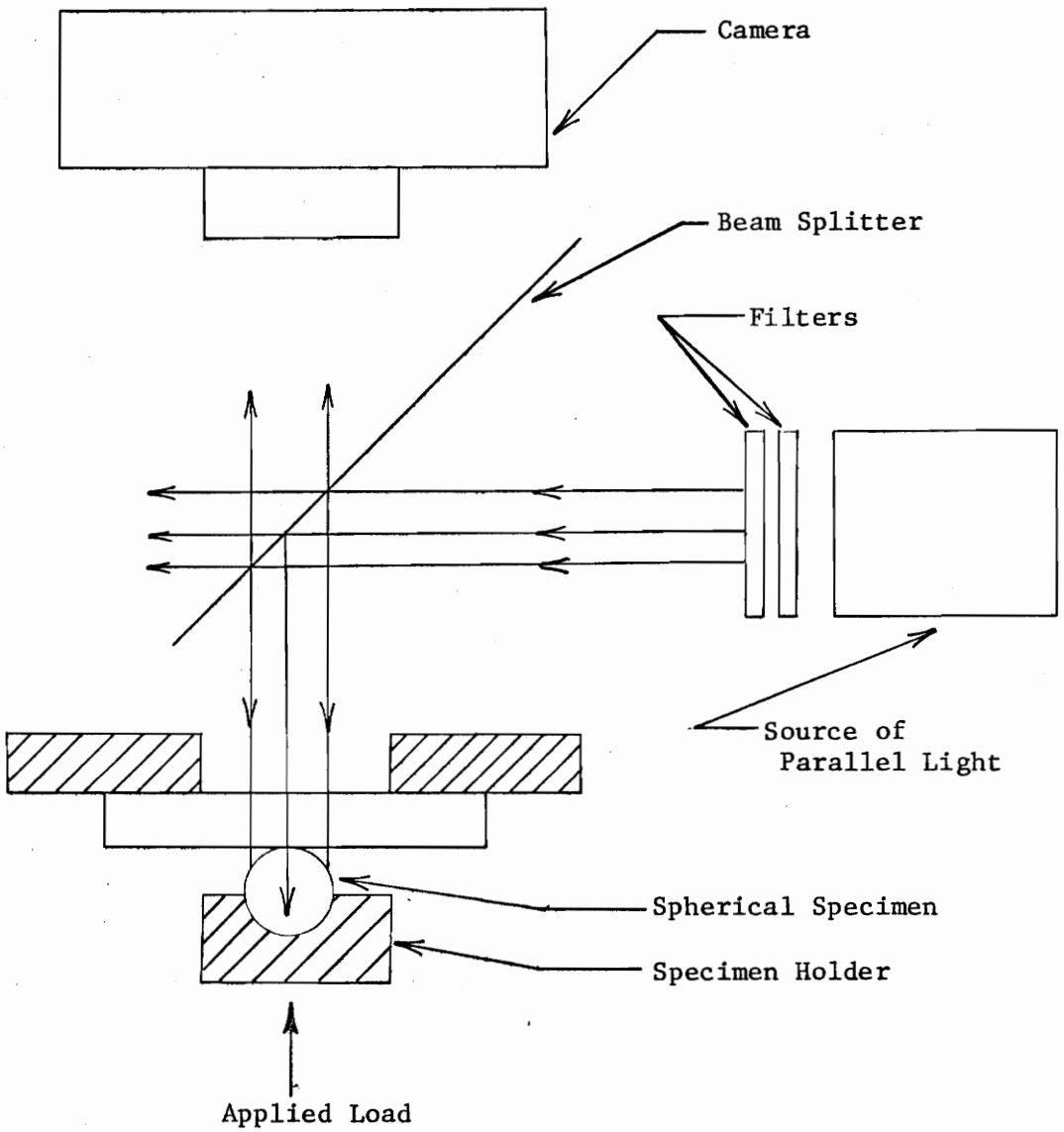

Figure 3. Extinction of Parallel Light

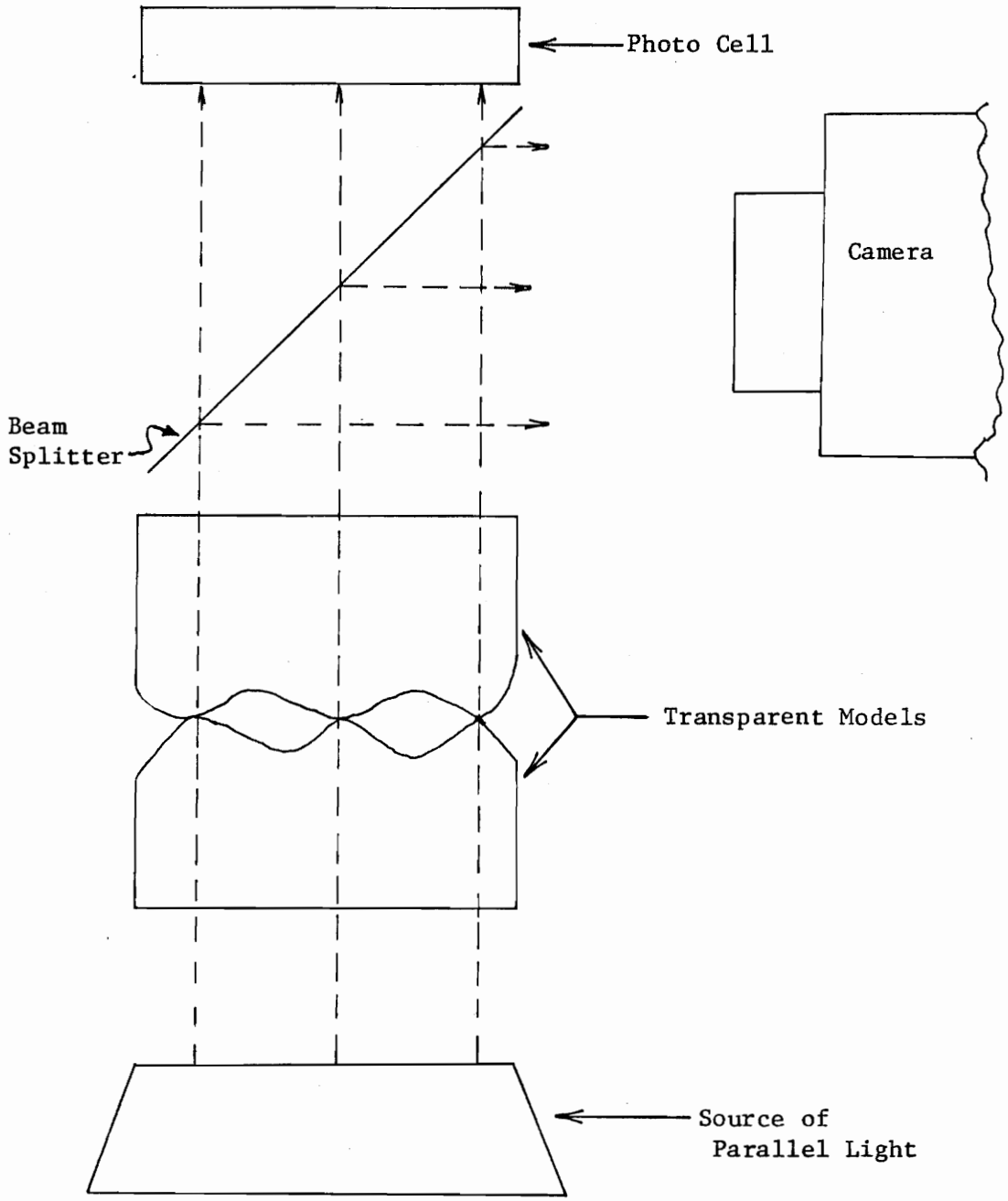

Figure 4. Transmittance of Parallel Light

light passes through the areas of contact and is recorded by the photocell. A beam splitter also allows the contact areas to be viewed through a microscope or photographed. This technique also works better with rough surfaces than with smooth ones and may be used for both static and dynamic measurements.

A variation of this method has been used by Janka (24) in studies of multiple asperity models against a flat (see Figure 5). To eliminate the problem of light reflected and refracted through the air gap, an opaque fluid was placed at the interface between the surfaces. At the points of contact, the fluid was squeezed out thereby allowing light to pass through the interface. However, at other areas the passage of light was blocked. Thus areas of contact show up as bright spots against a dark background.

D. Theoretical Approaches to The Contact Area Problem

Scientists believe that a knowledge of the true area of contact between solid surfaces is of fundamental importance in many studies. Furthermore, it has been shown that real surfaces are rather complex geometrically and random in nature. Since real surfaces defy a deterministic representation of their geometry, completely deterministic theoretical approaches to the contact area problem become extremely complex, if not impossible. However, a number of approaches based on various simplifying assumptions have been proposed.

Generally, theoretical approaches to the contact area problem

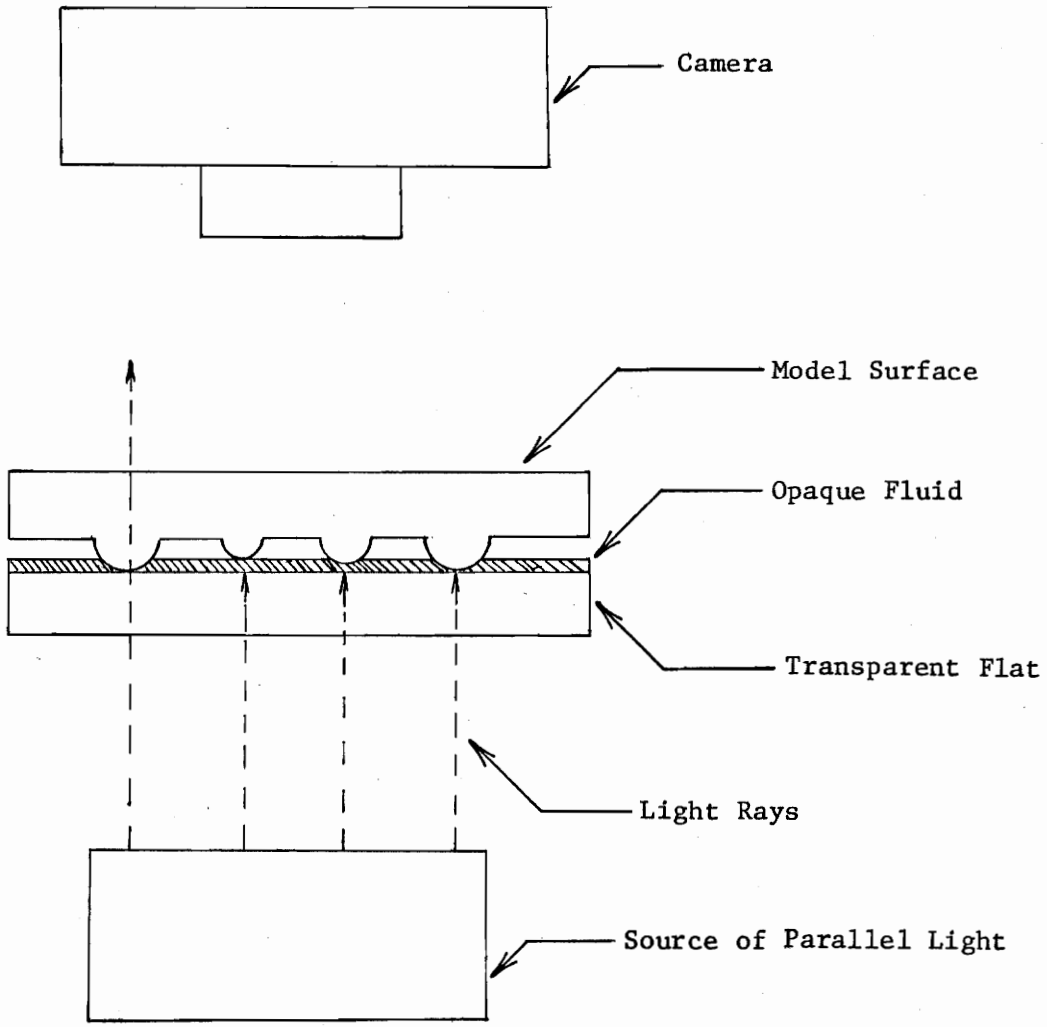

Figure 5. Opaque Fluid Technique

begin by assuming some convenient shape for model surface asperities, i.e., hemispheres, cones, pyramids, wedges, ellipsoids, etc. The contours of the real surface are simulated by having the heights and density of the assumed asperity models conform to certain distributions. Assumptions regarding the mode of deformation (elastic, plastic, or elasto-plastic) are also made. These assumptions are usually based on reasoning or experimental observation.

Theories which consider single or multiple contact have been proposed to predict the area of contact for purely elastic deformations, purely plastic, and elasto-plastic deformations. Other theories proposed consider the mode of deformation to be secondary in importance to the microgeometry of the contact surfaces. The problem is further simplified by assuming that the asperities deform independently of one another and often only contact between a rough surface and a smooth (sometimes rigid) plane is considered.

One factor which is often ignored in theories of static contact is the effect of tangential forces which may arise from an imposed tangential load or from off center contact (i.e., shoulder to shoulder contact) between asperities. Most theories simply do not consider the situation of an applied external tangential load. The few theories which consider the effects of shoulder to shoulder contact between asperities dismiss the tangential component as being negligibly small.

The following section briefly reviews some of the more significant theories of purely plastic, purely elastic, and elasto-plastic contact between solids. The situation of static contact between solids sub-

jected to both normal and tangential loading is also reviewed. Of course, other factors, such as a variation in mechanical, thermal, metallurgical and chemical properties can also influence the size of the real area of contact in a given system (21) but consideration of these factors is beyond the scope of this work.

1. Plastic Deformation

One of the earliest and simplest theories which have been proposed is that of Bowden and Tabor (26). From considerations of the roughness of real surfaces and the discrete nature of solid-solid contact, they reasoned that contact between real surfaces must take place at asperity peaks. The tremendous pressures resulting from peak to peak contact must result in plastic yielding of the asperities until the size of the area of contact is sufficient to support the normal load. Assuming constant properties, the mean pressure on the area of contact is equal to the yield pressure which is also assumed to be constant. Thus the area of contact (A) between asperities is:

$$A = \frac{W}{p_m}$$

where W = normal load

p_m = mean yield pressure of asperities

This theory predicts direct proportionality between the load and true area of contact, a result which greatly facilitates the explanation

of the Amonton-Coulomb laws of friction in terms of the Bowden and Tabor adhesion theory.

D'yachenko, et al. (8) have proposed a theory based on plastic contact of multiple asperities in which the most important factor affecting the contact area is the microgeometry of the surface. Their surface model is a set of cones on an elastic base. The cones have equal vertex angles, and are uniformly distributed on a base plane, but have heights which vary from zero to some maximum value. The cones are compressed by a smooth rigid surface. The area of contact is assumed to arise from the plastic deformation of the cones and is assumed to equal the geometric cross-section of the cone at the position of the rigid compressing plane. Based on experimental observations of machined surfaces, the assumptions are made that the asperities are cold hardened, i.e., somewhat harder than the base material and that plastic deformation of asperity peaks and elastic sinking of their bases begin simultaneously.

After a rather long derivation, the following equation results:

$$S_a = 0.2 \left\{\frac{P}{H_d}\right\}^{0.7} S_{nom}^{0.3} \left\{\frac{E}{\pi H_d \tan \gamma \, (1 - \nu)^2}\right\}^{0.7 \, (1 - \alpha)}$$

where S_a = actual contact area

S_{nom} = nominal contact area

E = modulus of elasticity

P = load

H_d = hardness

ν = Poisson's ratio

α = parameter related to mean height

γ = included half-angle of cone

Another multi-asperity contact theory has been proposed by Greenwood and Tripp (7). In treating contact between nominally flat rough surfaces, they assumed that individual contacts are sufficiently separated so that there is no interaction between two contacts. The real surface was modeled by a distribution of identically shaped asperities at various heights. The asperities were assumed to be symmetrical and the shape a function of the radius of curvature at the summit.

In the derivation, the separation between two rough surfaces was found to depend upon the sum of the heights of the two surfaces at the point under consideration and the separation of the two reference planes. Mathematically, it is justifiable to combine the height distributions (assumed Gaussian) of the two surfaces into one distribution by standard statistical techniques. Consequently, the static areas of contact between two rough surfaces were determined from considering one rough and one smooth surface. By assuming that both the contact area and normal load on two contacting asperities were functions of the overlap and by considering the statistical probability of contact occurring, general expressions for the total area of contact and total load were obtained.

For the case of plastic contact the area of contact was assumed to be the cross-sectional area of the asperity at the position of the

flat surface (i.e., plastically-deformed material at the top of the asperity was ignored). Using the Bowden and Tabor theory, the load was taken to be the product of the area of contact and the yield pressure. The equation for the area of contact and the load were found to be:

$$A(h\sigma) = \pi^2(\eta\beta\sigma)^2 \, A_{nom} \, F_2(h)$$

$$P(h\sigma) = 2\pi^2(\eta\beta\sigma)^2 \, HA_{nom} \, F_2(h)$$

where η = surface density of asperity heights

β = radius of curvature at the asperity peak

σ = standard deviation of the sums of asperity heights

H = mean pressure related to hardness

A_{nom} = nominal contact area

$F_n(u) = \int_u^{\infty} (s - u)^n \, \psi^*(s) ds$

$\psi^*(s)$ = standardized probability distribution of asperity heights

From various experiments it has been shown that plastically-deformed asperities at high loads deviate from the classical (directly proportional) relation with the area of contact. Uppal and Probert (27-29) point out that this is caused by subsurface plastic flow, interpenetration of the plastic zones under contacting asperities and the plastic flow of material from asperity summits. As cited in reference 28, Williamson et al. (30) have proposed a theory which takes into account the material displaced from the asperity summits.

Using a conservation of volume principle, Williamson postulates that the material plastically displaced from the asperity summits contributes to a uniform rise in the non-contacting surface. The theory predicts a directly proportional relation between the load and area of contact at low loads, but at higher loads where the plastic flow becomes significant the relation between load and the area of contact deviates from linearity.

2. Elastic Deformation

Not all workers in the area of surface contact believe that pure plastic deformation explains all contact phenomena. In one often cited example, Archard (20) stated that it was very difficult to believe that machine bearing surfaces, which may undergo millions of contacts, deform plastically during each loading cycle. Others have found experimentally that for relatively smooth surfaces contact is elastic. Accordingly, a number of theories based on the elastic deformation of surface asperities have been proposed.

Since all of the theories of elastic contact employ the Hertz theory of contact between two elastic bodies, it is appropriate to review that theory. In his derivation Hertz assumed the following (10, 31):

1. The contacting solids are isotropic and linearly elastic.
2. The dimensions of the contact area are small in comparison to the radii of curvature of the bodies near the contact surface.

3. The two bodies may be represented accurately enough by general surfaces of the second degree.

   (i.e., $Z = Ax^2 + By^2 + Hxy$)

4. In the region of the contact area, the two bodies are sufficiently "flat" to justify the use of analytical methods for semi-infinite solids.

5. The elastic bodies are perfectly smooth and only normal forces are present on the contact surface.

For the general case Hertz came to these conclusions:

1. The contact area is an ellipse with semi-axes a and b. The position of the contact area relative to the bodies in contact may be determined from geometric considerations.

2. The distribution of normal pressure is

$$p = p_o \left\{1 - \left\{\frac{x}{a}\right\}^2 - \left\{\frac{y}{b}\right\}^2\right\}^{\frac{1}{2}}$$

   The maximum pressure, p_o, is equal to 1½ times the average pressure and occurs at the center of the contact area.

3. The dimensions of the ellipse, a and b, are proportional to $N^{1/3}$.

4. The approach (decrease in separation between two reference points removed from the contact area) is proportional to $N^{2/3}$.

For the special case of two spheres with radii R_1 and R_2 considered by Lubkin (10), the Hertz equations reduce to:

$$a = (3NR_o/4E_o)^{1/3}$$

$$p = p_o(1 - r^2/a^2)^{1/2}$$

$$p_o = 3N/2\pi a^2$$

$$\alpha = R_o^{-1/3}(3N/4E_o)^{2/3} = a^2/R_o$$

where $1/E_o = (1 - \nu_1^2)/E_1 + (1 - \nu_2^2)/E_2$

$$1/R_o = 1/R_1 + 1/R_2$$

N = normal load

E_1, E_2 = modulii of elasticity

ν = Poisson's ratio

a = radius of contact area

p = normal pressure

α = approach = decrease in center distance

r = radial distance measured from center of contact area

The maximum shear stress is $0.31p_o$ (for materials with a Poisson's ratio of 0.3, i.e., steel) and is located at a point below the center of the contact area where the ratio of depth to the radius of the contact area is 0.47. (The magnitude of this stress varies slightly with Poisson's ratio.) The maximum compressive stress is p_o and is located at the center of the contact area.

The first to show that laws of elastic deformation could be used to explain direct proportionality between the normal load and area of contact was J. F. Archard (20). As mentioned above, for elastic contact of smooth spheres the area of contact is proportional to $N^{2/3}$. However, Archard found that for a sphere covered with smaller hemispheres the contact area is proportional to $N^{4/5}$. If these hemispheres are then covered by smaller hemispheres the contact area is proportional to $N^{14/15}$. As the asperity model becomes more complex by the superposition of hemispheres on hemispheres, the relation between N and A approaches linearity. Archard explained that the linear relation arises from the fact that new areas of contact come into existence with an increase in the load.

Kragelskii (21) considered two types of surface models involving elastic deformation. In one model each surface was modeled by a group or rods, each of which obeyed Hooke's Law. Considering a linear distribution of rod heights, Kragelskii derived the following equation:

$$A_r = 1.65 \frac{A_c^{1/3} \gamma_1^{1/3} \gamma_2^{1/3} (E_1 + E_2)^{2/3} 4\rho(1 - \mu^2)^{2/3}}{(E_1 E_2)^{2/3}} N^{2/3}$$

where A_r = real contact area

A_c = contour area

γ_1, γ_2 = constants characterizing the distribution of rod heights

E_1, E_2 = modulii of elasticity

ρ = radius of contact region

μ = Poisson's ratio

N = normal load

Kragelskii's other model was a group of hemispherical asperities of radius r, uniformly distributed on a flat plane. The height distribution was exponential. Using Hertz's equations and bearing area curves, Kragelskii derived the following equation

$$\eta_1 = \left\{ \frac{0.75 b^{\frac{1}{2}\nu} \pi r^{\frac{1}{2}} (1 - \mu^2)}{2^{\frac{1}{2}\nu} K_2 \nu h_{max}^{\frac{1}{2}} (\nu - 1)} \right\}^{2\nu/(2\nu + 1)} \left\{ \frac{q}{E} \right\}^{2\nu/(2\nu + 1)}$$

r = radius curvature

μ = Poisson's ratio

b, ν = surface coefficients

q = nominal pressure

E = modulus of elasticity

K_2 = constant related to asperity height

h_{max} = maximum asperity height

D'yachenco, et al. (8) have proposed an equation for elastic contact using an ellipsoidal model. The choice of this model was based upon observations of a number of perpendicular profilometer traces of ground surfaces, one of the most common surfaces in engineering. In this model, surface roughness was simulated by an assortment of ellipsoids with various radii of curvature. No interaction between asperities was considered but elastic deformation of the base was considered.

After an involved derivation, a rather complex equation for the

real area of contact as a function of material properties and coefficients from profilometer traces resulted. In solving the contact area problem, the load was first determined for a given approach and the true area of contact was obtained with the use of the aforementioned equation. A correction for a variable modulus of elasticity with depth was also included.

Greenwood and Tripp (32) extended the Hertz theory of elastic contact of smooth bodies to the contact of one rough on one smooth body. The case chosen was a rough plane in contact with a smooth sphere. It was assumed that the tops of the asperities were spherical with the same radius, followed a Gaussian height distribution, and deformed as predicted by the Hertz equations. The contact was not continuous but was spread over a number of discreet points. Greenwood and Tripp considered the most significant factor in determining the contact to be the statistical distribution of asperity heights.

At sufficiently high loads the equations derived agreed well with the Hertz equation. However, at lower loads significant differences were found. At low loads the contact area was predicted to be approximately ten times larger than the Hertz value. Consequently, the peak pressure was only one-third of the Hertz value.

Greenwood and Tripp (7) also obtained equations for the contact of two nominally flat rough surfaces. Following a procedure described in the section on plastic deformation, they derived general expressions for the contact areas and loads. However, in the case of elastic deformation, elastic relations were used to reduce the equation for

the total contact area to the following:

$$\tilde{A}(h\sigma) = \pi^2 (\eta B\sigma)^2 A_{nom} AF_2(h)$$

(see previous section for definition of terms).

3. Elasto-Plastic Deformation

As surface asperities come into contact and begin to carry part of the normal load they are deformed first elastically and then plastically. Various criteria have been used to determine the transition point from elastic to plastic deformation. D'ychenko, et al. (8) assumed that plastic deformation ensued after the asperity had been deformed to a critical depth. For his sinusoidal surface model Blok (33) proposed that for $\frac{h_{max}}{2\ell} < \frac{H}{\pi E'}$ deformations were completely elastic. (h_{max} = peak to valley height, ℓ = peak to peak length, H = hardness, E' = equivalent Young's modulus). Halliday (34) proposed criterion for the limit of elastic deformation

$$\tan\theta < (\text{constant}) \frac{H}{E} (1 - \nu^2)$$

where θ = asperity slope

H = Vickers hardness

E = modulus of elasticity

ν = Poisson's ratio

The constant depends upon asperity shape; for two flat surfaces covered by spherical caps it is 0.84.

Greenwood and Williamson (35) have also proposed a criterion for the limit of elastic deformation which they call a plasticity index. According to Tabor's work with indentation hardness, the onset of plastic flow occurs when the maximum Hertz pressure is approximately 0.6H, where H is the hardness. Using this criterion, they found the critical elastic deformation (W_p) for the onset of plastic deformation to be

$$W_p = .89B \left\{\frac{H}{E_o}\right\}^2$$

where B = summit radius of asperity.

However, since the criterion for plastic flow is exceeded first internally, plastic flow will be restricted by the surrounding elastic material. Therefore, for convenience Greenwood and Williamson assumed that the actual criterion for plastic flow is

$$W_p = B \left\{\frac{H}{E_o}\right\}^2$$

After nondimensionalizing and rearranging terms, the following plasticity index was obtained.

$$\psi = \frac{E_o}{H} \left\{\frac{\sigma}{B}\right\}^{\frac{1}{2}}$$

Greenwood and Williamson reasoned that even for a small amount of plastic deformation the predictions of load and contact area based on elastic theory would be accurate. Accordingly, they allowed a limit of 2% of the total contact to be plastically deformed before considering the limits of elastic behavior to be exceeded. For a plasticity index of

less than 0.6 a surface behaves elastically except at very large nominal pressures. When the plasticity index is greater than 1.0, the mode of deformation is plastic, even at very low nominal pressures.

D'yachenko et al. (8) have extended the ellipsoidal model of elastic deformation to include deformations in the elasto-plastic regime. It was assumed that some of the asperities were plastically deformed and others elastically deformed, that as soon as the criterion of plastic deformation was exceeded the entire asperity became plastically deformed, and that the plastic contact area was equal to the geometric cross-section of the asperity at the depth of the crushing surface. In order to determine the area of plastic contact and the area of elastic contact, the normal load as a function of the approach of the crushing plane was first determined. The second step involved the separate determination of the elastic and plastic contact areas. This procedure is complicated and difficult to use in practical situations.

In experimental observations of polymethyl methacrylate replicas of real surfaces, D'yachenko noted that the deformation of surface asperities was of an elasto-plastic nature. The peaks deformed plastically while the base deformed elastically.

4. Effect of Tangential Loads

The effect of tangential loading on both plastically and elastically deformed junctions has been treated by Bowden and Tabor (26) as

part of their development of the adhesion theory of friction. This theory assumes that under a normal load, asperity peaks become plastically deformed. Since the area of contact is already at the yield stress, the addition of a tangential load causes the contact area to deform and become larger (junction growth) until it is large enough to withstand the combined stress. Bowden and Tabor obtained the following relation to predict the growth of the contact area:

$$1 + \alpha\psi^2 = \left\{\frac{A}{A_o}\right\}^2$$

where A_o = contact area due to normal load acting alone

A = contact area due to combined normal and tangential loads

ψ = ratio of tangential load to normal load

α = a constant varying from 3 to 30 depending on the junction shape and material properties

The phenomenon of junction growth has been observed by a number of investigators. Courtney Pratt and Eisner (36), experimenting with a spherically ended cone on a flat, obtained experimental verification of the above equation.

Mindlin (37) has extended Hertz's treatment of smooth elastic bodies in contact to include the effects of a tangential load less than that required to produce sliding. Although he was primarily interested in the tangential compliance of the bodies, Mindlin did reach conclusions concerning the area of contact. The size of the contact area is determined solely by the normal load. The effects

of the shear stress are to displace the contact area without changing its size or shape and to produce an annulus of slip around the outside portions of the contact area.

O'Connor and Johnson (38) used specially prepared surfaces to check the behavior of asperities in transmitting tangential loads. Their data tended to support the Bowden and Tabor theory for plastically deformed asperities and the Mindlin theory for elastically deformed asperities.

After reviewing the results obtained by O'Connor and Johnson, Bowden and Tabor (26) offered the following explanation for the elastic case. Even though the bulk deformation of the materials involved was elastic, asperities at the interface of the contacting solids were deformed plastically. Since the tangential elastic displacements of the materials were on the same order of magnitude as the asperity heights, there must have been a growth in the size of the individual contact areas even though the bulk behavior was determined by elastic deformations.

Experimental studies of the effect of tangential loads on the optical area of contact between a sphere and an opitcal flat have been performed by Furey (39). Spheres of various metals (Ag, Cd, In, Sn, Au, Pb, and Bi) and polymers (polymethyl methacrylate, polyethylene, nylon, and cellulose acetate) were tested. Upon the application of a fixed tangential load there was generally an increase in the area of contact. However, in all cases the increase was smaller than that of indium which had been used in previous studies

by others (e.g., 18).

The application of gradually increasing tangential loads generally resulted in a large increase in contact area--especially with the softer metals. For sliding contact the contact areas decreased, increased, or remained the same depending upon the materials used.

The contact of elastomers sliding against an optical flat was studied by Bartenev, Lavrentjev, and Konstantinova (25). They found the contact area to remain almost constant for sliding velocities up to one cm/sec. At higher velocities the contact area was observed to decrease.

III. APPROACH TO PROBLEM

A. Introduction

As evidenced in the previous sections, the problem of determining static contact areas between real surfaces has not been fully resolved from either the experimental or the theoretical point of view. The theories of static contact between rough surfaces remain just theories; none has been sufficiently verified to attain the status of a law of static contact. Each of the experimental methods has its limitations; none offers a convenient means of continuous determination of both the size and location of the true area of contact between real surfaces commonly used in engineering.

An approach to this problem has been outlined by Dr. M. J. Furey (1) in a research proposal to the National Science Foundation. The rather ambitious approach was addressed to two interrelated topics:

1. The mechanisms of friction and wear
2. The nature and area of contact between solids

The main objective of the first part of the proposal was to observe as completely as possible contact between three-dimensional models of real surfaces. Carefully designed experiments between simple geometric models were proposed to study plastic-plastic contact, plastic-elastic contact, and elastic-elastic contact. It was anticipated that much of the initial experimental work would involve the use of transparent solids such as polymethyl methacrylate. Previous work by Dr. Furey (40) had proven that the proposed optical technique could be used to study the area of contact between a spheri-

cal asperity model and a flat. Furthermore, for polymethyl methacrylate spheres used in that study, the size of observed contact areas were quite close to values predicted from the Hertz equation.

The objectives of the second part of the proposal were to carry out:

1. A careful review of previous theoretical studies
2. A review of previous experimental techniques
3. An investigation of ways of mathematically describing real and model surfaces
4. Continued experimental studies with the existing solid-solid contact device
5. Experimental contact studies of multi-asperity surface models against a flat or another surface model
6. Further development of the theory of contact between rough surfaces
7. A comparison of experimental and theoretical results
8. A comparison of significant results from each part of the study

This project represents a continuation of previous detailed studies by Dr. Furey (40) of the contact between single spherical asperity models and flat surfaces. Recently, Janka (24) has dealt with the problem of multi-asperity models against a flat surface. It is the purpose of the present study to develop the necessary techniques to implement the above approach to the problem of solid/

solid contact between two multi-asperity models. The remainder of this section describes these techniques.

B. Model Design

The goal of the model design procedure was to obtain the geometric specifications for multi-asperity, macroscopic surface models for use in both theoretical and experimental contact studies. There were also a number of constraints (maximum size, shape, etc.) which were placed on the model design. Since a number of different model configurations could satisfy these constraints, it was decided to select the model geometry based on the most important constraints and then ascertain that none of the other constraints was exceeded.

The most obvious constraint is that of geometric similitude between the model and some representative real surface. Another less obvious constraint is similitude in the behavior of the model and of the real surface. In other studies in which a model is compared with a prototype, similitude of behavior corresponds to several levels of similitude--kinematic, dynamic, and sometimes thermodynamic. In modeling real surfaces for contact studies, similitude in behavior corresponds to similarity between the deformation of the real surface and that of the models. This implies that under corresponding conditions both the amount and mode of deformation is the same.

As mentioned previously, El-Refaie and Halling (3) have listed the following parameters as essential for characterizing the geometry

of a surface:

1. The asperity shape and size
2. The asperity height distribution
3. The distribution of asperities in the plane of the surface.

Unfortunately, in the past the bulk of information presented for characterizing surfaces dealt with only one or two surface parameters--usually asperity slopes or the center line average of the heights. However, as a result of their work in surface topography, Greenwood and Tripp have published values of the above parameters for bead-blasted aluminum. These values are summarized in Table I. From the table it is seen that there can be a wide variation in the surface geometry.

In order to achieve strict geometric similitude it would only be necessary to multiply linear dimensions of some real surface by a scale factor K. Table II shows the effect of changing the size of two asperities in elastic contact on various contact parameters. Once the scale factor K and the materials are chosen, the only other variable which may be freely manipulated is the load N.

From Table II it is seen that by increasing the load for the macroscopic models by a factor of $C = K^2$, the ratios of approach, radius of contact area, area of contact, and maximum elastic approach of the macroscopic models to the corresponding parameters of the real surface become equal to K. In other words, by suitable manipulation of the load, the contact behavior of the macroscopic models can be made to

TABLE I

Surface Parameters for Bead Blasted Surfaces

	Typical Values	Bead Blasted Aluminum
Asperity height	10 to 300 μin	
Mean		200 μin
Std. dev.		46 μin
Max		360 μin
Summit Density		$2 \times 10^6 \frac{\text{Summits}}{\text{Sq. in.}}$
Mean Summit Radius	400 to 800 μin	
Separation between	50 to 3000 μin	2000* μin
Slope	5° - 10° Occasionally 25°	10° Average

*Roughness of 40 μin cla

**Separation between major summits

NOTE: The distinction between a summit and a major summit should be made clear. Greenwood and Tripp defined a summit to be a spot on the surface which was higher than its eight nearest neighbors. Major summits, as the name implies, were only the highest, most significant of all the summits.

TABLE II

Effect of Changing the Size of Two
Contacting Hemispherical Asperities on Elastic Contact Behavior

Asperity Parameters	Asperities on real surface	Macroscopic Asperity Models
Summit Radii	R1	R1' = KR1
	R2	R2' = KR2
Equivalent Radius	$R = (R1 \cdot R2)/(R1 + R2)$	R' = KR
Equivalent Modulus of Elasticity	E	E' = E
Elastic Limit of Material	s	s
Normal Load	N	N' = CN
Contact Parameters		
Approach	$\alpha = R^{-1/3}(3N/4E)^{2/3}$	$\alpha' = (C^2/K)^{1/3}\alpha$
Radius of Contact Area	$a = (3NR/4E)^{1/3}$	$a' = (CK)^{1/3}a$
Area of Contact	$A = \pi(3NR/4E)^{2/3}$	$A' = (CK)^{2/3}A$
Maximum Elastic Load	$Np = (2\pi s/3)^3(3R/4E)^2$	$Np' = K^2Np$
Maximum Elastic Approach	$\alpha p = R(\pi s/2E)^2$	$\alpha p' = K\alpha p$

correspond to that of the real surface.

Several other constraints were also placed on the design of the models:

1. There should be a statistically significant number of asperities.
2. A point of reference should be provided to facilitate alignment of models in the NSF contact device.
3. The asperities should deform elastically.
4. The summit radius of the asperities should be an easily reproducible dimension.
5. The maximum load should not exceed the limit of the experimental apparatus.
6. The maximum sizes of the asperity surfaces are 3 in. x 8 in. and 3 in. x 4 in.
7. The model should be thick enough to withstand the applied loads without appreciable deflection.
8. Standard machining operations would probably limit tolerances to $\pm$0.001 inch in the x-y plane and $\pm$0.0005 in the z-plane.

After consideration was given to the constraints, the following model specifications were selected for this study: (See Figures 6 and 7)

1. Size of asperity surface:

   upper model - 3 in. x 4 in.

   lower model - 3 in. x 8 in.

2. Summit radius:

   0.5 inches

3. Asperity height:

   mean - 0.050 inches

   standard deviation - 0.012 inches

4. Number of asperities:

   upper model - 37

   lower model - 75

5. Distribution of asperities in x-y plane:

   random - coordinates selected from a table of random numbers (41)

   - minimum separation approximately 0.3 inch

Several comments should be made regarding the heights. The distribution of heights was calculated from a table of the cumulative normal distribution function using the values of the mean and standard deviation listed above and a sample size of 200 for the lower model and 100 for the upper model. However, since the lower asperities almost never come into contact these asperities were not included in the model. The difference in the heights of the tallest asperities in the original height distribution was 0.002-0.003 inches. Since the tallest peaks greatly influence contact, it was possible that contact would occur first at one of these asperities; thus in order to bring other asperities into contact (to obtain the desired multiple contact between models) it would be necessary to deform the taller asperities beyond their elastic limit into the mode of plastic deformation. Of

course, this situation can occur with real surfaces, but the object of this particular study was to achieve multiple elastic contact in order that the well verified Hertz equations could be used to predict the size of contact areas. There were two means of correcting the situation: the value of the standard deviation could have been reduced by a factor of two in order to obtain models of a smoother surface or the highest asperity heights could be excluded. The latter approach was taken, resulting in a Gaussian distribution of heights which was truncated at both ends. See Table III for the location and heights of the asperities. (The x- and y-coordinates are referenced from edges A and B respectively. See Figures 6 and 7.)

C. Model Fabrication

One objective of the project was to develop a technique whereby it would be possible to fabricate models of rough surfaces in a few hours of laboratory work. The technique was to provide optically clear models with various numbers and distributions of asperities whose position and height were accurately controllable.

Polymethyl methacrylate was selected as the model material because of its good optical qualities and its commercial availability as a casting syrup. The material used initially, Klearmount, was obtained from Vernon-Benshoff Company, Inc. After the proper ratios of the monomeric casting syrup and catalyst are mixed, a polymerization takes place at room temperature and pressure. After approxi-

TABLE IIIA

LOCATIONS AND HEIGHTS OF ASPERITIES ON UPPER MODEL

ASPERITY INDEX NUMBER	SUMMIT LOCATION X-COORD (CM)	Y-COORD (CM)	HEIGHT (CM)
1	8.199	2.482	0.1661
2	2.652	6.431	0.1656
3	2.202	2.690	0.1722
4	7.318	2.035	0.1638
5	5.651	4.928	0.1598
6	2.911	7.541	0.1521
7	5.517	2.913	0.1598
8	4.122	5.933	0.1534
9	10.505	6.302	0.1369
10	4.188	2.045	0.1572
11	10.645	1.801	0.1440
12	1.801	7.673	0.1420
13	3.950	4.862	0.1478
14	2.758	4.613	0.1496
15	8.755	4.780	0.1392
16	3.967	7.135	0.1392
17	4.437	4.140	0.1438
18	7.937	6.088	0.1341
19	9.017	7.668	0.1222
20	8.120	7.015	0.1275
21	1.580	5.331	0.1400
22	9.594	5.568	0.1382
23	6.853	3.477	0.1374
24	5.804	6.574	0.1300
25	3.399	3.053	0.1400
26	10.615	5.210	0.1224
27	6.607	4.915	0.1308
28	10.269	7.661	0.1110
29	6.657	5.662	0.1273
30	7.744	4.816	0.1280
31	9.799	2.322	0.1265
32	4.818	7.475	0.1212
33	6.571	2.682	0.1306
34	7.861	3.835	0.1257
35	10.437	3.973	0.1191
36	9.576	4.044	0.1196
37	1.867	6.203	0.1247

TABLE IIIB

LOCATIONS AND HEIGHTS OF ASPERITIES ON LOWER MODEL

ASPERITY INDEX NUMBER	SUMMIT LOCATION X-COORD (CM)	Y-COORD (CM)	HEIGHT (CM)
1	14.844	2.146	0.1674
2	10.160	6.568	0.1836
3	19.845	4.173	0.1326
4	10.178	1.989	0.1831
5	6.419	1.816	0.1859
6	7.620	1.466	0.1844
7	6.091	5.306	0.1831
8	8.529	4.935	0.1811
9	9.469	3.134	0.1806
10	9.469	4.648	0.1783
11	9.942	5.476	0.1758
12	1.605	5.352	0.1725
13	12.515	1.773	0.1679
14	8.618	3.853	0.1775
15	3.480	6.032	0.1745
16	9.870	6.431	0.1699
17	19.695	5.618	0.1191
18	13.797	3.020	0.1323
19	5.992	5.268	0.1758
20	18.011	6.104	0.1293
21	6.881	2.466	0.1737
22	12.606	6.104	0.1590
23	5.220	6.190	0.1699
24	3.881	1.750	0.1694
25	11.918	2.652	0.1605
26	12.921	3.886	0.1560
27	1.438	6.487	0.1598
28	3.889	2.921	0.1692
29	5.408	3.706	0.1704
30	13.914	6.871	0.1468
31	2.715	1.714	0.1643
32	19.360	1.161	0.1140
33	6.746	6.322	0.1648
34	3.459	5.029	0.1643
35	18.029	1.128	0.1318
36	7.653	1.140	0.1593
37	19.167	3.927	0.1138
38	19.398	2.395	0.1102

TABLE IIIB (CONTINUED)

ASPERITY INDEX NUMBER	SUMMIT LOCATION X-COORD (CM)	Y-COORD (CM)	HEIGHT (CM)
39	9.759	3.665	0.1605
40	10.676	3.416	0.1577
41	14.148	5.126	0.1420
42	16.462	5.293	0.1275
43	18.992	1.847	0.1110
44	17.440	1.900	0.1206
45	17.404	4.313	0.1224
46	11.036	1.816	0.1527
47	3.299	4.000	0.1577
48	15.636	3.772	0.1552
49	2.332	2.708	0.1572
50	9.959	2.939	0.1554
51	14.712	6.441	0.1323
52	16.739	1.989	0.1240
53	19.139	6.723	0.1031
54	14.257	4.117	0.1374
55	13.200	0.975	0.1402
56	12.644	5.029	0.1427
57	16.251	6.320	0.1209
58	14.783	1.753	0.1300
59	3.881	6.576	0.1501
60	9.327	2.484	0.1501
61	9.759	1.770	0.1519
62	1.382	1.935	0.1445
63	19.705	4.709	0.0955
64	15.509	5.306	0.1242
65	18.059	2.520	0.1095
66	17.523	5.451	0.1102
67	11.656	4.933	0.1420
68	18.796	4.983	0.1013
69	7.597	5.789	0.1496
70	4.867	7.198	0.1466
71	14.773	2.776	0.1275
72	3.409	7.206	0.1435
73	17.739	3.066	0.1087
74	14.920	4.735	0.1247
75	5.212	2.830	0.1478

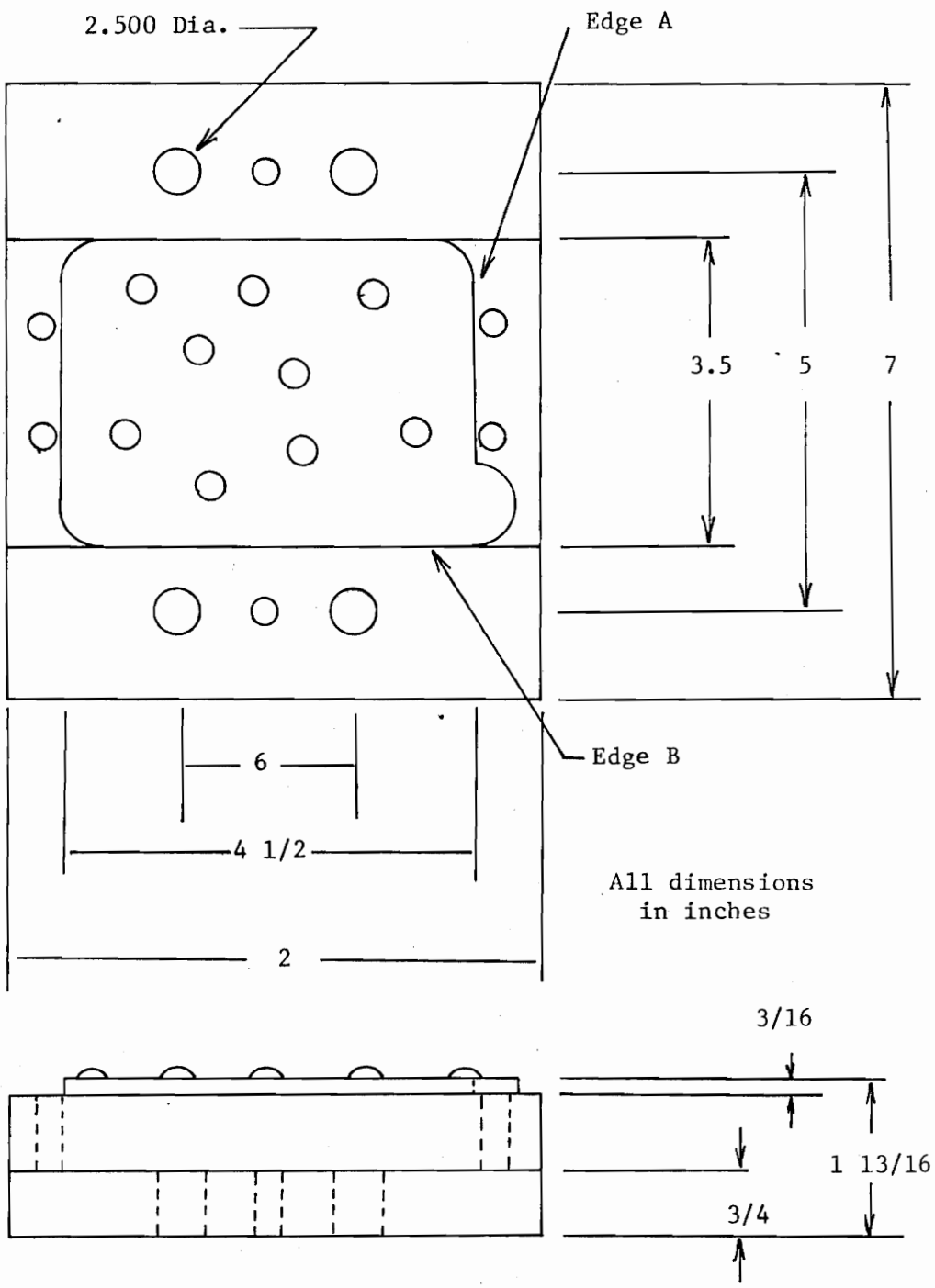

Figure 6A. Small Surface Model

(See Figure 7A)

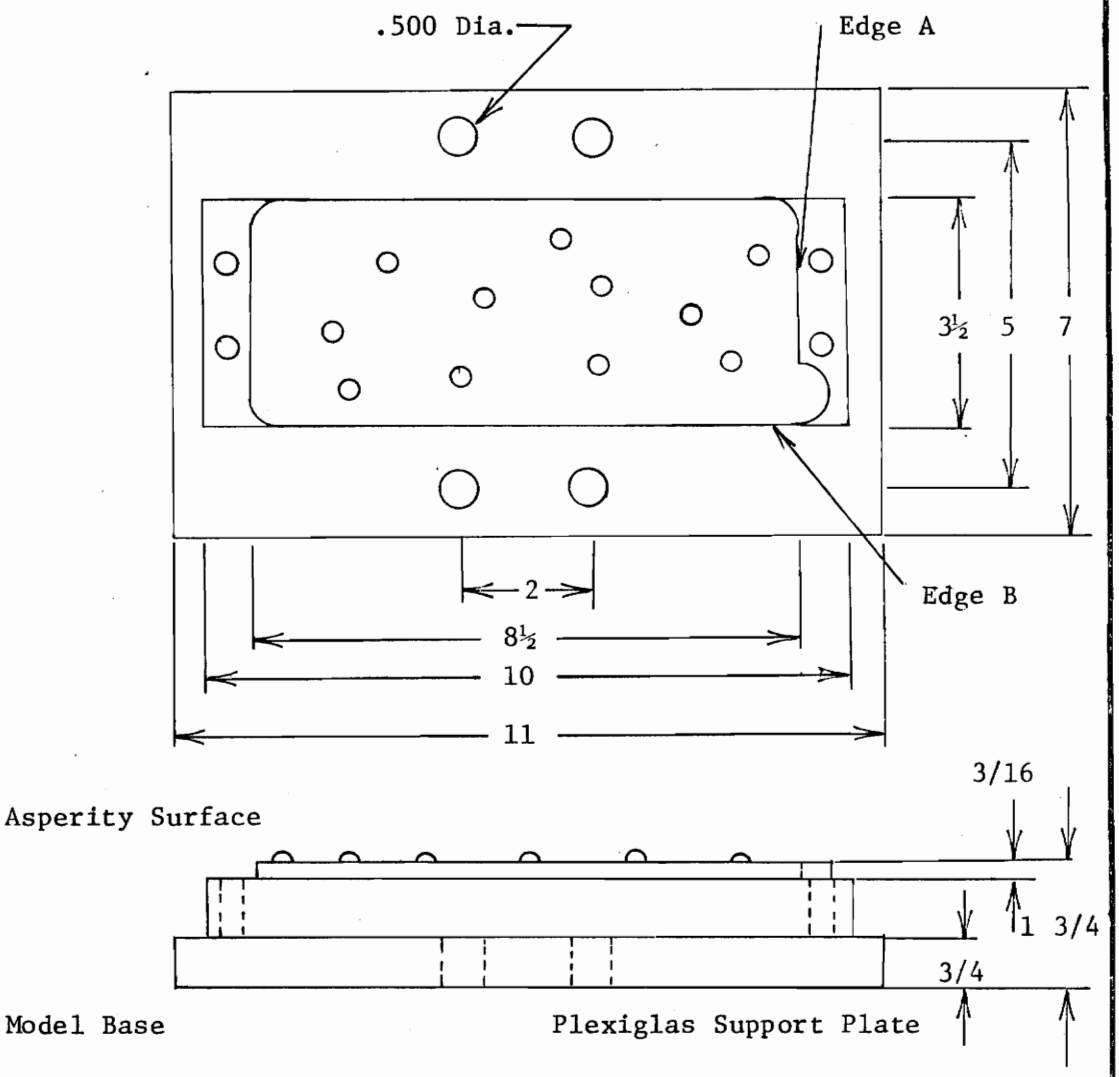

All dimensions in inches

Figure 6B. Large Surface Model
(See Figure 7B for location of Asperities)

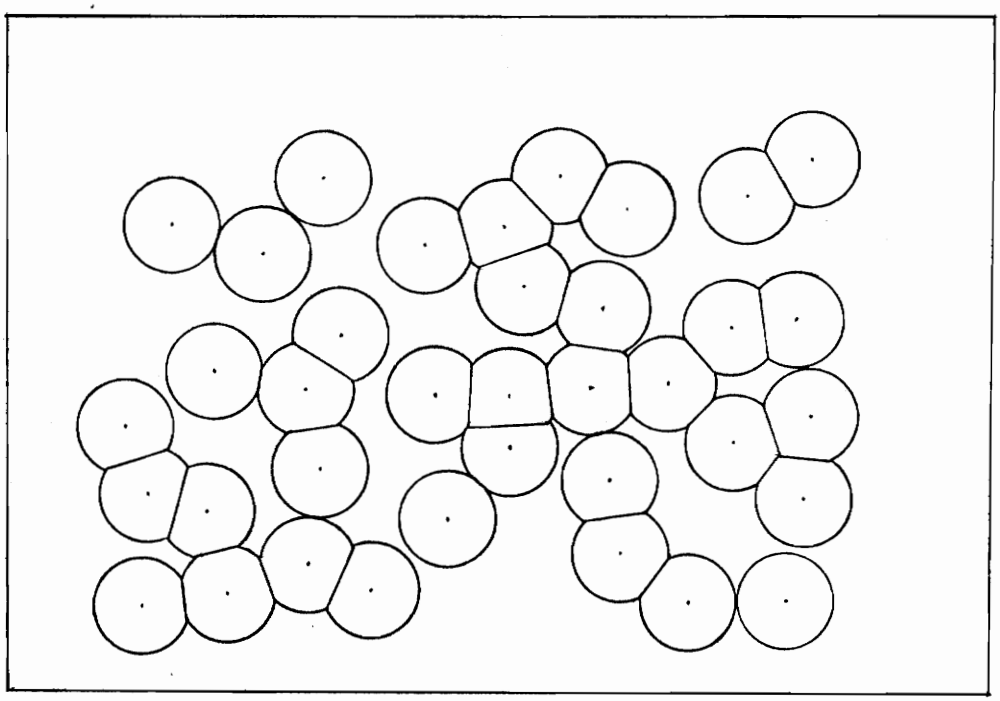

Figure 7A. View of Asperities on the Small Model

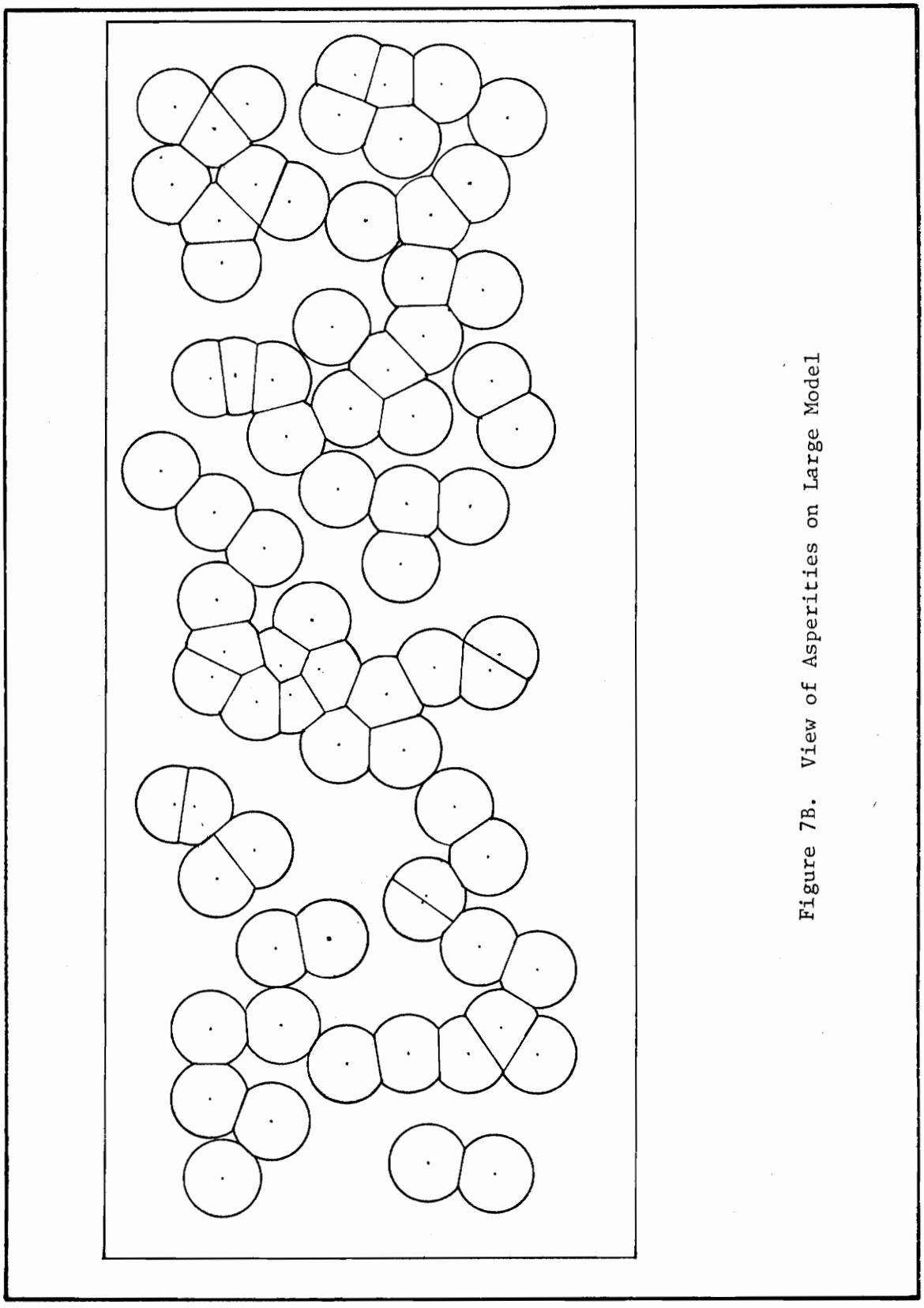

Figure 7B. View of Asperities on Large Model

mately 60-70 minutes the polymerization is complete.

Using polymethyl methacrylate in this form dictated the use of an open mold and a casting technique. Initial attempts at this open mold casting were not successful. Air bubbles entrapped in the casting, the irregular nature of the free surface of the casting, and cracks made the optical clarity of these early specimens unacceptable. These defects arose from the introduction of air bubbles during the mixing process as well as heat generation and shrinkage of the polymer during the curing process. The air bubbles could be eliminated by mixing and pouring the casting solution carefully to reduce the number of bubbles formed and by allowing those bubbles which were formed to rise to the top of the casting and pushing them to the side or raking them from the mold with a stainless steel wire before the casting solution polymerized.

The problem of the irregularity of the free surface was solved by simply changing the position of the mold. In initial casting trials, a mold consisting of spherical cavities machined or pressed into a flat aluminum or magnesium plate was placed flat on the table top. Aluminum blocks were then placed around the mold to provide retaining walls for the casting. With this method the free surface was always opposite the surface containing the asperities, a situation which made observation of the asperities through the model impossible. However, by changing the orientation of the mold, i.e., standing the mold on its end, and placing an optical flat or a commercially available Plexiglas plate opposite the mold surface,

the irregular free surface was placed on one of the edges of the model where it would not interfere with the observation of the contact surface.

Several methods for eliminating the shrinkage defects were mentioned in the manufacturer's literature:

1. Casting the polymer in an autoclave
2. Heat treating the polymer in an oven for periods of up to one week
3. Making the casting in several stages
4. Reducing the size of the casting.

Since the latter two methods were easier to use and did not require additional expenditures or long curing periods, most of the subsequent efforts to eliminate shrinkage problems in the castings involved these two methods.

It was determined that by casting 1 inch x 1 inch x ½ inch models in successive stages, optically acceptable models could be obtained. This technique was adapted by Janka (24) to obtain some of the models used in his work. However, his findings indicated that the modulus of elasticity of the material used in these models was less than that of commercially available polymethyl methacrylate. Furthermore, as a result of his findings, questions were raised regarding the consistency of material properties and the presence of residual stresses in the models.

For these reasons an investigation of the material properties and state of stress of the models was undertaken. As a nondestruc-

tive test for detecting a change in material properties, the indentation hardness test was selected. Although this test is not a direct measure of the modulus of elasticity, the test is sensitive to changes in E and it did not require specially prepared specimens. Indentation hardness tests following ASTM Standard D785 were performed on models which had been made over a period of a half year to one and one half years before the test as well as on a commerical grade of Rohm and Haas Plexiglas plate. Four of the older specimens were tested and found to have values of 68, 68, 70 and 70 Rockwell M. The six month old specimen was 83 Rockwell M and a section of ½ inch thick Rohm and Haas Plexiglas plate measured 105 Rockwell M.

Since polymethyl methacrylate is a photoelastic material, stress fields in this material show up as a pattern of light and dark fringes when a model is placed between crossed polaroid filters.

Observations were made on a number of models including:

1. Multibatch castings
2. Spheres embedded in Klearmount
3. Castings cemented to a Plexiglas plate
4. A specially prepared beam specimen in which a severe bending stress was induced to cause cracking
5. Plexiglas plate with machined holes
6. Hemispheres glued to Plexiglas plates.

No attempt was made to quantitatively analyze the stress patterns observed. However, a qualitative comparison with the beam specimen indicated that there was a moderate degree of residual stress in all

of the castings. Stresses appeared to be largest at any interface where the casting solution polymerized while in contact with previously polymerized material, i.e., the Plexiglas support plate, the embedded spheres, the hemispheres, and previously polymerized sections of the model.

From these observations it was obvious that although the techniques of multi-stage casting and casting in thin sections could eliminate optical defects due to shrinkage, residual stresses were still present. Residual stresses can, of course, be present in real surfaces, but residual stresses of varying magnitudes in the models could influence the results of contact experiments. For this reason it was decided to seek methods of eliminating the residual stresses.

The manufacturer's literature mentions heat treatment as a means of stress relief. However, further study of the properties of polymethyl methacrylate revealed that heating the polymer to the critical temperature relieved only the secondary bonds; the primary bonds remained unaffected. Therefore, the heat treatment would only partially relieve residual casting stresses and could conceivably induce warping.

The literature further revealed that some of the criteria for models used in photoelastic stress analysis were similar to the criteria for the rough surface models: transparency, freedom from residual stress, and no characteristics of excessive creep. Furthermore, the casting procedure required to obtain large epoxy castings used in photoelastic work requires that a careful technique be

employed and closely controlled temperature conditions be maintained for periods of up to two weeks (42).

At this point the results of the model making study were evaluated. Although the investigation was not quantitative, a considerable amount of information and experience with the properties and casting of polymethyl methacrylate was gained. The investigation indicated that a simple model making technique requiring only a few hours was not likely to be developed. It was then decided to purchase models from an outside supplier.

Figure 6 is a sketch of the models ordered from Universal Plastics Inc., a firm specializing in casting polymethyl methacrylate. The model consists of a base with a raised surface containing the asperities. Surfaces A and B were to serve as reference surfaces for aligning and positioning the models in the experimental apparatus. The models obtained from the firm were optically very good. There were no flaws which would interfere with the use of optical techniques to observe contact. However, the models were found to fall short of three important criteria.

Examination of the models between crossed polaroid filters revealed that residual casting stresses were present. The stresses were tensile in the x-y plane and seemed to emanate from along the line of intersection between reference edge A and the model base. As before, no quantitative analysis was undertaken, but it was estimated that the maximum stress was on the order of a few thousand pounds per square inch. Generally, residual stresses in models whose

deformation is being studied is undesirable, but for the purpose of testing this experimental approach, the estimated level of stress was deemed tolerable.

Further examination of the models revealed that five surfaces on each model (including one surface which was intended for use as a reference surface) had been machined and polished. The machining of an unknown amount of material from the reference surface required that the position of this surface relative to the position of the asperities be re-established. This was accomplished with the use of an optical comparator.

Examination of the models on a surface plate with a dial indicator showed that the model surface was bowed (0.010-0.020 inches higher in the center) and that the polished surfaces were wavy and not parallel. Since errors of this nature and magnitude seriously affected the distribution of asperity heights, it was necessary to use the surface plate and dial indicator to determine the height of each asperity on each model. (This was done after the models had been mounted on their Plexiglas support plates in order to compensate for any variations of the thickness of the support plate.)

It has been suggested that the warping of the models resulted from machining a material which contained residual stress. Since this problem poses a serious limitation to the ability to obtain cast models of a known, predetermined geometry, it is important that the problem be overcome. Several suggested means of reducing residual stresses and eliminating the need for machining and

polishing of the models are listed in Recommendations.

D. Mold Fabrication

In order to obtain a smooth surface on the asperities of the models, it was decided to specify a high quality finish on the cavity surfaces of the mold, against which the asperity surfaces would be formed. To reduce nonrandom variations in the surfaces arising from hand operations such as polishing, it was specified that these operations not be used. A final mold specification was accurate location of mold cavities: $\pm$0.001 inch in the x-y plane and $\pm$0.001 inch or better in depth. (Note: after model fabrication the asperity heights may be more accurately measured.)

Initially, the most obvious technique of mold preparation, that of machining the cavities with a ball end mill, was ruled out. Previous experience with milling spherical cavities in steel resulted in tool marks which were considered unacceptable in this work. Therefore other methods of fabricating the mold were sought.

The first method investigated was one which was known to yield excellent surface finishes, i.e., pressing hardened and polished steel balls into a soft metal. Since copper is incompatible with polymethyl methacrylate casting solution, other metals such as aluminum and magnesium were used. Cavities of high surface quality were formed, but there were a number of disadvantages associated with this method. Since the hardened steel balls deformed elastically under the load

required to press them into another surface and after removal of the load there was a certain amount of elastic recovery of the cavity, there was some question about the sphericity of the cavity thus formed. Although this problem could be solved by using a material with a lower modulus of elasticity, there were other more serious disadvantages associated with this method. Accurate positioning of the cavity would be difficult without the use of a special fixture. Furthermore, as a result of plastic flow of metal during the formation of the cavity, an area surrounding the cavity of 2 to 4 times the depth was deformed. Clearly, a minimum separation between cavities must be maintained in order to prevent the formation of one cavity from distorting a neighboring cavity. All cavities could be pressed simultaneously, but very large pressures would be required.

Other trials were made by pressing hardened steel balls into premachined cavities of various shapes in aluminum and magnesium. Little success was achieved with this method. Pressing hardened balls into matching spherical cavities resulted in little improvement in the surface finish of the cavities. After pressing hardened balls into premachined cavities of other shapes, there was usually a flaw in the bottom of the cavity where material flowing down from the sides of the cavity met, but failed to fuse together.

Burnishing a premachined cavity in aluminum with a ball bearing was also attempted, but severe galling resulted.

The use of a Silastic rubber mold material was also investigated. This material is a very viscous, yet pourable fluid, which, when mixed

with a catalyst, cures to form a Silastic rubber. A method of mold preparation involving this technique has been described by Janka (24). Basically, the technique involves accurately positioning an array of spheres approximately one half inch above the bottom of a shallow container. By filling the mold with the catalyzed Silastic rubber until the lower portions of the suspended spheres were immersed to the desired depth, molds with high quality cavity surface finishes may be obtained. However, certain disadvantages are also associated with this method. There is a minimum separation distance between the cavities, which is determined by either the diameter of the spheres used or the clearance required for screw assemblies supporting the spheres. Another disadvantage is that the Silastic rubber adheres to the surface of the spheres and forms a small ridge around the perimeter of each sphere. After the Silastic rubber cured and the array of spheres was removed, the ridge remained. Removing the ridge was accomplished by using a razor blade, but the process was tedious.

Since the molds produced by these techniques failed to meet the specified criteria, the process of machining the molds was re-evaluated. Positioning the cavities to within the specified tolerance is not difficult with a milling machine. The main disadvantage appeared to be tool marks in the machined cavities. However, by using a new tool to machine cavities in aluminum 6031 rather than in steel, a better surface finish was obtained. Although some tool marks were visible in the aluminum, the surface quality of the cavities was

better than that of the cavities in the steel mold.

For fabrication of molds for the model surfaces, the technique of machining cavities in an aluminum plate was selected. Coordinates for the x-y location of each hole were punched onto tape and a numerically controlled milling machine was used to position the cavities to within $\pm$.001 inch of the desired value. A dial indicator was used to enable the machinist to machine the cavity to within $\pm$.0005 inch of the specified depth.

E. Experimental Apparatus

In order to observe the contact between macroscopic models, it was necessary to design and construct a machine which would perform the following functions:

1. Firmly hold one model over the other for static and sliding contact
2. Allow one model to be positioned in the x-y plane to within $\pm$0.001 inch of a desired position relative to the stationary model
3. Allow vertical motion of one model
4. Allow the application of known loads
5. Allow observation of the contact areas by various optical techniques such as transmittance or reflectance of parallel light
6. Facilitate the collection of the following data:

1. Applied normal load
2. Contact area
3. Friction force
4. Sliding speed
5. Separation distance between the two models.

The first task was that of establishing the design criteria, i.e., the size models to be used, the desired loads, speeds, and the amount of travel in the x, y, and z directions. This was a difficult task since little was known about the size of the models. However, some calculations for the contact of arrays of various diameter polymethyl methacrylate spheres against a flat surface were made. From these calculations it was estimated that 1000 pounds would be a reasonable maximum capacity. The maximum size of the models was conveniently selected to be 3 inches x 4 inches and 3 inches x 8 inches. From this a maximum travel of 8 inches in the y direction and 9 inches in the x direction was established. Since relatively low sliding speeds were desired (on the order of a few inches per minute) determination of exact sliding speeds was not necessary during the initial design.

As shown in Figures 8, 9, and 18 (pg. 110) the device consists of two basic components: an x-y table on which the lower surface model is mounted and an upper model support plate which can move vertically. On each support plate the surface models are mounted over large slots which enable light to pass through the models and allow the contact process to be observed.

The x-y table consists of two plates, one mounted over the

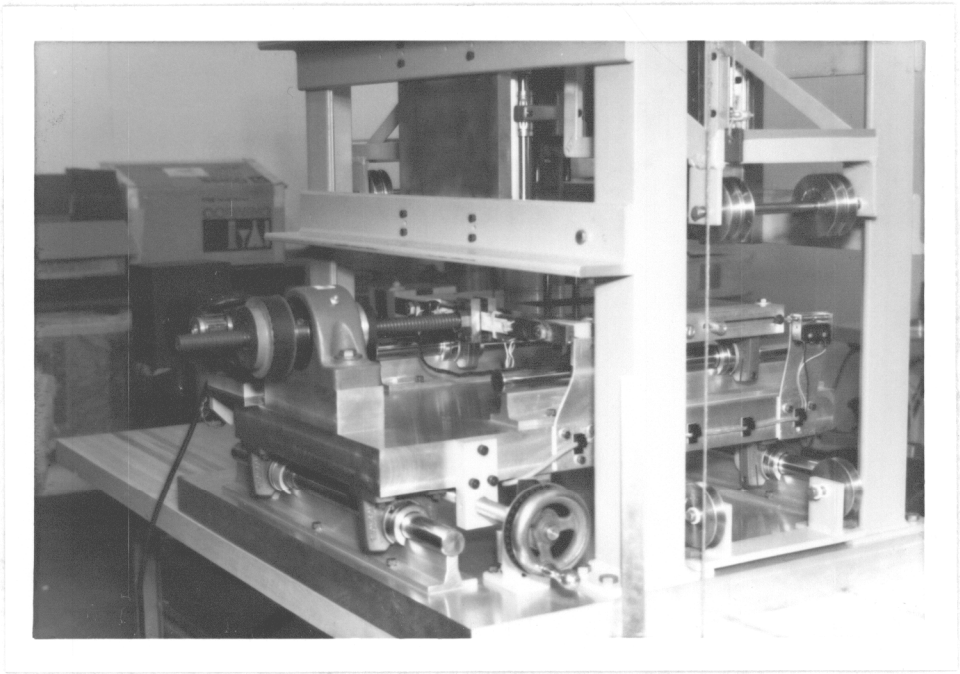

Figure 8. View of Experimental Apparatus

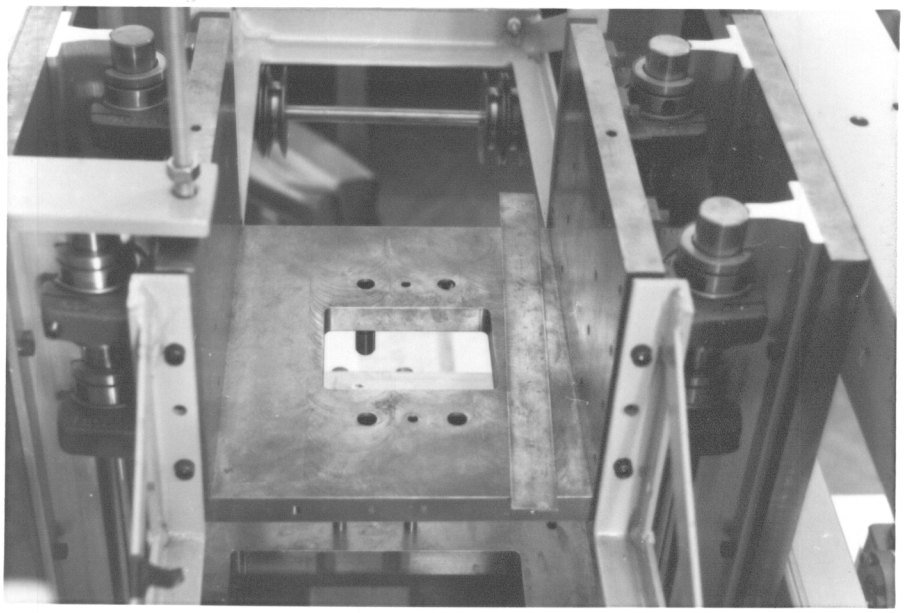

Figure 9. Top View of Upper Model Support Plate

other, which move in perpendicular horizontal directions. Each plate is mounted on four linear ball bushings which travel on two parallel, hardened and ground shafts. Positioning the bottom plate at the desired y-coordinate is achieved by a hand operated positioning screw which has a pitch of 0.100 inches. The model support plate (the upper plate on the x-y table) is positioned at the desired x-coordinate with a ball screw assembly which is driven by an electric motor through a worm gear speed reducer. The electric motor also provides the x-axis motion required for sliding experiments. (Limit switches were provided to prevent the table from being driven off the shafts.) The ball screw is attached to the model support plate by a strain bar to which strain gages are attached. The strain bar assembly enables one to measure friction forces in static and dynamic experiments. The entire x-y table is mounted to a 2¼ inch thick aluminum plate which rests on a laboratory table with a laminated wooden top.

The upper model support plate is attached to eight linear ball bushings which travel vertically on four accurately aligned (less than $\pm$0.0001 inch total indicator reading) hardened and ground steel shafts. The shafts are securely mounted to a framework of 3 in. x 3 in. x ½ in. steel angle which is also bolted to the aluminum base plate. The top model support plate assembly is counter-weighted at each end with a pulley and cable arrangement. Loads may be applied to the models by removing part or all of the counter weights, by placing weights on the top model support plate assembly, or by

placing weights on a cable and pulley loading system. A camera bracket is provided for facilitating the use of a 35-mm camera to record contact areas.

The experimental device has also been described by Janka (24) who made several important contributions to the design of the device, supervised its construction, and conducted a number of performance tests. The experimental device was used for a study by Janka (24), but was not used in this study.

(See Appendix 2 for a description of the operation of the device.)

F. Description of a Computer Program for Multiple Elastic Contact

The objective of the theoretical approach was to develop a computer program to predict the elastic contact behavior of two macroscopic models of known geometry. Information regarding the size and location of the areas of contact as well as the load and pressure on each contact area was desired. The problem was divided into two parts. The first part concerned locating the points of contact while the second part dealt with calculating the contact parameters at each contact area.

Predicting the points of contact between two surfaces with a known, regular geometry is a relatively straightforward process. The surfaces used in this work may be idealized as two-dimensional arrays of spheres. When these two arrays are brought together, con-

tact will occur at the points of the second, third, fourth, fifth, etc. least separation.

In order to find these points of least separation for a given orientation of the surfaces, the program considers the possibility of contact between each sphere (asperity) in the upper surface with each sphere (asperity) in the lower surface. Initially, the reference planes of each surface are assumed to be sufficiently far apart that contact does not occur. Contact between two asperities is possible only if they are within a certain radial distance (measured in the x-y plane) of each other. For all possible contact pairs, the minimum vertical separation is calculated. The thirty-seven smallest separations are stored along with the index numbers of the asperity pairs involved.

For a given separation of the reference planes, the points of contact may be determined by subtracting the difference between the initial and given separation of the reference planes from the minimum vertical separations of the asperity pairs determined previously. Contact occurs where the separation of the asperities is less than or equal to zero. (See Appendix 5 for sample calculations.)

The problem of calculating contact areas, and pressures is also a straightforward procedure. By assuming that the asperities deform independently (which is justifiable if the contacts are sufficiently far apart), each contact may be idealized as two contacting spheres. This is a special case of the Hertz equations for the contact of elastic bodies.

When multiple contact is considered, the problem of determining the distribution of the total load and area of contact arises. For a given load, it is not immediately obvious how many contacts will be involved. This can be determined only through an iterative procedure involving determination of deformations and the number of points of contact for the various deformations.

A better method is to assume that the approach (separation of reference planes) of the surfaces is the independent variable. For a given approach the number and location of the contact areas may be obtained using the results of the first part of the program. The amount of "negative separation" or "overlap" at each contact point may be substituted into the Hertz equations to obtain the load and area of each contact. From these results plots of the total area and total load as functions of the approach may be obtained. These plots may be combined to yield a contact area vs. load curve from which the contact area for any given load may be obtained.

The Hertz equations, the use of which was described above, were derived for a load applied perpendicularly to the area of contact. This condition is met exactly only for contacting asperities which are perfectly aligned. When the contacting asperities are not perfectly aligned, there is a tangential component of the load acting in conjunction with a component normal to the contact area (See Figure 25). Shoulder to shoulder contact may influence the observed contact areas in three ways:

1. The component of the load acting perpendicular to the

contact area is less than the applied load. Therefore, the area of contact will be less.

2. The projection of the contact area onto the plane of the surface (i.e., the projected contact area) will be smaller than the calculated contact area.
3. The tangential component of the load can affect the contact area.

These effects may be taken into account in the prediction of the calculated and the projected contact areas by:

1. Using the actual decrease in the hypothetical center distance between the contacting asperities instead of the amount of negative separation. (See Figure 26)
2. Determining the angle between the area of contact and the plane of the surfaces in order to calculate the projected area of contact.
3. Noting that according to Mindlin (37) tangential forces do not affect the area of contact between elastically deformed bodies.

G. Criterion for the Limit of Elastic Behavior

Normally, the criterion for determining the compressive stress at which the deformation of a body is no longer elastic is the compressive yield strength of the material. Strict adherence to this principle in the use of the Hertz equations dictates that the limit

of applicability is reached as soon as the stress at any point in the contacting bodies exceeds the yield strength of the material. Taking the largest value for the elastic limit of polymethyl methacrylate reported in reference 22 (2,550 $\frac{N}{cm^2}$ = 3,700 psi) and applying it to the contact of two 2.54 cm (1 inch) diameter spheres, one obtains a maximum elastic load of 2N (approximately ½ pound). This value is surprisingly small.

Furey (1) has found the deformation of 1.27 cm (½ in.) diameter polymer spheres against a rigid flat to be generally elastic for loads up to 145N (32 lb.). Janka has reported that the point of transition from elastic to plastic contact between a 1.35 cm (17/32 in.) diameter polymethyl methacrylate sphere and flat to occur at an average contact pressure of approximately 5,200 $\frac{N}{cm^2}$ (7,500 psi). This corresponded to a load of approximately 300N (65 lb.) For both of these systems the equivalent radius, R_o, is approximately the same as that for two 2.54 cm (1 in.) diameter spheres in contact. Thus, the results are directly applicable to this work. In making the comparison with theoretical and experimental results it becomes evident that the load at which the Hertz pressure exceeds the elastic limit is not the maximum load for which the overall deformation is elastic.

One explanation of this difference is obtained from the nature of the stress distributions involved. Normally, tests of the mechanical properties of materials are performed on specimens of uniform cross-section (at least over the test length) in uniaxial tension or compression. Measures are taken to insure that the stress is uniformly

distributed over the entire cross-section. In the case of spheres in elastic contact the distribution of stress over the contact area is not uniform but varies from zero at the edge to a maximum at the center. Furthermore, the highest stresses occur just below the surface of contact. Thus, as reported by Greenwood and Williamson (35), at the point where stress initially exceeds the elastic limit, the material is restrained from deforming plastically by the surrounding material.

As mentioned previously, the criterion for the onset of plastic deformation used by Greenwood and Williamson (35) was based on the maximum Hertz pressure exceeding a value of 0.6 times the Vickers or Brinell hardness. The plasticity index based on this criterion has been used to predict the nature of contact between metal surfaces and would be a convenient criterion for use with polymethyl methacrylate.

The following properties for polymethyl methacrylate were taken from reference 21:

$E = 2 \times 10^4 \frac{Kg}{cm^2}$ = modulus of elasticity

$H = 22 \frac{Kg}{mm^2}$ = hardness

B = 0.635 cm = equivalent radius for asperities used in this work

Substituting into the following equation from Greenwood and Williamson (35):

$$Wp = B \left\{\frac{H}{E_o}\right\}^2$$

Wp = 0.021 cm = critical value of elastic displacement

This corresponds to a load of 380N (85 lb.), which is somewhat larger than the value determined experimentally by Janka (24).

An analytical approach to the problem of determining the range of applicability of the Hertz equations could be quite difficult. However, Hardy, et al. (43) have used a finite element technique to obtain a solution to the problem of the indentation of an elasto-plastic half-space by a rigid sphere. Some of their results are relevant to the problem of determining the range of applicability of the Hertz equations.

The range of loads considered by Hardy, et al. (43) ranged from the maximum elastic load to one hundred times this value. The threshold of plastic deformation, based on the von Mises criterion, was found to be

$$p_o = 2.76\ (\tau_{yp})$$

where p_o = maximum Hertz pressure evaluated at the threshold of plasticity

τ_{yp} = shear yield stress

Over this range of load various parameters were determined including: the area of contact, the approach, stress and pressure distributions over the area of contact, subsurface stress distributions, and a plot showing the progressive yielding of the half-space. Theoretical results were compared with experimental data obtained by Tabor (44) for ball indentation tests and found to be in good agreement. Extrapolated theoretical plots were compared with data for contacting spheres

obtained by Johnson (45) and found to be in good agreement.

The results indicated that at loads higher than that required for the onset of plastic deformation the pressure distribution deviated from the elliptical Hertz distribution. At increased loads the distribution tended toward a rectangular distribution and the maximum pressure increased somewhat. Nevertheless, predictions of the contact area and the approach based on the Hertz equations were accurate up to a load of more than ten times the load at the onset of plastic deformation. At higher loads both the area of contact and the approach were larger than those predicted by the Hertz equations.

Direct application of these results to the problem under consideration is complicated by the viscoelastic behavior of polymethyl methacrylate. As with most other viscoelastic materials at very low stresses the deformation of polymethyl methacrylate is elastic, at intermediate stresses the deformation is viscoelastic, and the deformation is plastic at higher stresses. In the region of viscoelastic deformation the contact parameters are time dependent. Immediately after the application of the load contact parameters are approximately equal to Hertz values, but with increasing time the contact area and approach increase while the maximum pressure decreases.

Viscoelastic behavior is also strain rate dependent. The ultimate compressive strength can vary from 5,500 to 20,700 $\frac{N}{cm^2}$ (8,000 to 30,000 psi) and the compressive yield stress from 2,100 to 9,700 $\frac{N}{cm^2}$ (3,000 to 14,000 psi) as the strain rate increases from 2×10^{-4} to 760 $\frac{in}{in}$/sec (46).

In order to use the results obtained by Hardy, et al. (43), the magnitude of the strain rate must be determined or estimated. It is assumed that the strain rate will be on the order of 10^{-2} $\frac{in}{in}$/sec. From reference 46 the compressive yield stress associated with this strain rate is 3,500 $\frac{N}{cm^2}$ (5,000 psi). For uniaxial tension or compression the shear yield strain is equal to 0.707 τ_{yp}. Substituting this into the expression for the onset of plasticity, one obtains the following yield criterion:

$$p_o^* = 2.76\ (.707\ \tau_{yp})$$

$$= 2.76\ (.707)(3{,}500\ \frac{N}{cm^2})$$

$$p_o^* = 6{,}700\ \frac{N}{cm^2}\ (9{,}800\ psi)$$

The following equation gives the load at the onset of plasticity:

$$N^* = \left\{\frac{3}{2}\ \pi\ p_o^*\right\}^3 \left\{\frac{3}{4}\ \frac{R_o}{E_o}\right\}^2$$

$$N^* = \left\{\frac{3}{2}\ \pi\ 6{,}700\right\}^3 \left\{\frac{3}{4}\ \frac{.25}{2.43 \times 10^5}\right\}^2$$

$$N^* = 19N\ (4.1\ lb.)$$

Based on the previous assumption, 19N (4.1 lb.) is the maximum load for which all the conditions for the application of the Hertz equations are met. However, the work of Hardy, et al. (43) indicates that even though the pressure distribution deviates from Hertz values at higher loads, contact area and approach calculations based on the Hertz equations are accurate up to a load of $10N^*$ or 190N (41 lb.).

If another value of the strain rate had been assumed, then another value for the limit of applicability of the Hertz equations could have been obtained. However, the value obtained indicates the order of magnitude of the range of applicability. To more accurately determine the maximum load between two contacting asperities for which the Hertz equations are valid, a series of experiments with polymethyl methacrylate spheres should be performed.

IV. Results and Discussion of Computer Study

Calculations of contact parameters for the two model surfaces described in the previous section were performed using the computer program shown in Appendix 4. Average properties of polymethyl methacrylate were used. (See Tables IV and V.) Calculations for relative x-displacements of the models ranging from 0.0 to 10.0 cm in 0.1 cm increments were made. The relative y-displacement was not varied but remained constant at 0.0 cm. At each relative position of the models the decrease in approach was incremented from the point of first contact to the onset of plastic deformation in 0.001 cm increments. At each value of the approach the following parameters were determined for each individual contact area:

1. Center coordinates
2. Index numbers of contacting asperities
3. Calculated contact area
4. Projected contact area
5. Load
6. Average Hertz pressure
7. Maximum Hertz pressure
8. Indication of whether or not the elastic limit was exceeded

Also at each value of the approach various individual contact area parameters were summed to obtain the values for the following parameters:

1. Total number of points in contact

TABLE IV

Average Properties of Polymethyl Methacrylate (47)

Specific Gravity	1.18 - 1.19
Refractive Index	1.49 - 1.50
Light Transmission	
"As Received" -	
Parallel	91%
Total	92%
Haze	1%
Tensile Strength	
(1/4 in. specimen - 0.2 in/min)	
Maximum	9,000 - 11,000 psi 6,200 - 7,600 N/cm^2
Rupture	9,000 - 11,000 psi 6,200 - 7,600 N/cm^2
Elongation, Maximum	4.9%
Elongation, Rupture	4.9%
Modulus of Elasticity	400,000 - 450,000 psi 280,000 - 310,000 N/cm^2
Compressive Strength	
(0.2 in/min)	
Maximum	14,000 - 19,000 psi 9,700 - 13,100 N/cm^2
Modulus of Elasticity	400,000 - 450,000 psi 280,000 - 310,000 N/cm^2
Shear Strength	8,000 - 9,500* psi 5,500 - 6,500 N/cm^2
Rockwell Hardness	M-80* to M93*

*This value is somewhat dependent upon the thickness. The value quoted is for a 0.250 inch thick specimen.

TABLE V

INPUT DATA

	ASPERITY PROPERTIES			MATERIAL PROPERTIES		
	NO.	SUMMIT RADIUS (CM)	MAX HEIGHT (CM)	ELASTIC MODULUS (NT/CM2)	POISSONS RATIO	MAX ALLOW. STRESS (NT/CM2)
UPPER MODEL	37	1.270	0.1778	275760.	0.420	7721.
LOWER MODEL	75	1.270	0.1778	275760.	0.420	7721.

THETAU=0.0 RADIANS THETAL=0.0 RADIANS

2. Total calculated area

3. Total projected area

4. Total load

The variance of a number of these contact parameters evaluated at the point at which the elastic limit was exceeded is given in Table VI. The nature of contact is shown to vary from the case of a single pair of contacting asperities dominating contact to the case of multiple asperity contact between eight pairs of asperities. The average number of asperities in contact at the limit of elastic behavior was found to be two. The maximum total load varied from 289 to 1438N while the average total load was 427N. The total contact area varied from 0.0276 to 0.1550 cm^2 with an average of 0.0433 cm^2. This indicates that with the models used the limit of elastic behavior is generally reached before a large number of asperities come into contact. This explains why the average total load and the average total contact areas are nearer the minimum values than the maximum values. Table VI also shows that the slope of the individual contact areas varied from 0.011 to 0.240 with an average of 0.110. The misalignment of contacting asperities caused the difference in the calculated and projected individual contact areas to vary from 0.0 to 2.8% with an average of 0.7%. The difference in the calculated and projected total contact areas varied from 0.0 to 1.8% with an average of 0.3%. This shows that even though the misalignment of the contacting asperities may result in a contact area which is not horizontal, the difference between the calculated contact area and the

TABLE VI

VARIANCE OF CONTACT PARAMETERS
FOR MODEL POSITIONS TESTED

CONTACT PARAMETER	UNITS	MAXIMUM	MINIMUM	AVERAGE
TOTAL LOAD	(NT)	1438.	289.	427.
TOTAL CONTACT AREA	(CM2)	0.1550	0.0276	0.0433
NUMBER OF CONTACT POINTS		8	1	2
APPROACH	(CM)	0.3213	0.2571	0.2836
SLOPE OF CONTACT AREAS		0.240	0.011	0.110
DIFFERENCE IN CALCULATED AND PROJECTED CONTACT AREA	(%)	1.8	0.0	0.3
DIFFERENCE IN CALCULATED AND PROJECTED INDIVIDUAL CONTACT AREAS	(%)	2.8	0.0	0.7

area projected onto the horizontal plane is small. Finally, the approach varied from 0.2571 to 0.3213 cm with an average of 0.2571 cm.

The data given in Tables VIIA, VIIB, and VIIC (Appendix 6) illustrate various contact situations from a single pair of contacting asperities to multiple elastic contact. The most significant data are plotted in Figures 10, 11, and 12.

Figure 10 shows the number of asperities in contact as a function of load for three relative x-displacements of the upper model. The figure shows that the number of contacting asperities increases or remains the same as the load increases. At a relative x-displacement of 1.3 cm there was only one asperity in contact at the onset of plastic flow. At a relative x-displacement of 5.6 cm there were two asperities in contact at a load of 10N and the number increased to eight contacting asperities before the elastic limit was exceeded. The number of contacting asperities at a relative x-displacement of 5.5 cm increased from one to three. For the models studied it is obvious that the number of asperities in contact depends upon the relative position of the models as well as the load.

Figure 11 shows the decrease in approach versus load for the three values of relative x-displacement of the upper model. At a relative x-displacement of 1.3 cm where only a single asperity pair were in contact, the curve is linear with a slope of 0.66. At a relative displacement of 5.5 cm the curve is only approximately linear and has a slope of 0.54. At a relative x-displacement of 5.6 cm the curve is not linear but seems to approach linearity at higher

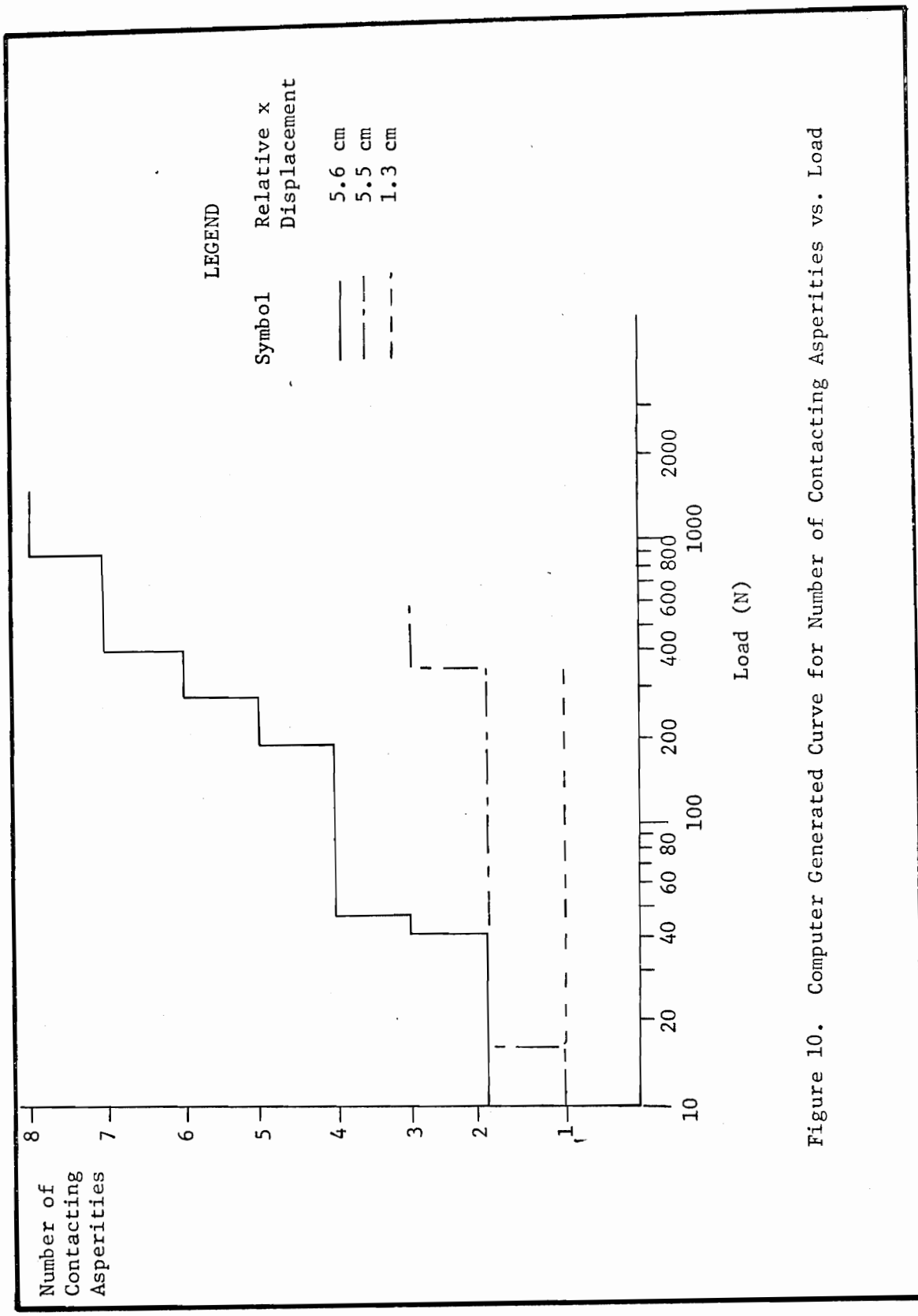

Figure 10. Computer Generated Curve for Number of Contacting Asperities vs. Load

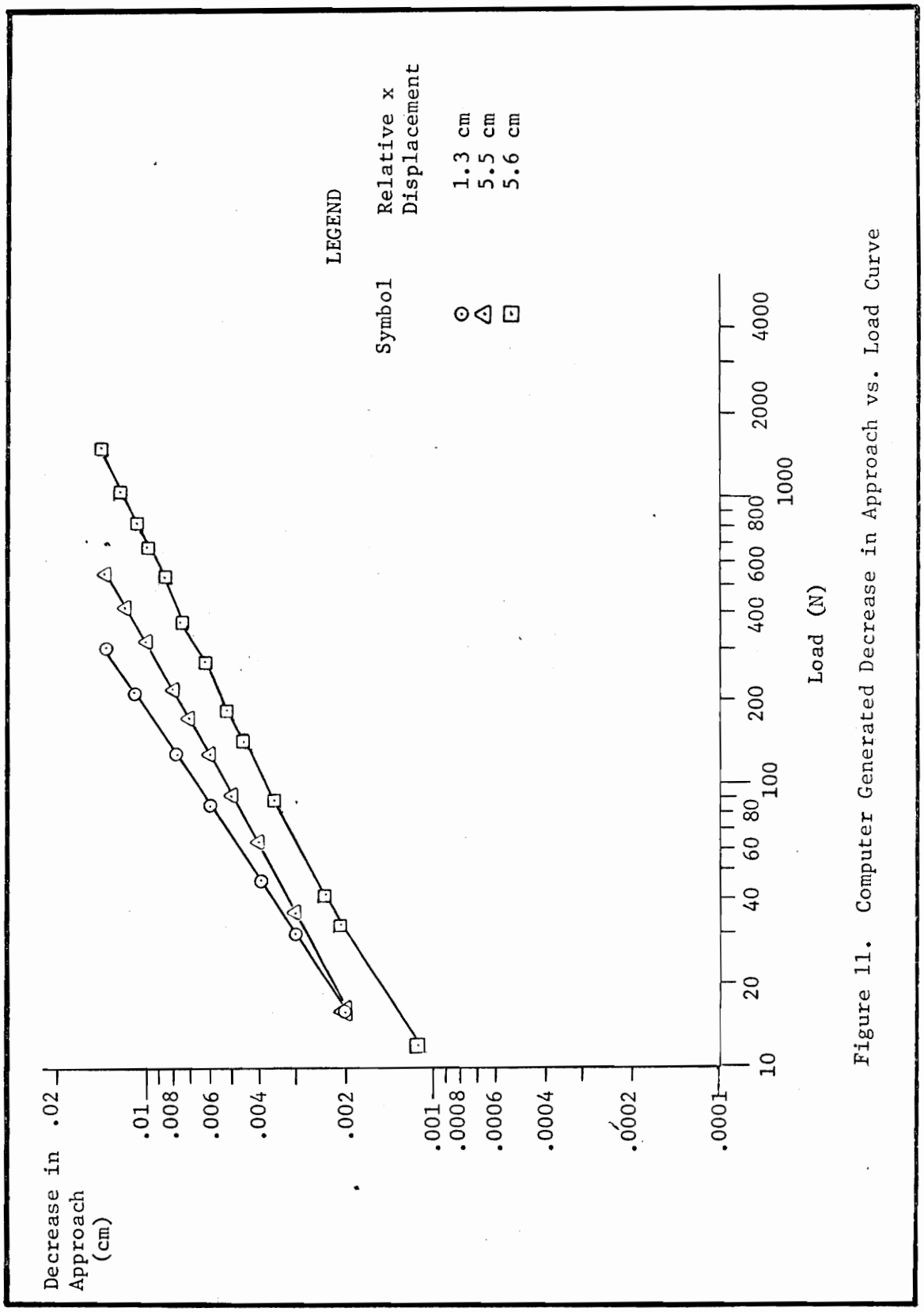

Figure 11. Computer Generated Decrease in Approach vs. Load Curve

loads. The departures from linear behavior and the differences in the slopes are probably caused by newly contacting asperities as they begin to support significant portions of the load. The three curves terminate at the same value of the decrease in approach. This is to be expected since the limit of elastic behavior is reached after the first pair of contacting asperities have deformed by a certain critical amount (0.014 cm). It is also apparent that for a given load, the decrease in approach is less for the case of multi-asperity contact.

Figure 12, a plot of total contact area versus load for each of the three relative x-displacements, shows that the total contact area increases with increasing load. At a relative x-displacement of 1.3 cm, where there is only a single pair of contacting asperities, the curve is linear with a slope of 0.67 as predicted from the Hertz equations. At a relative displacement of 5.5 cm there is a change in slope from 16 to 40N, but at higher loads the curve is linear with a slope of 0.72. At a relative x-displacement of 5.6 cm the curve is approximately linear, but it is not completely linear throughout the entire load range. At those points where newly contacting asperities come into contact and begin to support a significant portion of the load, changes in slope occur. Below loads of 16N the total contact area curves for relative x-displacements of 1.3 cm and 5.5 cm coincide. With higher loads more asperities come into contact at the relative x-displacement of 5.5 cm and the two curves separate. The most interesting aspect of the three curves is that they show that with the

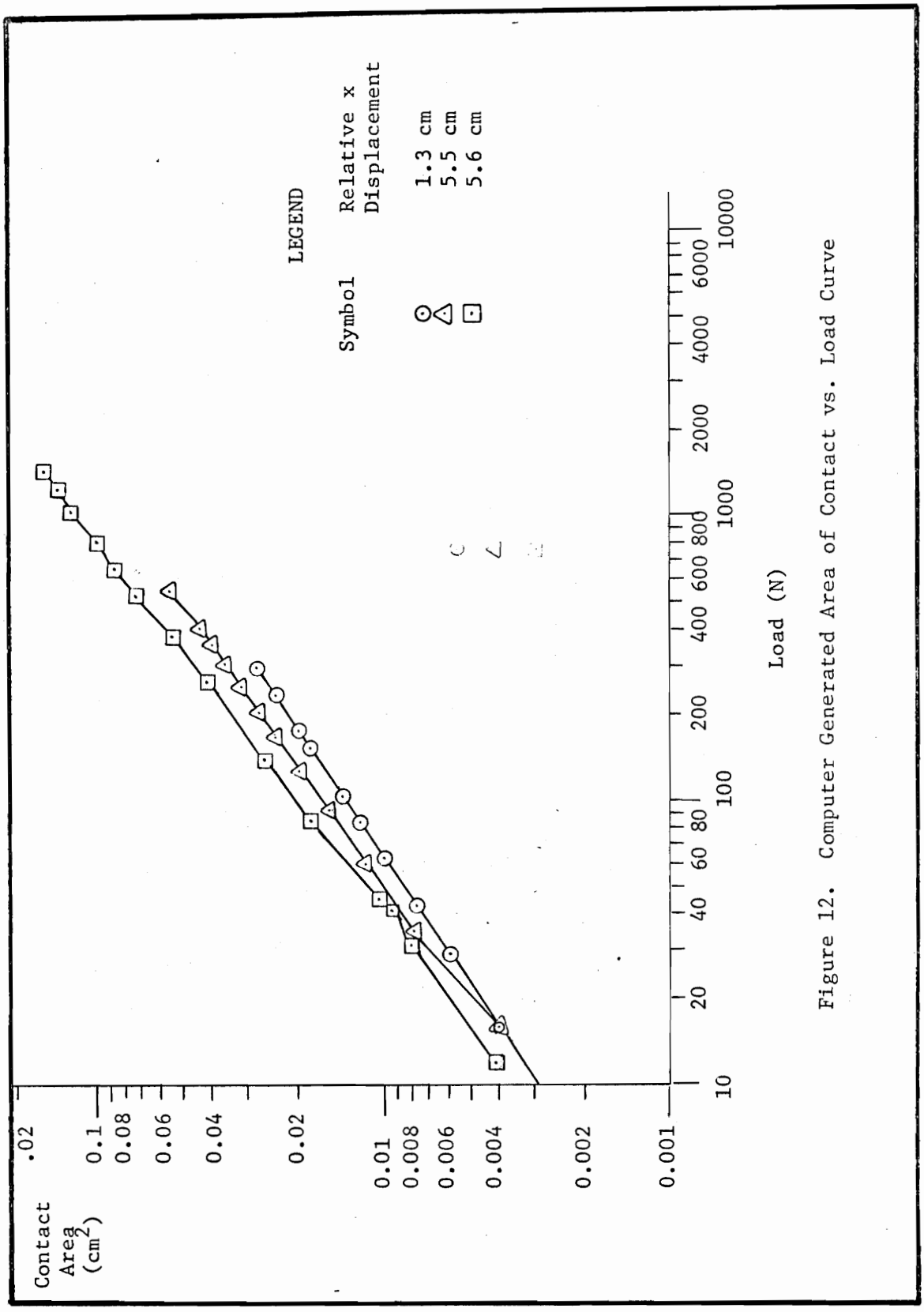

Figure 12. Computer Generated Area of Contact vs. Load Curve

models used in this study for a given load the total area of contact can be different for various relative positions of the upper model. The total area of contact depends upon the number of contacting asperities as well as the load. The contact area for a given load increases as the number of contacting asperities increases.

Using material properties of polymethyl methacrylate taken from reference 21, the Greenwood and Williamson plasticity index for the models used in this study was found to be 0.92. This value indicates that the deformation behavior of the models is in the transition region between surfaces which deform completely elastically and those which deform completely plastically. Calculation of the nominal bearing pressure on the models at the limit of elastic deformation from the following formula

$$P_{nom} = \frac{\text{Total Load}}{(\text{Model length})(\text{Model width})}$$

Shows the average nominal bearing pressure to be 5.50 $\frac{N}{2}$ (8.0 psi) and the maximum nominal bearing pressure to be 18.5 $\frac{N^{cm}}{cm^2}$ (27 psi). These are relatively low bearing pressures.

Figure 28 shows the locations of the contact areas for various loads with a relative x-displacement of the upper model of 5.6 cm. Although all the contacts occur on the right half of the model, no special significance should be placed on this fact because the location of the contact areas was probably determined by the amount of warping of the models. At two locations (8 cm, 8 cm) and (10 cm, 2 cm) contact areas are very close together. At both of these

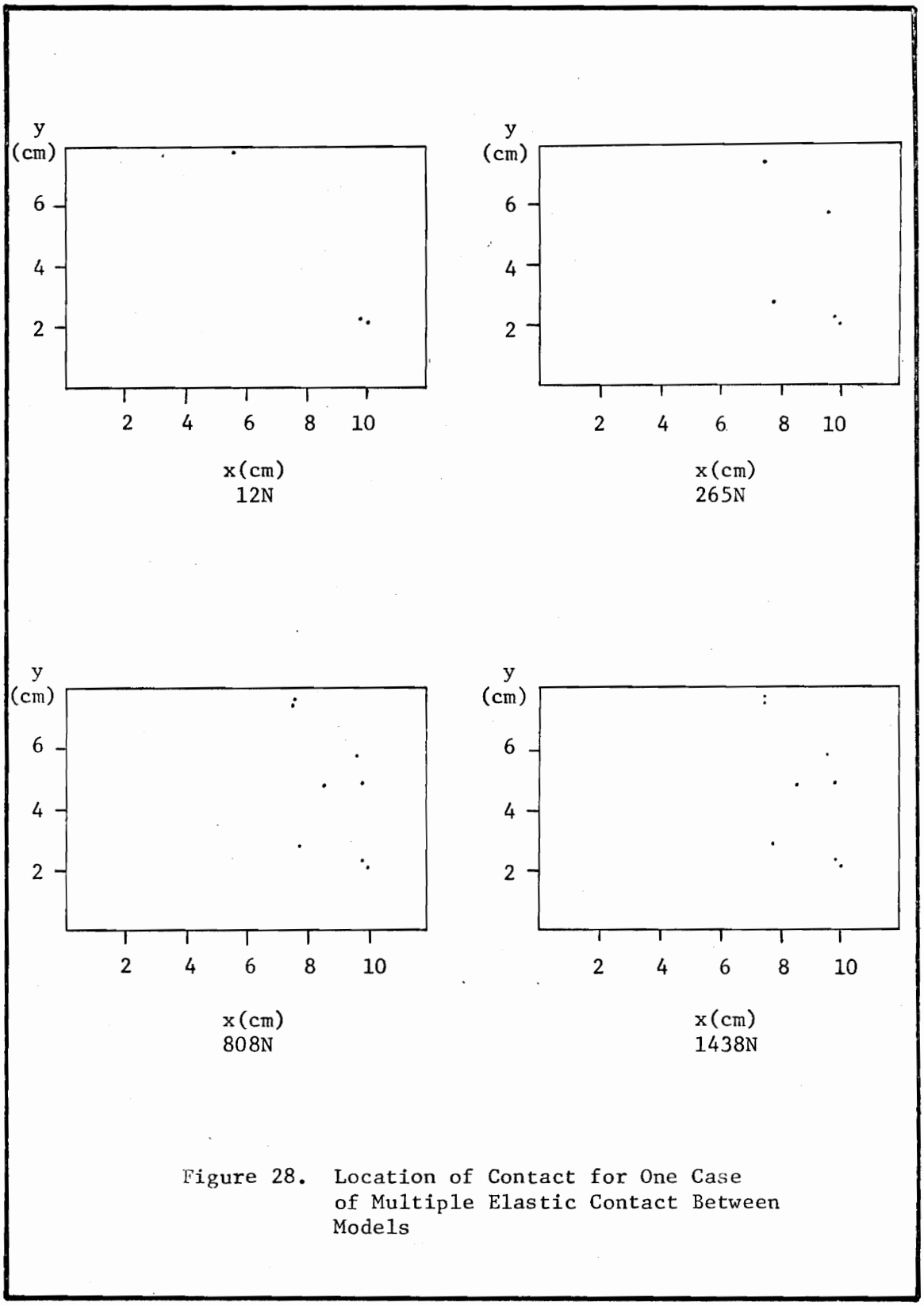

Figure 28. Location of Contact for One Case of Multiple Elastic Contact Between Models

locations a single asperity on the upper model contacts two asperities on the lower model. During the manufacture of the mold for the lower model, a machining error was made which resulted in several positions where two asperities were very close together. Due to the complexity of the distribution of the asperities, the error was not detected until after the fabrication of the models. Thus the contact areas which are very close together result from an asperity on the upper model contacting a pair of asperities on the lower model which are very close together.

V. CONCLUSIONS

Model Design

Various constraints which must be met in the design of three-dimensional models of rough surfaces have been determined. A procedure of modifying certain average dimensions of a "scaled-up" real surface to obtain model specifications which conform to the various constraints has been proposed. However, any procedure which produces model specifications meeting the design constraints may be used.

Model Fabrication

A mold design and a method of machining spherical asperity cavities has been developed. Due to complications of residual stresses, it has been found necessary to purchase models from an outside fabricator. Although models obtained so far are not completely satisfactory from the standpoint of the presence of residual stresses, it is felt that resolving this problem requires the use of appropriate casting and curing techniques by the supplier.

Experimental Device

Through the efforts of several persons, a device for solid-solid contact studies has been designed, built, tested and made operable.

Computer Program

A computer program has been developed which predicts elastic contact parameters between surface models of various materials and geometries. Input data required are the mechanical properties and the size and location of asperities. The parameters calculated at each contact area for each value of the approach are:

1. Center coordinates of the contact area
2. Index numbers of asperities in contact
3. Calculated contact area
4. Projected contact area
5. Slope of contact area
6. Load
7. Average Hertz pressure
8. Maximum Hertz pressure
9. Indication of whether or not an elastic limit is exceeded

The parameters for which total values are calculated are:

1. Number of contact points
2. Calculated contact area
3. Projected contact area
4. Load

When calculations are made at several relative x-displacements of the upper model maximum, minimum, and average values of the following contact parameters are determined:

1. Total load

2. Total calculated contact area
3. Number of points in contact
4. Approach
5. Slope of individual contact areas
6. Difference in calculated and projected individual contact area
7. Difference in calculated and projected total contact areas

Elastic contact studies of the models designed in a previous section indicate that for a given load the approach, contact area, and average contact pressure are dependent upon the number of asperities in contact. At a given load the number of asperities in contact depends upon the relative position of the models. The off-center contact of asperities causes projected contact area to differ from the calculated contact area by less than 1%.

VI. RECOMMENDATIONS

Mold Design and Model Fabrication

To help reduce the residual casting stresses, the mold should be redesigned to eliminate the raised face on the model. The new model would then be simply a rectangular block with asperities on one surface. A sketch of the proposed mold is shown in Figure 13. During fabrication of the mold the location of the cavities should be referenced from the reference surfaces. It should be clearly specified that these reference surfaces on the models should not be machined or polished in order that they might be used to position the models in the NSF device. In order to provide points of reference to be used in interpreting photograophs of the models, shallow slots could be machined in the mold as shown in Figure 13.

The problem of residual casting stresses should be discussed with the firm supplying the models to ascertain if it is possible to obtain models with less residual stress.

Machining and polishing of the models should be eliminated if possible. In order to obtain a smooth flat surface opposite the asperity surface without machining, it may be necessary to use the technique of placing a polymethyl methacrylate plate or an optical flat across the top of the mold and standing the mold on one of its edges. A section of the mold opposite this edge, i.e., the "top" edge of the mold, should be removed to provide an opening for filling the mold.

If these recommendations are not successful in producing accept-

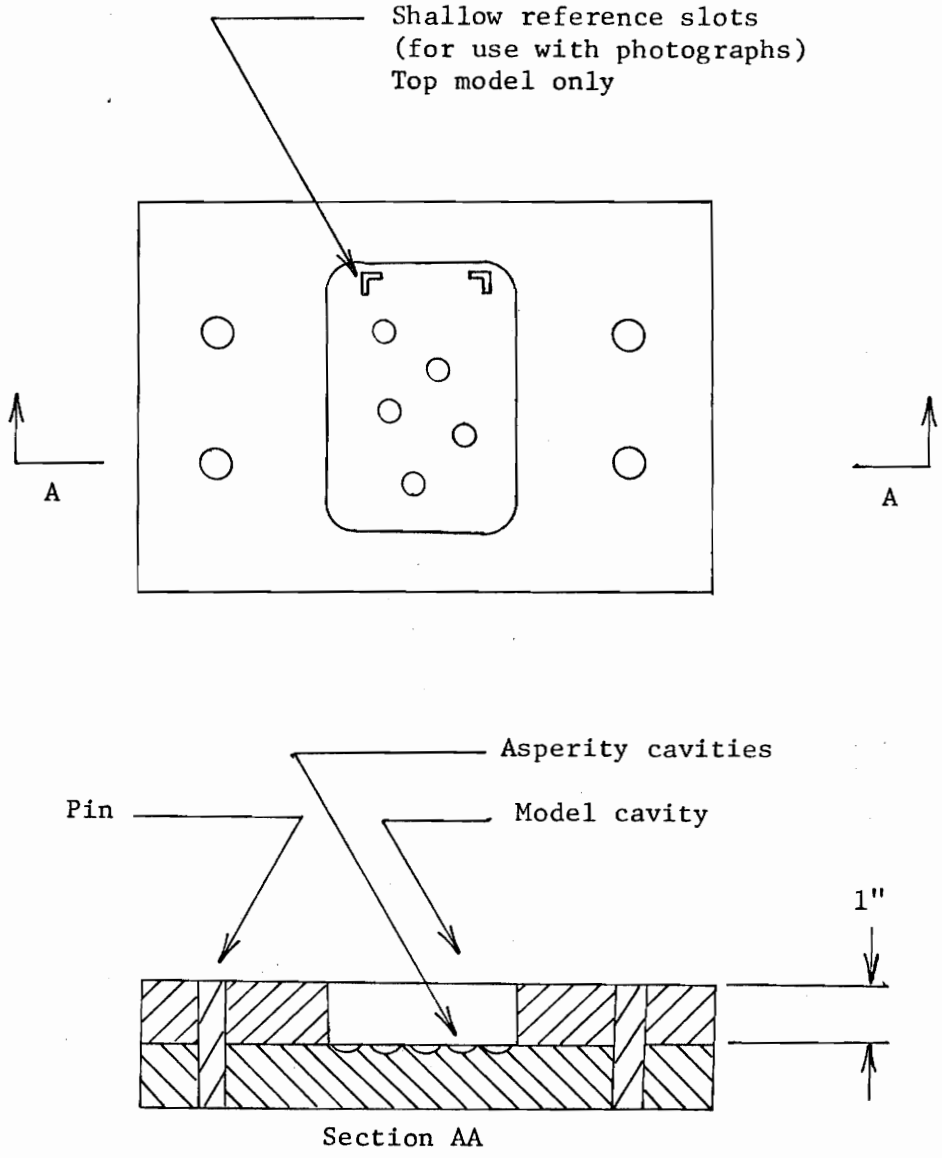

Figure 13. Recommended Mold Design

able models, then consideration should be given to using materials used in photoelastic studies (See reference 42). Although the curing cycle for some of these materials is long and the technique for producing stress free models tedious, experimentalists as well as commercial enterprises have been successful in obtaining models which meet the more stringent criteria of photoelastic studies.

Model Design

In designing subsequent models, the generation of random x-y coordinates and the assignment of asperity heights following a statistical distribution should be computerized. This would be a straightforward procedure.

In expanded theoretical studies, an investigation of the minimum real area represented by the model which is necessary to make statistically significant predictions of the contact parameters of the entire real surface, should be fruitful. One means of achieving this might be to mathematically model two real surfaces, each several square centimeters in area. Once contact parameters for these surfaces have been calculated, parameters for the contact between successively smaller sections from these surfaces could be determined. It should be recognized that the minimum areas required to make statistically significant predictions regarding the contact of real surfaces may be a function of the parameters characterizing those surfaces.

Experimental

Before continuing theoretical studies of solid/solid contact, it is recommended that the results of the computer study be correlated with experimental investigations. Studies of a single pair of contacting hemispheres could determine the load range for which predictions based on the Hertz equations are valid (i.e., the point at which plastic deformation significantly altered the deformation of the contacting asperities), the effect of applied tangential loads on the static contact area, and the effect of misaligned contact between asperities. After the preliminary experiments, experimental studies of the contact of two rough surfaces could be performed.

VII. APPENDIX

APPENDIX 1

An Investigation of the Friction in the Loading System of the Experimental Apparatus

Previous work in which the mechanical advantage of the pulley and cable loading system was determined, showed the mechanical advantage of the system to be less than the theoretical mechanical advantage. Furthermore, it was found that the mechanical advantage of the system was smaller at light loads. These two phenomena were attributed to friction in the pulleys and in the bending of the cables. In the case of static contact, it was found that by carefully adding weights to the loading system, reproducible loads could be placed on the model surfaces. However, it was decided to investigate the effects of friction in the loading system for the case of sliding contact.

In terms of the demands placed upon the loading system, sliding contact differs from static contact in one important aspect. For static contact, after the load has been applied there is no additional movement of the loading system. In dynamic contact the lower model moves horizontally. Since the contacting surfaces are rough, the separation between the surfaces will vary as different asperities come into contact. This causes the top model support assembly (and also the loading system) to move up and down slightly during the sliding process.

The reader is now referred to Figure 14 which is a simplified free body diagram of the loading system. It is the inherent nature

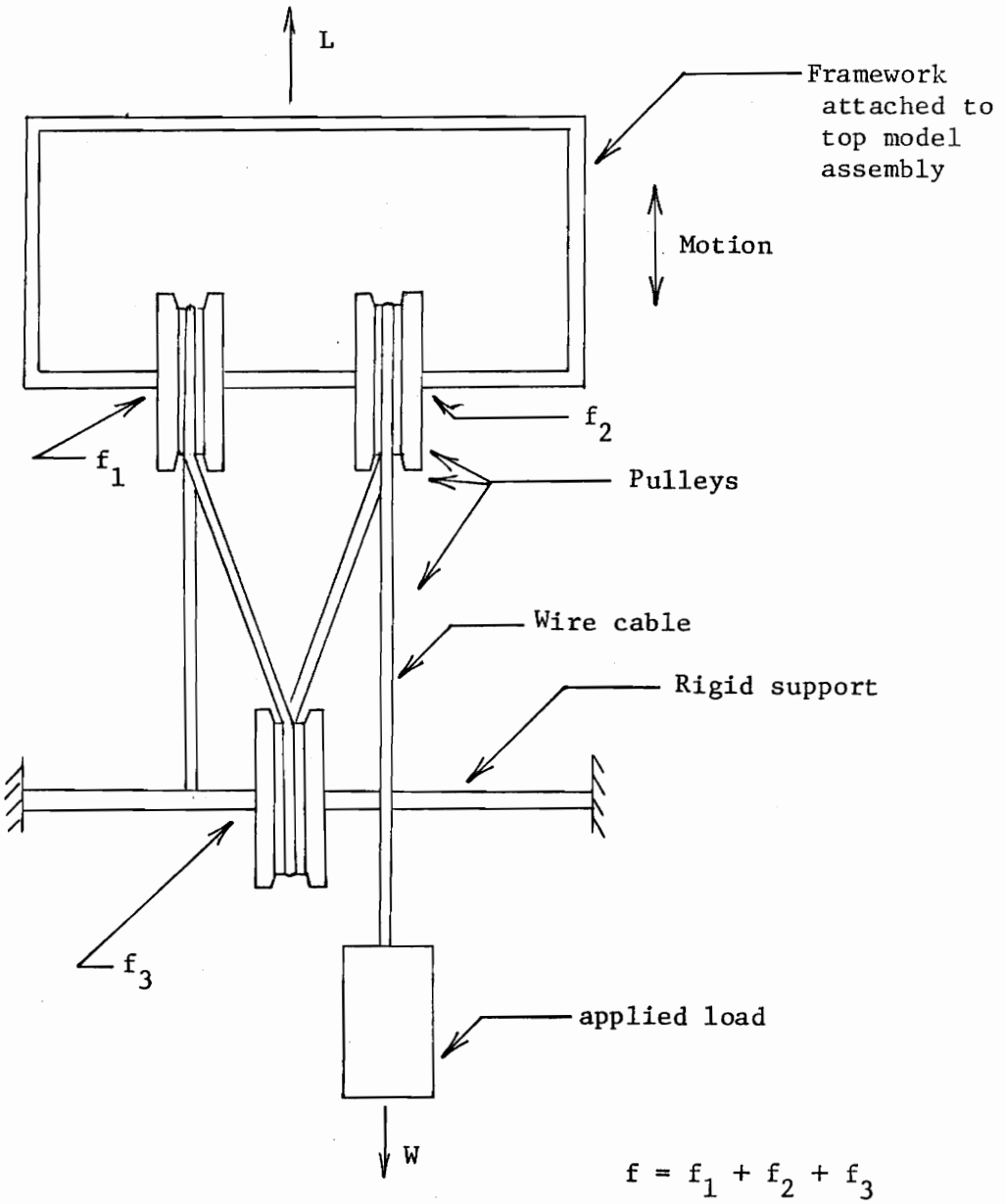

Figure 14. Schematic Diagram of the Pulley Loading System

of friction to act in a direction opposite to motion or impending motion. This fact leads to the following force balance:

$$W \cdot MA = L \pm f$$

where W = applied load

MA = the mechanical advantage of the system

L = load at the model surfaces

f = total frictional resistance of system

The graph of this equation, Figure 15, shows that for any applied load, the load on the models can vary as much as $2 \cdot f$. The exact value of the output load will depend upon the previous loading history of the system. This effect may be reduced by at least two methods. The first is to use a feedback control loop to reduce the error between the desired load and the actual load. The second approach, which was used in this work, is to reduce the magnitude of the frictional forces.

In order to determine the total frictional resistance of the loading system, several tests were performed on the experimental device. Initially, tests were conducted by adding or subtracting weights from the loading system and counter weight system. Since these two systems act in opposition, changing the weight on one would necessitate changing the weight on the other in order to bring the system into balance. By noting these differences some estimates of the friction were obtained. This method indicated that at low loads (less than 50 pounds), the load on the models

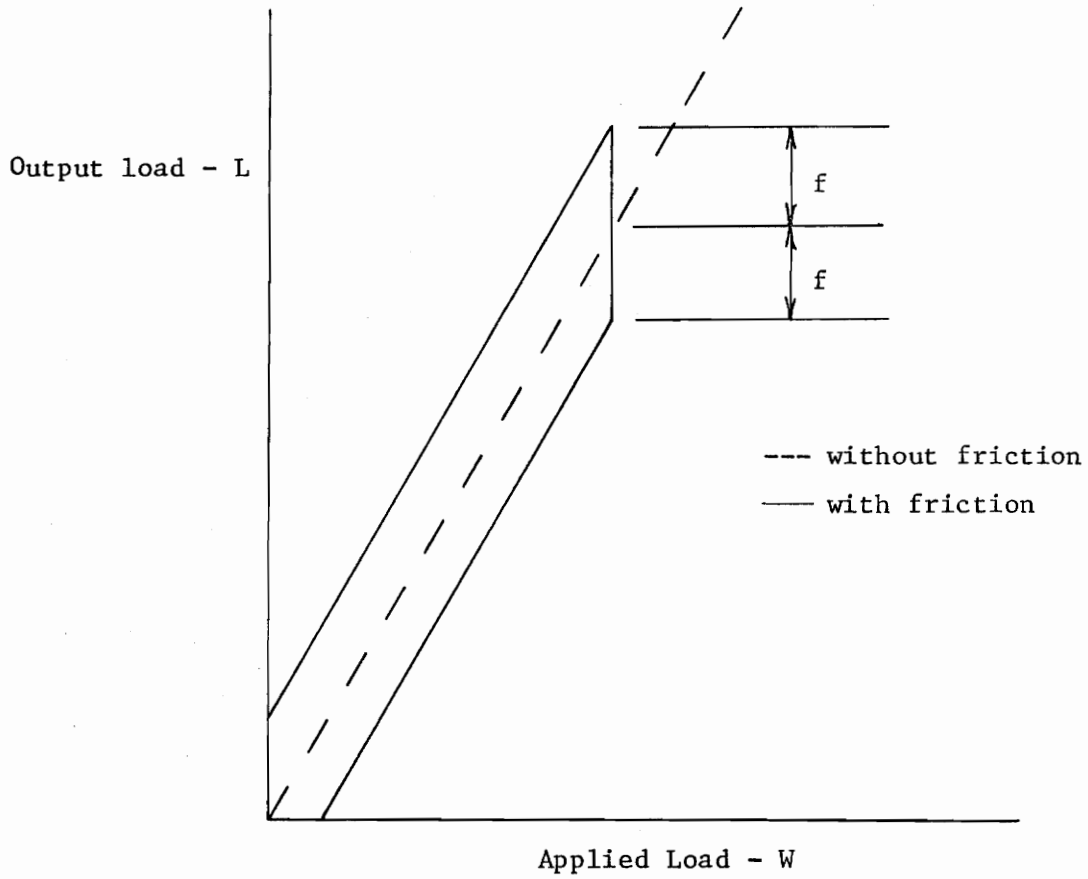

Figure 15. Input-Output Curves for a Loading System with and without Friction

could vary as much as fourteen pounds. Since the friction was rather high, additional tests were made to more accurately determine the total friction and also the contribution of each component of the loading system.

Figure 16 shows a schematic diagram of the apparatus used. A strain bar was mounted on a special fixture and bolted to the lower surface of the top model support plate. A small hydraulic jack was placed under the x-y table with the end of the lifting rod protruding through the viewing slots of the table. The top model support assembly was then lowered until the center of the strain bar rested on the top of the lifting rod of a hydraulic jack. This arrangement allowed the actual load on the models (measured by the strain bar and a strain gage circuit) to be measured as the support plate assembly was moved up and down by the hydraulic jack.

After the strain bar was calibrated, friction tests were performed on the entire loading system, on the system with the loading cables removed (i.e., on the counterweight pulleys and cables plus the linear bearings attached to the model support plate), and on the system with both the loading cables and counterweight cables removed. By comparing results of each of these tests, it was possible to make some determinations of the friction associated with each of the components.

Initial tests revealed that the friction in the linear bearings was larger than expected (on the order of ± 5 pounds). However,

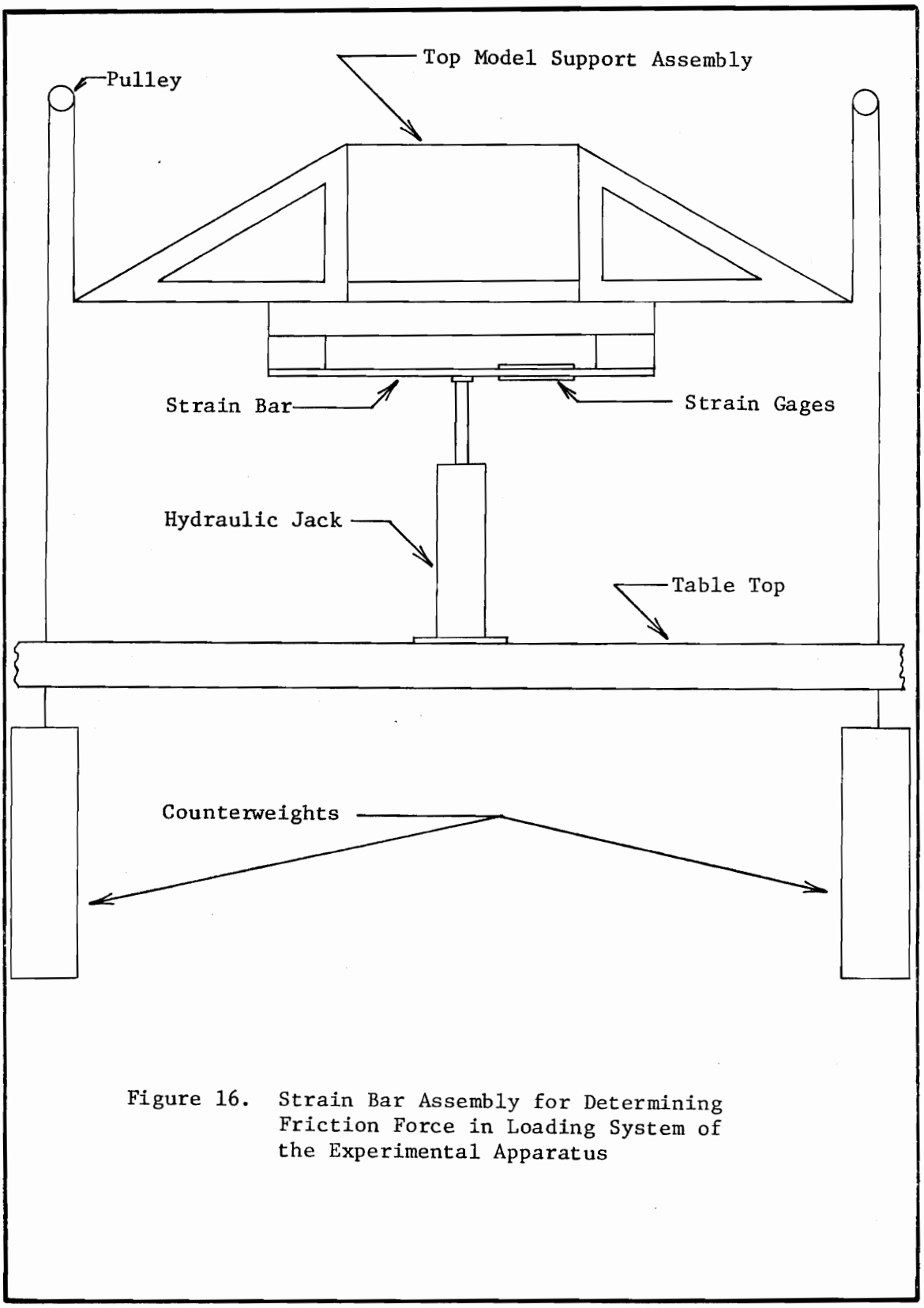

Figure 16. Strain Bar Assembly for Determining Friction Force in Loading System of the Experimental Apparatus

further investigation revealed that set screws in the bearing pillow blocks had been tightened. This caused the bearings to clamp the shafts. Loosening these screws greatly reduced the friction of the bearings.

A number of interesting observations were made during the course of the experiments. The friction of the linear bearings alone was not constant but varied considerably (from $\pm$1 lb. to $\pm$10 lb.). The average friction of the bearings was probably around $\pm$2 lb. Usually, a popping or cracking sound from the bearings was heard when the friction was at a maximum. The friction varied with the speed of the model support assembly. Lowering the assembly more slowly resulted in higher friction. During repeated tests these friction peaks sometimes, but not always, occurred at approximately the same position of the model support assembly. With the counterweight cables attached, the friction ranged from approximately a minimum of $\pm 3\frac{1}{2}$ lb. to $\pm$14 lb. at the friction peaks.

From these tests it was concluded that foreign matter in the linear bearings gave rise to the erratic frictional forces. Furthermore, considerable error could be introduced by using the cable loading system for dynamic experiments.

APPENDIX 2

Operation of Experimental Apparatus

Mounting Models in Device

As designed, both the upper and lower model mounting plates on the experimental friction device have four accurately machined and located alignment pins. The Plexiglas support plates on which the models are mounted (pinned) contain four accurately located holes which match the alignment pins. During the process of attaching the models to these support plates, care must be taken that the reference surfaces on the model are accurately aligned and located with respect to the alignment holes. Mounting the models in the NSF device is accomplished by placing the model and support plate over the alignment pins. Since the upper model will be hanging upside down from the alignment pins in the upper mounting plate of the device, provision has been made for a small screw to hold the upper model in place (see Figures 17 and 18).

Establishment of a Point of Reference Between the Top and Bottom Model Support Plates

In order to determine the relative position of the asperities on the upper model with respect to the asperities of the lower model, it is necessary to establish a point of reference between the top and bottom model support plates. This is accomplished by employing

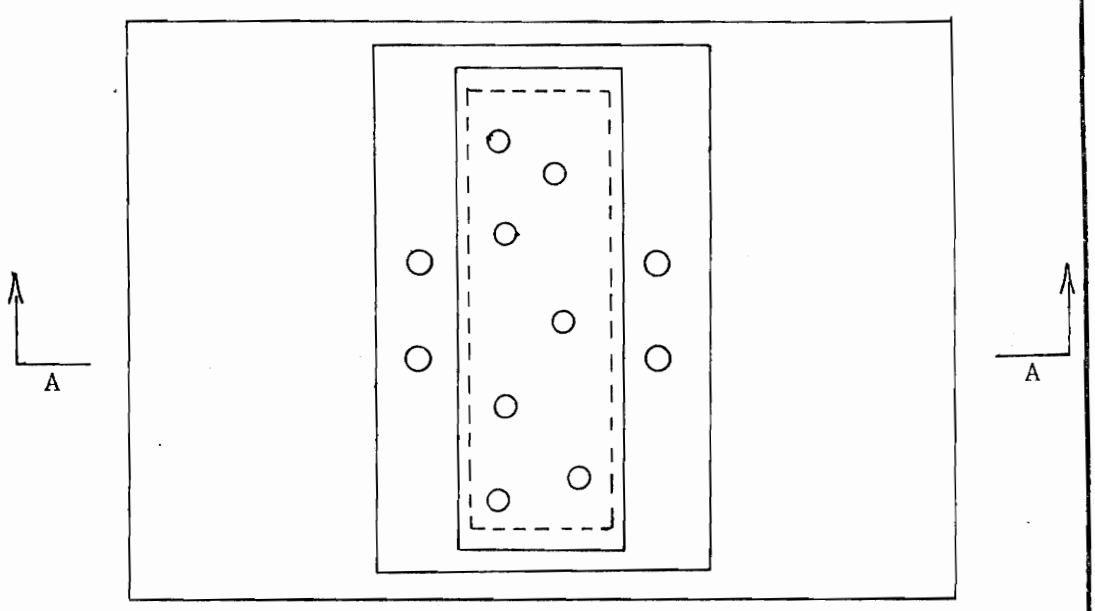

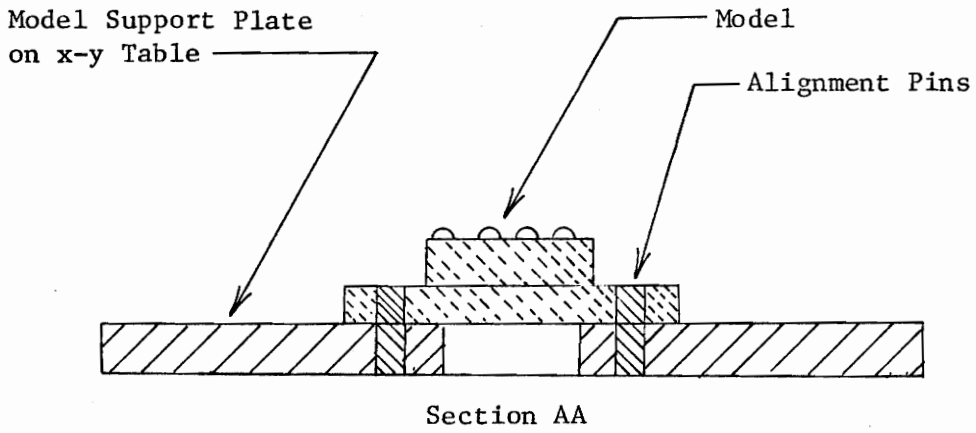

Figure 17. Mounting Models to Experimental Apparatus

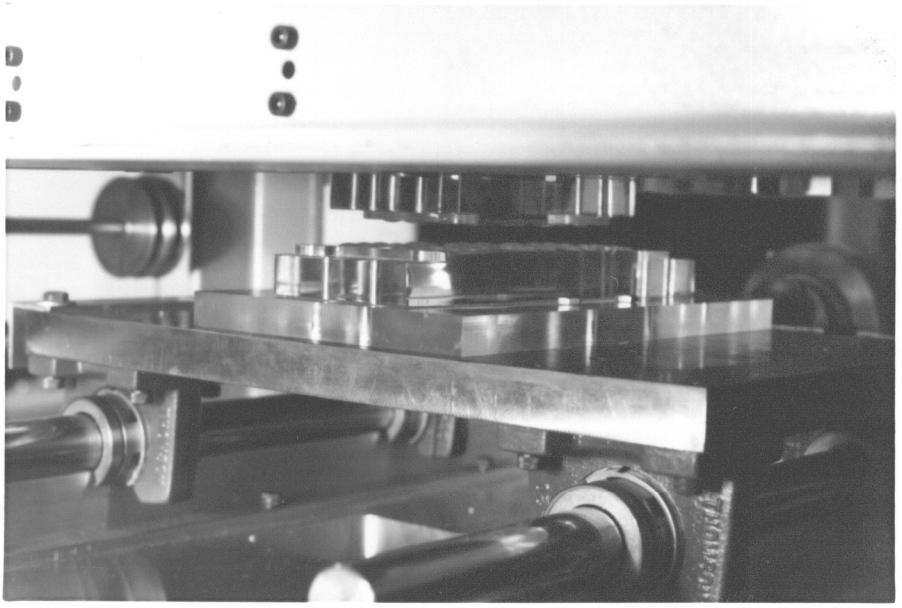

Figure 18. View of Models Mounted in Experimental Apparatus

standard machine shop practices.

Items required for this alignment procedure are a piece of lens cleaning tissue and a machinist's parallel bar approximately 1/4" x 3/4" x 6". The parallel bar is placed on its edge against the alignment pins as shown in Fig. 19. The upper mounting plate is lowered until the separation between it and the lower mounting plate is approximately an inch. The lower mounting plate is moved slowly in the negative y direction until the lens tissue is lightly clamped between the parallel bar and the upper alignment pins. The lens tissue should not be so tightly clamped that it cannot be removed without tearing. The upper mounting plate is raised and the y position of the lower mounting plate noted. By moving the lower table in the negative y direction a distance equal to the sum of the radius of the upper alignment pin, the thickness of the tissue, the thickness of the parallel bar, and the radius of the lower alignment pin, the alignment pins of the upper and lower mounting plates will be aligned in the x-z plane.

By following the same procedure the pins may also be aligned in the y-z plane. If these results are combined, it is possible to align the four pins of the upper mounting plate directly over the pins of the lower mounting plate (unless there was a misalignment of the upper and lower mounting plates during the assembly of the machine). This location of the lower mounting plate may be taken as a point of reference. Since the reference surfaces of both the upper and lower models have been accurately located with respect to

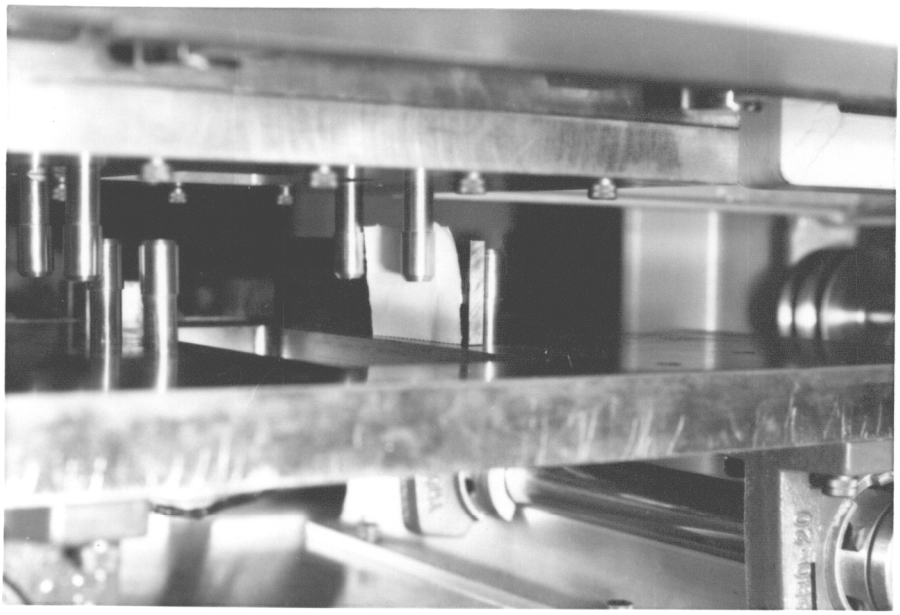

Figure 19. Establishing a Point of Reference Between Alignment Pins

the alignment holes (and therefore the alignment pins), it is possible to determine the relative position of the reference surfaces of the models at any position by determining the displacement of the lower mounting table from the reference position.

As of this writing, stainless steel alignment pins have not been placed on the model support plates of the NSF device because electroplating the support plates as a rust-preventive measure is being considered. Since the plating process would add material to the pins, their diameter would change. This would require that the pins be remachined. Until such time as the pins are placed on the machine an alternate method of attaching and aligning the models in the NSF device must be used.

To secure the models to the mounting plates, 1/2 in. diameter bolts are used. Since the diameter of the mounting holes in the friction device is 7/16 in., there is a sufficient amount of clearance to allow the model to be positioned properly. First, the reference surfaces of the model are aligned parallel to the x and y motion of the x-y table by eye and the bolts are tightened until they are snug but not tight. To more accurately align the reference surfaces with the travel of the table, a dial indicator is used. To align the upper model the dial indicator if firmly clamped to the lower model support plate. The tip of the indicator is placed on the x-reference surface of the model. By turning the hand feed screw on the y axis of the x-y table the dial indicator, one can move the dial indicator in the y-direction across

the x-reference surface. If the x-reference surface is aligned parallel to the y-axis of the table, then the reading of the dial indicator will not change. However, if the x-reference surface is misaligned, the amount of misalignment will be detected by the dial indicator as it moves from one end of the surface to the other. The position of the model is adjusted until there is zero indicator run out. The bolts are tightened after the model is aligned. To align the lower model, a similar procedure is followed with the dial indicator attached to the top model support plate.

After aligning the models with the travel of the x-y table, it is necessary to establish a point of reference from which the relative displacement of the models may be determined. To establish an x-reference position one face of a machinist's parallel bar is placed against the x-reference surface of the lower model as shown in Figure 20. The face of the parallel bar should protrude at least 3/8 in. above the top surface of the model. The tip of a dial indicator which is clamped to the lower support plate is placed behind the parallel bar as shown. With the top model positioned approximately 1/4 in. above the lower model, the lower model is moved in the x-direction. When the parallel bar contacts the x-reference surface of the upper model, the two x-reference surfaces are aligned. Contact is detected by a slight deflection of the dial indicator.

This technique cannot be used to align the y-reference surfaces because these surfaces were machined and polished and conse-

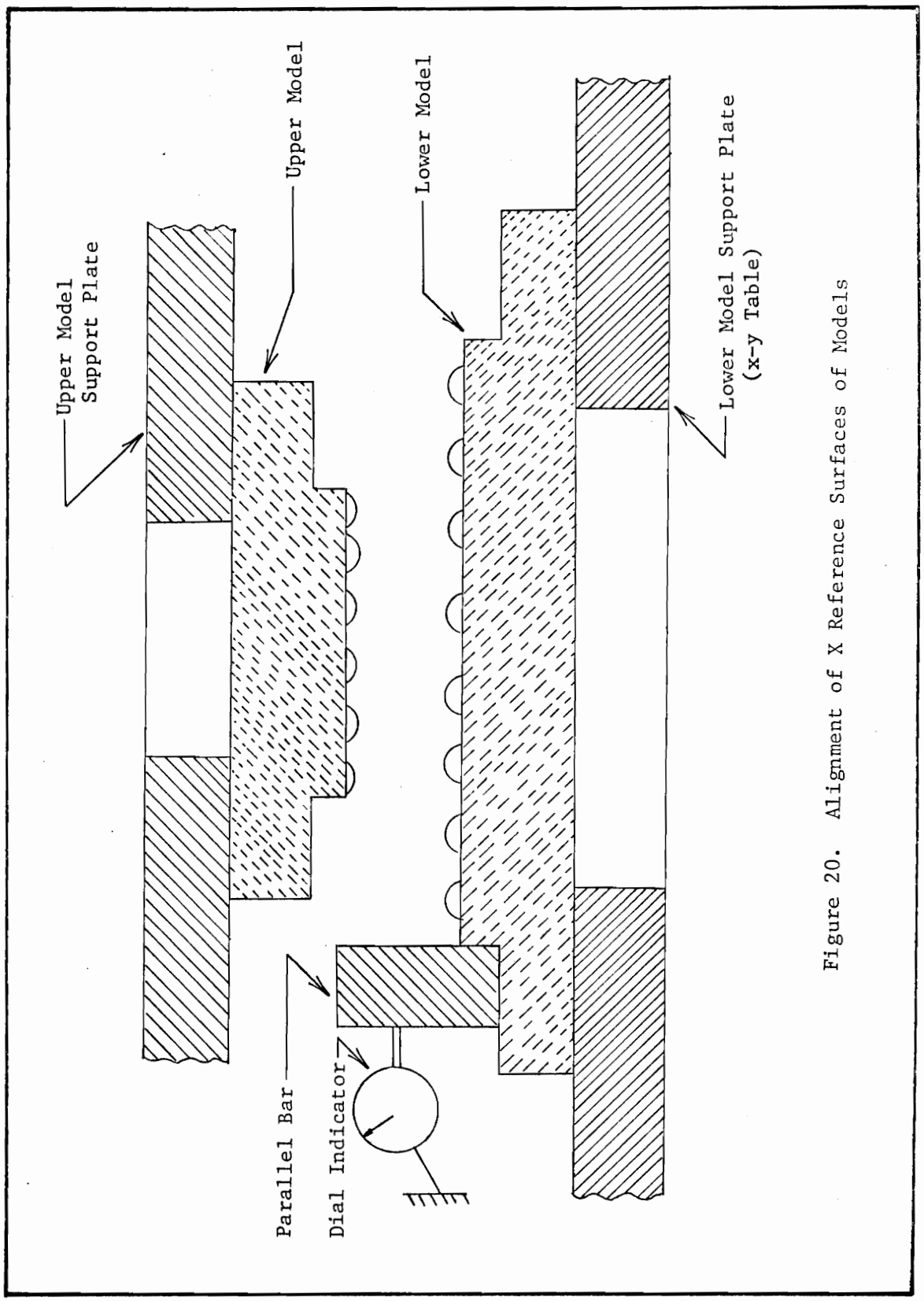

Figure 20. Alignment of X Reference Surfaces of Models

quently are warped. To establish a y-reference point the following technique is suggested. An accurately ground pin is securely held against the y-reference surface of a model directly opposite an asperity. Using an optical comparator, the distance between the edge of the pin and the center of the asperity is determined. The procedure is repeated for the other model. The models are then mounted and aligned in the experimental device as previously described. The pin is securely clamped against the y-reference surface of the lower model directly opposite the asperity which was previously located with respect to the y-reference surface. The upper model is then lowered and the x-y table positioned so that the pin can make contact with the y-reference surface of the upper model directly opposite the asperity previously referenced with the aid of the optical comparator (see Figure 21). Contact between the pin and the y-reference surface of the upper model is determined with the aid of a piece of lens cleaning tissue as described previously. This procedure allows the two warped reference surfaces to be aligned at one point. Since the position of one asperity on each model relative to this point of alignment has been previously determined with the aid of the optical comparator, the relative positions of the other asperities may also be determined.

Alignment of Single Asperity Models

Since the existing single asperity models were obtained by gluing a polymethyl methacrylate hemisphere to a Plexiglas plate with no

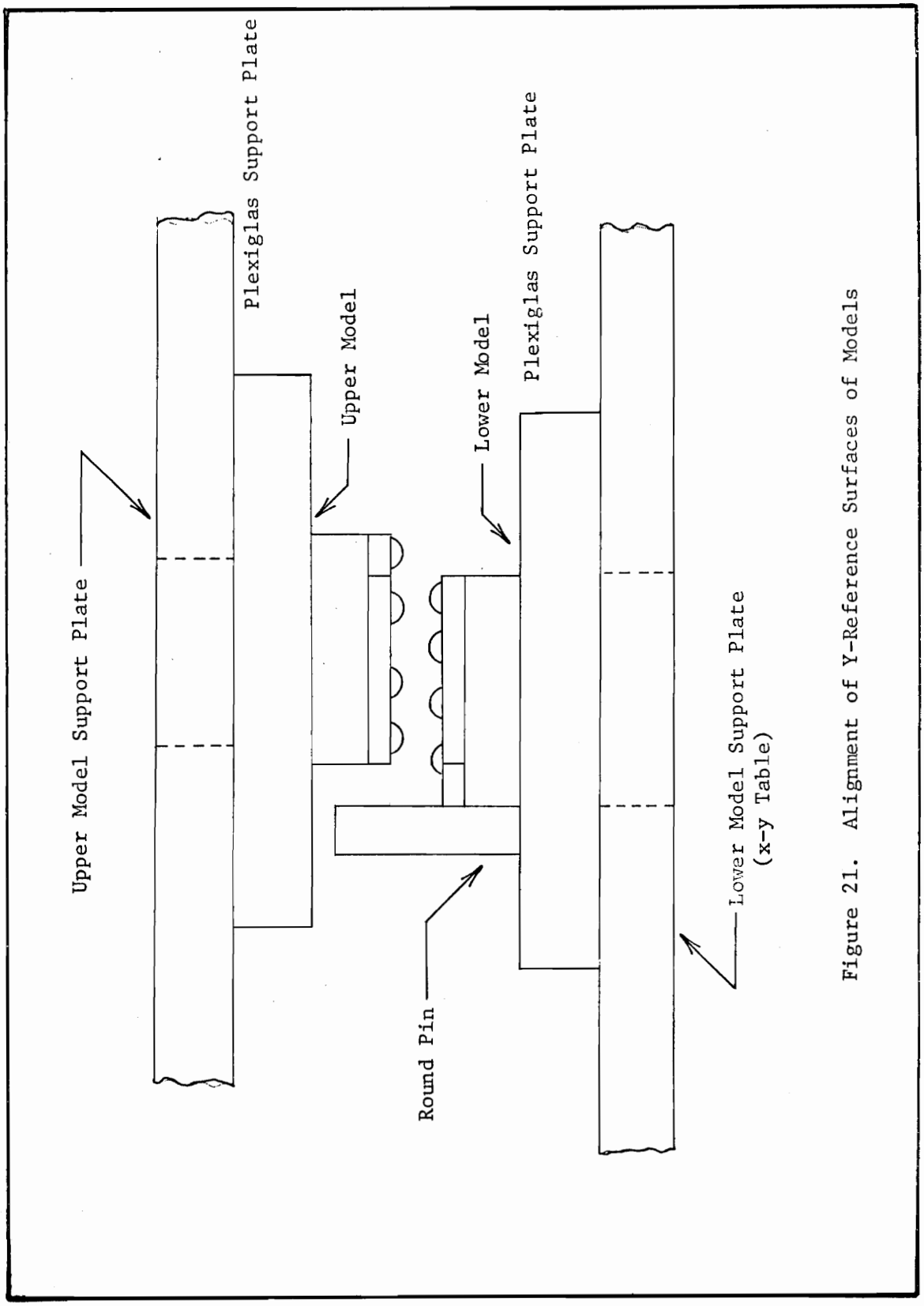

Figure 21. Alignment of Y-Reference Surfaces of Models

special aligning fixtures, the location of the hemispheres cannot be referenced to the edge surfaces. For this reason, a special alignment plate was made for aligning the summits of the single asperity models in the experimental apparatus. The alignment plate is simply a 1/2 inch thick Plexiglas plate with a 3/4 inch diameter hole in the center.

To align the single asperity models in the experimental apparatus one model is first bolted to the lower model support plate (x-y table) with two bolts placed in diagonally opposite holes. Next, the alignment plate is placed over model with the hemispherical asperity protruding into the 3/4 inch alignment hole (see Figure 22). The alignment plate is then bolted to the x-y table and leveled with the aid of a dial indicator. Then the hemispherical asperity of the other single asperity model is placed in the alignment hole, the upper model support plate assembly lowered, and the upper model bolted in place. After the alignment plate is removed, the centers of the asperity summits are aligned.

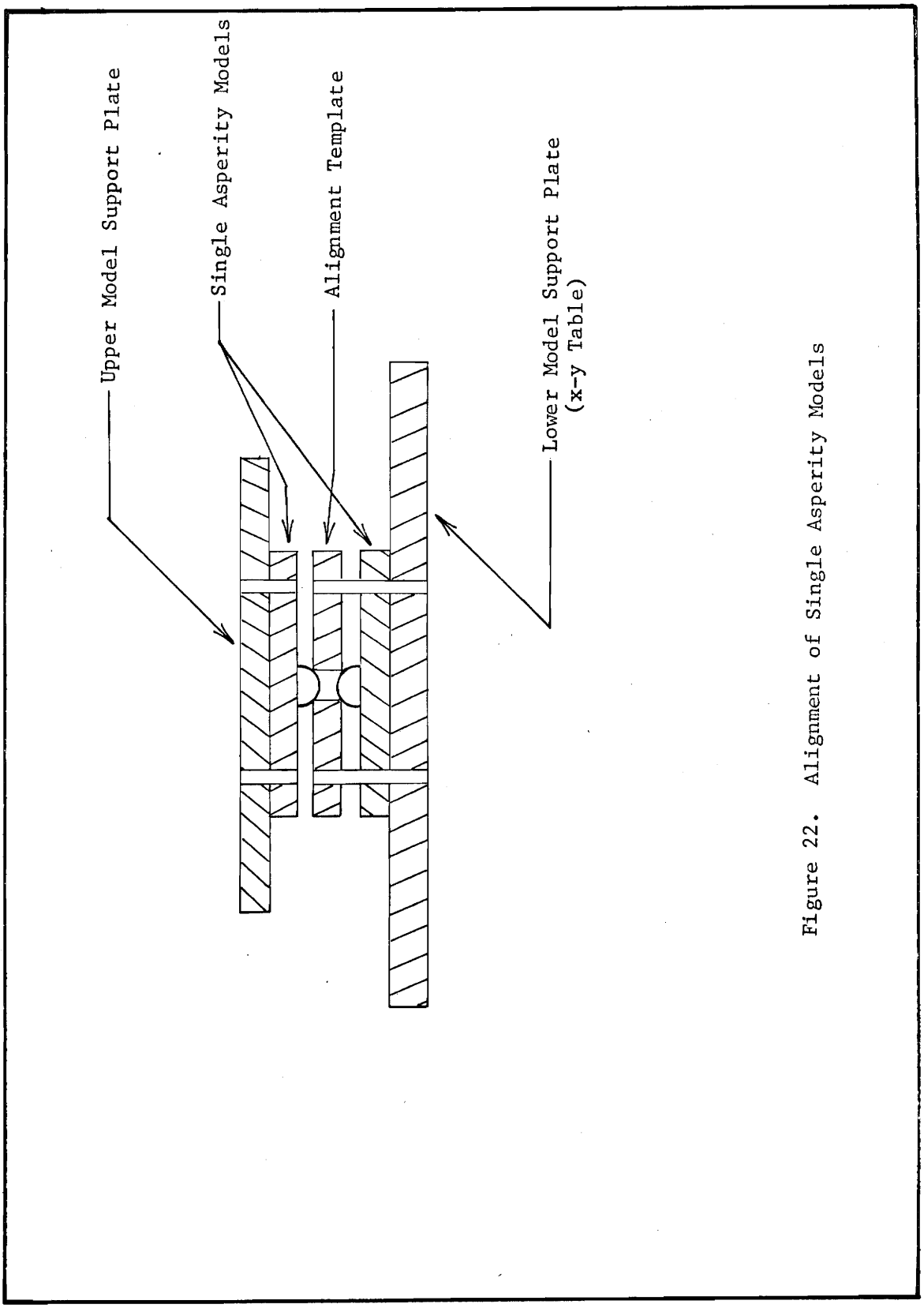

Figure 22. Alignment of Single Asperity Models

APPENDIX 3

Suggested Improvements to the Experimental Apparatus

1. To prevent rusting, the two model support plates and the plates supporting the Thompson bearings in the top support plate assembly should be electroplated. The plates to which the vertical shafts are mounted should be painted. (Considerable time was required to align the vertical shafts and they should not be moved.)
2. The Thompson bearings should be cleaned and proper measures taken to keep them clean (i.e., obtaining a plastic cover for the machine and maintaining a clean environment). (The set screws on the Thompson bearings should never be tightened because they can significantely increase friction.)
3. After the model support plates are electroplated, the alignment pins should be installed.
4. The wooden table top should be reinforced with a steel angle frame.
5. To measure the x-y position of the lower model support plate, two Trav-a-Dials should be purchased and installed. The separation of the models should be measured with a device such as an LVDT. Nuri (42) uses measurements of the approach of two surfaces under load and after the load is removed to determine the amount of plastic deformation present.

6. Due to the friction of the cables and pulleys, it is recommended that the pulley system not be used for low loads. By placing weights on the top model support (and its framework) and by removing the counterweights, loads of up to 300 pounds may be obtained without using the pulley loading system. At loads below 80 pounds it is necessary to use counterweights. To apply the full load in one smooth continuous action, a small hydraulic jack placed under one end of the angle frame (which is attached to the top model support assembly) may be used. The loading mechanism should be redesigned.

```
C                              APPENDIX 4
C
C                    CONTACT PARAMETERS FOR ELASTIC CONTACT
C                     BETWEEN TWO MODELS OF ROUGH SURFACES
C
C              THE PURPOSE OF THIS PROGRAM IS TO CALCULATE VARIOUS
C     CONTACT PARAMETERS FOR STATIC ELASTIC CONTACT BETWEEN TWO MODELS
C     OF ROUGH SURFACES. THE MODELS CONSIST OF SPHERICAL SEGMENTS
C     (WHICH SIMULATE SURFACE ASPERITIES) RANDOMLY LOCATED ON A PLANE.
C     THE SPHERICAL SEGMENTS ON A GIVEN SURFACE EACH HAVE THE SAME
C     RADIUS. THE PROGRAM ACCOUNTS FOR MISALIGNMENT OF THE MODELS IN THE
C     EXPERIMENTAL DEVICE AND THE SLIGHT MISALIGNMENT OF THE MODEL
C     SUPPORT PLATES ON THE EXPERIMENTAL DEVICE. THE PROGRAM ACCEPTS
C     INPUT DATA IN ENGLISH UNITS AND PROVIDES RESULTS IN STANDARD
C     INTERNATIONAL UNITS.
C              THE REQUIRED INPUT DATA ARE
C     NU,RU,ZUMAX,EU,MUU,ELIMTU                AS PER FORMAT 3
C     NL,RL,ZLMAX,EL,MUL,ELIMTL,WIDTHL         AS PER FORMAT 3
C     THETAU, THETAL,XDISPL, YDISPL            AS PER FORMAT 4
C     THE COORDINATES OF THE MOLD FROM WHICH THE MODEL IS MADE
C     XSU(I),YSU(I),ZSU(I)                     AS PER FORMAT 10
C     XSL(I),YSL(I),ZSL(I)                     AS PER FORMAT 10
C
C          ************************  SYMBOLS   ************************
C
C     APPR       =APPROACH OR SEPARATION DISTANCE BETWEEN REFERENCE
C                 SURFACES OF THE UPPER AND LOWER MODELS
C     CAREA      =AREA OF CONTACT BETWEEN TWO ASPERITIES
C     CAREAP     =AREA OF CONTACT BETWEEN TWO ASPERITIES PROJECTED ONTO
C                 THE REFERENCE PLANE OF THE  UPPER MODEL
C     CF         =COSINE OF ANGLE BETWEEN PLANE OF CONTACT AND HORIZONTAL
C                 PLANE
```

```
C      CFL         =FACTOR FOR CONVERTING INCHES TO CENTIMETERS
C      CFP         =FACTOR FOR CONVERTING LB/IN2 TO NT/CM2
C      CLOAD       =NORMAL LOAD BETWEEN TWO CONTACTING ASPERITES
C      CTAVPR      =AVERAGE PRESSURE ON A PARTICULAR CONTACT AREA
C      CTMXPR      =MAXIMUM PRESSURE ON A PARTICULAR CONTACT AREA
C      DAPPR       =INCREMENTAL CHANGE IN THE APPROACH
C      DXDISP      =INCREMENTAL CHANGE OF XDISPL
C      DYDISP      =INCREMENTAL CHANGE OF YDISPL
C      EP          =COMBINED ELASTIC MODULUS
C      EL          =ELASTIC MODULUS FOR MATERIAL OF THE LOWER MODEL
C      ELIMTL      =COMPRESSIVE YIELD STRESS FOR MATERIAL OF LOWER MODEL
C      ELIMTU      =COMPRESSIVE YIELD STRESS FOR MATERIAL OF UPPER MODEL
C      EU          =ELASTIC MODULUS FOR MATERIAL OF THE UPPER MODEL
C      F1          =INDICATES WHETHER OR NOT AN ELASTIC LIMIT IS EXCEEDED
C      MNL(K)      = THE INDEX NUMBER OF THE ASPERITY ON THE LOWER MODEL AT
C                   SEPMIN(K)
C      MNU(K)      =THE INDEX NUMBER OF THE ASPERITY ON THE UPPER MODEL AT
C                   SEPMIN(K)
C      MUL         =POISSONS  RATIO FOR THE MATERIAL OF THE LOWER MODEL
C      MUU         =POISSONS  RATIO FOR THE MATERIAL OF THE UPPER MODEL
C      NAPMAX      =MAXIMUM NUMBER OF INCREMENTAL CHANGES IN APPR
C      NCTPT       = NUMBER OF CONTACT POINTS
C      NL          =NUMBER OF ASPERITIES ON THE LOWER MODEL
C      NU          =NUMBER OF ASPERITIES ON THE UPPER MODEL
C      OFSTMX      =AN UPPER LIMIT FOR THE MAXIMUM MISALIGNMENT (MEASURED
C                   IN THE X-Y PLANE) OF ASPERITY CENTERS AT WHICH CONTACT
C                   MAY TAKE PLACE
C      Q           =CONSTANT DEPENDING ON RU AND RL
C      R           =COMBINED RADIUS
C      RL          =SUMMIT RADIUS OF ASPERITIES ON THE LOWER MODEL
C      RU          =SUMMIT RADIUS OF ASPERITIES ON THE UPPER MODEL
C      SEP         =SEPARATION BETWEEN THE UPPER AND LOWER MODELS AT A
```

```
C                 PARTICULAR POINT
C      SEPMIN(K) =THE K-TH SMALLEST SEPARATION DISTANCE BETWEEN THE UPPER
C                 AND LOWER MODELS
C      SLOPE     =TANGENT OF ANGLE BETWEEN PLANE OF CONTACT AND
C                 HORIZONTAL PLANE
C      TAREA     =TOTAL CALCULATED CONTACT AREA
C      TAREAP    =TOTAL PROJECTED CONTACT AREA
C      THETAL    =ANGLE OF MISALIGNMENT BETWEEN THE X REFERENCE SURFACE
C                 ON THE LOWER MODEL AND THE DIRECTION OF X DISPLACEMENT
C                 OF THE LOWER MODEL ON THE NSF CONTACT DEVICE
C                 (RADIANS)
C      THETAU    =ANGLE OF MISALIGNMENT BETWEEN THE X REFERENCE SURFACE
C                 ON THE UPPER MODEL AND THE DIRECTION OF X DISPLACEMENT
C                 OF THE LOWER MODEL ON THE NSF CONTACT DEVICE
C                 (RADIANS)
C      TLOAD     =TOTAL LOAD
C      W         =DECREASE IN DISTANCE BETWEEN CENTERS OF CONTACTING
C                 ASPERITIES
C      WIDTHL    =WIDTH OF LOWER MODEL
C      WLIMIT    =MAXIMUM ELASTIC LOAD
C      XCA       =X COORDINATE OF THE CENTER OF AN AREA OF CONTACT
C      XDISPL    =RELATIVE DISPLACEMENT IN THE X DIRECTION OF THE UPPER
C                 MODEL WITH RESPECT TO THE LOWER MODEL
C      XLSLOP    =SLOPE OF THE LOWER MODEL SUPPORT PLATE RELATIVE TO THE
C                 DIRECTION OF X DISPLACEMENT OF THE LOWER MODEL SUPPORT
C                 PLATE ON THE NSF CONTACT DEVICE
C      XSL(I)    =X COORDINATE OF THE ASPERITY NUMBER I ON THE LOWER
C                 MODEL
C      XSU(I)    =X COORDINATE OF THE ASPERITY NUMBER I ON THE UPPER
C                 MODEL
C      XUSLOP    =SLOPE OF THE UPPER MODEL SUPPORT PLATE RELATIVE TO THE
C                 DIRECTION OF X DISPLACEMENT OF THE LOWER MODEL SUPPORT
```

```
C                  PLATE ON THE NSF CONTACT DEVICE
C      YCA        =Y COORDINATE OF THE CENTER OF AN AREA OF CONTACT
C      YDISPL     =RELATIVE DISPLACEMENT IN THE Y DIRECTION OF THE UPPER
C                  MODEL WITH RESPECT TO THE LOWER MODEL
C      YLSLOP     =SLOPE OF THE LOWER MODEL SUPPORT PLATE RELATIVE TO THE
C                  DIRECTION OF Y DISPLACEMENT OF THE LOWER MODEL SUPPORT
C                  PLATE ON THE NSF CONTACT DEVICE
C      YSL(I)     =Y COORDINATE OF THE ASPERITY NUMBER I ON THE LOWER
C                  MODEL
C      YSU(I)     =Y COORDINATE OF THE ASPERITY NUMBER I ON THE UPPER
C                  MODEL
C      YUSLOP     =SLOPE OF THE UPPER MODEL SUPPORT PLATE RELATIVE TO THE
C                  DIRECTION OF Y DISPLACEMENT OF THE LOWER MODEL SUPPORT
C                  PLATE ON THE NSF CONTACT DEVICE
C      ZL         =HEIGHT OF A POINT ON THE LOWER MODEL ABOVE THE
C                  REFERENCE PLANE ON THE LOWER MODEL
C      ZLMAX      =MAXIMUM ASPERITY HEIGHT ON LOWER MODEL
C      ZSL(I)     =Z COORDINATE OF THE ASPERITY NUMBER I ON THE LOWER
C                  MODEL
C      ZSU(I)     =Z COORDINATE OF THE ASPERITY NUMBER I ON THE UPPER
C                  MODEL
C      ZU         =HEIGHT OF A POINT ON THE UPPER MODEL ABOVE THE
C                  REFERENCE PLANE ON THE LOWER MODEL
C      ZUMAX      =MAXIMUM ASPERITY HEIGHT ON UPPER MODEL
C
    2 FORMAT (10X,2I10,F10.4)
    3 FORMAT (I5,2F5.3,F10.0,F5.3,F10.0,3F7.4)
    4 FORMAT (2F8.4,2F7.3)
    5 FORMAT (2A4)
    8 FORMAT (1H1/////////53X,7HTABLE V)
    9 FORMAT (          //52X,10HINPUT DATA)
   10 FORMAT (2F6.3,F7.4)
```

```
12 FORMAT (13X,F7.4,I3,2F8.3,I3,I4,1X,F8.5,8X,F6.3,F6.0)
13 FORMAT (13X,F7.4,I3,2F8.3,I3,I4,1X,2F8.5,F6.3,F6.0,2F8.0,3X,A4)
14 FORMAT (47X,2F8.5,F12.0,5X,5HTOTAL)
15 FORMAT (  //41X,8HASPERITY,16X,8HMATERIAL/(40X,
  5 10HPROPERTIES,14X,10HPROPERTIES/))
16 FORMAT (37X,43HNO. SUMMIT  MAX     ELASTIC  POISSONS   MAX/(41X,
  6 41HRADIUS HEIGHT   MODULUS    RATIO   ALLOW.)/(76X,6HSTRESS))
17 FORMAT(42X,22H(CM)   (CM)   (NT/CM2),10X,8H(NT/CM2)//
  7 (30X,5HUPPER))
18 FORMAT (30X,5HMODEL,I5,F7.3,F7.4,F11.0,F7.3,F10.0)
19 FORMAT (/30X,5HLOWER)
20 FORMAT (/////30X,7HTHETAU=, F5.3,2X,7HRADIANS,10X,7HTHETAL=,
  1  F5.3,2X,7HRADIANS)
21 FORMAT (          //(24X,50HLOCATIONS AND HEIGHTS OF ASPERITIES ON
  1 LOWER MODEL))
22 FORMAT (          //(24X,50HLOCATIONS AND HEIGHTS OF ASPERITIES ON
  1 UPPER MODEL))
24 FORMAT (          //(31X,36HASPERITY   SUMMIT  LOCATION   HEIGHT)/
  4(32X,25HINDEX    X-COORD  Y-COORD)/(32X,6HNUMBER))
25 FORMAT (43X,23H(CM)     (CM)      (CM))
26 FORMAT (31X,I5,3X,2F9.3,F10.4)
27 FORMAT (1H1//////)
28 FORMAT (22X,43HRELATIVE DISPLACEMENT OF UPPER MODEL    X  , F6.3,
  1 9H CM   Y  ,F6.3,3H CM//)
29 FORMAT (41X,12HU   L   AREA,39X,8HEXCEEDED)
30 FORMAT(15X,53HAPPR  AREA CENTER COORD ASPERITY  CALC    PROJ  SLOP
  1E,31H  LOAD    AVG     MAX   ELASTIC)
31 FORMAT(15X,52H       NO.   X      Y    INDEX   CONTACT  AREA
  1 ,10X,20HPRESS   PRESS  LIMIT)
32 FORMAT (15X,4H(CM),8X,11H(CM)   (CM),11X,13H(CM2)   (CM2),8X,
  2   22H(NT) (NT/CM2) (NT/CM2))
33 FORMAT (1H1//// //44X,10HTABLE IIIA)
```

```
   34 FORMAT (1H1//// //44X,22HTABLE IIIA (CONTINUED))
   35 FORMAT (1H1//// //44X,10HTABLE IIIB)
   36 FORMAT (1H1//// //44X,22HTABLE IIIB (CONTINUED))
   37 FORMAT(1H1/////////53X,10HTABLE VIIA///49X,18HCONTACT PARAMETERS/)
   38 FORMAT(1H1/////////53X,10HTABLE VIIB///49X,18HCONTACT PARAMETERS/)
   39 FORMAT(1H1/////////53X,10HTABLE VIIC///49X,18HCONTACT PARAMETERS/)
   40 FORMAT (1H1/////////48X,8HTABLE VI)
   41 FORMAT (25X,10HTOTAL LOAD,10X,4H(NT),3F10.0//(25X,25HTOTAL CONTACT
     1 AREA  (CM2),F9.4,2F10.4)/)
   42 FORMAT (25X,17HNUMBER OF CONTACT/(25X,6HPOINTS,18X,3I10)//(25X,
     2 8HAPPROACH,12X,4H(CM),3F10.4)/)
   43 FORMAT (25X,16HSLOPE OF CONTACT/(25X,5HAREAS,19X,3F10.3)/)
   44 FORMAT (       //(37X,30HVARIANCE OF CONTACT PARAMETERS)/(39X,
     4 26HFOR MODEL POSITIONS TESTED)//)
   45 FORMAT(25X,54HCONTACT PARAMETER   UNITS  MAXIMUM   MINIMUM   AVERA
     5GE/)
   46 FORMAT (25X,18HDIFFERENCE IN CAL-/(25X,16HCULATED AND PRO-)/(25X,
     6 19HJECTED CONTACT AREA,1X,4H(%) ,3F10.1)/)
   47 FORMAT (25X,13HCONTACT AREAS,7X,4H(%) ,3F10.1)
   48 FORMAT(25X,18HDIFFERENCE IN CAL-/(25X,16HCULATED AND PRO-)/(25X,
     8 17HJECTED INDIVIDUAL))
   49 FORMAT (1H1/////////)
      DIMENSION XSU(37),YSU(37),ZSU(37)
      DIMENSION XSL(75),YSL(75),ZSL(75)
      DIMENSION SEPMIN(37),MNU(37),MNL(37)
      INTEGER PTMX,PTMN,PTAV
      REAL MUU, MUL, NO
C*************************************************************************
C     SECTION I
C     DECLARES VALUES OF CONSTANT VARIBLES AND INITIAL VALUES OF
C     OTHER VARIBLES
      CFL = 2.54
```

```
CFP = 0.6894
XUSLOP = 0.00400
YUSLOP = -0.00058
XLSLOP = -0.00067
YLSLOP = -0.00045
WLIMIT = 65. * 9.8 / 2.205
DXDISP = 0.10
DYDISP = 0.00
NAPMX = 25
DIFAMX = 0.
DIFAMN = 100.
DIFCMX = 0.
DIFCMN = 100.
TLODMX = 0.
TLODMN = 10000.
TARMX = 0.
TARMN = 100.
PTMX = 0
PTMN = 100
APPRMX = 0.
APPRMN = 100.
SLOPMX = 0.
SLOPMN = 100.
CP = 0.
SUMLOD = 0.
SUMAR = 0.
SUMAPP = 0.
SUMPOS = 0.
SUMDFA = 0.
SUMDFC = 0.
SUMSLO = 0.
ISUMPT = 0
```

```
C      SECTION I          END
C*****************************************************************************
C      SECTION II
C      READS DATA
C      CORRECTS FOR MISALIGNMENT
C      REVERSES Y-COORDINATES OF THE LOWER MOLD CAVITIES TO OBTAIN
C      MODEL DIMENSIONS
C      PRINTS INPUT DATA AND THE POSITION OF THE CENTERS OF THE
C      ASPERITIES
       READ (5,5) NO,YES
       READ (5,3) NU,RU,ZUMAX,EU,MUU,ELIMTU
       READ (5,3) NL,RL,ZLMAX,EL,MUL,ELIMTL,WIDTHL
       READ (5,4) THETAU,THETAL,XDISPL,YDISPL
       DO 50 I=1,NU
       READ (5,10) X,Y,Z
       XSU(I)= X*COS(THETAU) -Y*SIN(THETAU)
       YSU(I) = X*SIN(THETAU) + Y*COS(THETAU)
       ZSU(I) = .5 +RU -Z + XSU(I)*XUSLOP + YSU(I)*YUSLOP
       XSU(I) = XSU(I) * CFL
       YSU(I) = YSU(I) * CFL
       ZSU(I) = ZSU(I) * CFL
   50  CONTINUE
       DO 60 I=1,NL
       READ (5,10) X,Y,Z
       XSL(I) = X*COS(THETAL) - Y*SIN(THETAL)
       YSL(I) = X*SIN(THETAL) +Y*COS(THETAL)
       YSL(I) = WIDTHL - YSL(I)
       ZSL(I) = Z - RL + XSL(I)*XLSLOP  + YSL(I)*YLSLOP
       XSL(I) = XSL(I) * CFL
       YSL(I) = YSL(I) * CFL
       ZSL(I) = ZSL(I) * CFL
   60  CONTINUE
```

```
XDISPL = XDISPL * CFL
YDISPL = YDISPL * CFL
RU = RU *CFL
RL = RL * CFL
ZUMAX = ZUMAX * CFL
ZLMAX = ZLMAX * CFL
EU = EU * CFP
EL = EL * CFP
ELIMTU = ELIMTU * CFP
ELIMTL= ELIMTL * CFP
WRITE (6,8)
WRITE (6,9)
WRITE (6,15)
WRITE (6,16)
WRITE (6,17)
WRITE (6,18) NU,RU,ZUMAX,EU,MUU,ELIMTU
WRITE (6,19)
WRITE (6,18) NL,RL,ZLMAX,EL,MUL,ELIMTL
WRITE (6,20) THETAU,THETAL
WRITE (6,33)
WRITE (6,22)
WRITE (6,24)
WRITE (6,25)
IMAX = 38
DO 65 I=1,NU
WRITE (6,26) I,XSU(I),YSU(I),ZSU(I)
IF (I.EQ.NU) GO TO 65
IF (I.LT.IMAX) GO TO 65
WRITE (6,34)
WRITE (6,24)
WRITE (6,25)
IMAX = IMAX + 39
```

```
   65 CONTINUE
      WRITE (6,35)
      WRITE (6,21)
      WRITE (6,24)
      WRITE (6,25)
      IMAX = 38
      DO 75 I=1,NL
      WRITE (6,26) I,XSL(I),YSL(I),ZSL(I)
      IF (I.EQ.NU) GO TO 75
      IF (I.LT.IMAX) GO TO 75
      WRITE (6,36)
      WRITE (6,24)
      WRITE (6,25)
      IMAX = IMAX + 39
   75 CONTINUE
C     SECTION II          END
C*************************************************************************
C     SECTION III
C     DETERMINES VARIOUS MODEL AND MATERIAL PARAMETERS
      Q = RU/(RU+RL)
      EP = 1./(((1.-MUL**2)/EL) + (1.-MUU**2)/EU)
      R = RL*RU/(RU + RL)
      APPR = .5
      APPR = APPR * CFL
      ZMAX = ZLMAX
      IF (ZUMAX.LT.ZMAX) GO TO 110
      ZMAX = ZUMAX
  110 CONTINUE
      ELIMIT = ELIMTU
      IF (ELIMIT .LT. ELIMTL) ELIMIT = ELIMTL
      OFSTMX=2*SQRT(RU*ZMAX)
C     SECTION III         END
```

```
C*************************************************************************
C      SECTION IV
C      CALCULATES CONTACT PARAMETERS AT EACH DESIRED RELATIVE DISPLACEMENT
C      OF THE MODELS
       DO 600 M=1,100
C*************************************************************************
C      SECTION IV A
C      ESTABLISHES INITIAL VALUES OF SEPARATION PARAMETERS
C      INCREMENTS X-Y POSITION OF UPPER MODEL
       DO 301 I=1,37
       MNU(I) = 0
       MNL(I) = 0
       SEPMIN(I) = 100.
       XSU(I) = XSU(I) + DXDISP
       YSU(I) = YSU(I) + DYDISP
  301  CONTINUE
       XDISPL = XDISPL + DXDISP
       YDISPL = YDISPL + DYDISP
C      SECTION IV A       END
C*************************************************************************
C      SECTION IV B
C      FINDS THE SEPARATION AND THE INDEX NUMBERS OF THE ASPERITIES
C      INVOLVED FOR POINTS OF LEAST SEPARATION
       DO 300 J=1,NU
       DO 300 K=1,NL
       DIST=SQRT((XSU(J)-XSL(K))**2+(YSU(J)-YSL(K))**2)
       IF (DIST.GE.OFSTMX) GO TO 300
       DO 210 L=1,NU
       DU = SQRT(RU**2 -(DIST*Q)**2)
       DL = SQRT(RL**2 -(DIST*(1.-Q))**2)
       ZU = ZSU(J) - DU
       ZL = ZSL(K) + DL
```

```
      SEP = ZU-ZL
      IF (SEPMIN(L) - SEP) 210,210,140
  140 CONTINUE
      LX=NU
      NP = NU-L
      IF (NP.EQ.0) GO TO 160
      DO 150 LL=1,NP
      SEPMIN(LX) = SEPMIN(LX-1)
      MNU(LX) = MNU(LX-1)
      MNL(LX) = MNL(LX-1)
      LX = LX - 1
  150 CONTINUE
  160 CONTINUE
      SEPMIN(L) = SEP
      MNU(L) =J
      MNL(L) = K
      GO TO 300
  210 CONTINUE
  300 CONTINUE
C     SECTION IV B       END
C*****************************************************************
C     SECTION IV C
C     WRITES HEADINGS FOR CONTACT PARAMETERS
      J = MNU(1)
      K = MNL(1)
      DAPPR = SEPMIN(1)
      F2MAX = 21.
      F2 = 0.
      IF (M .EQ. 13) GO TO 701
      IF ( M .EQ. 55) GO TO 702
      IF ( M.EQ. 56) GO TO 703
      GO TO 705
```

```
  701 WRITE (6,37)
      GO TO 704
  702 WRITE (6,38)
      GO TO 704
  703 WRITE (6,39)
  704 CONTINUE
      WRITE (6,28) XDISPL,YDISPL
      WRITE (6,30)
      WRITE (6,31)
      WRITE (6,29)
      WRITE (6,32)
  705 CONTINUE
C     SECTION IV C       END
C*************************************************************************
C     SECTION IV D
C     CALCULATES CONTACT PARAMETERS AT EACH DESIRED APPROACH FOR A GIVEN
C     X-Y POSITION OF THE MODELS
      FLAG = 0.
      DO 500 NAP=1,NAPMX
C*************************************************************************
C     SECTION IV D.1
C     DECREASES APPROACH TO DESIRED VALUE
C     DECLARES INITIAL VALUES OF CONTACT PARAMETERS
      IF ( FLAG .GT. 0. ) GO TO 501
      APPR = APPR-DAPPR
      DO 304 JJ=1,NU
      ZSU(JJ) = ZSU(JJ) - DAPPR
  304 CONTINUE
      NCTPT = 0
      TAREA = 0.
      TLOAD = 0.
      TAREAP= 0.
```

```
C      SECTION IV D.1     END
C*****************************************************************
C      SECTION IV D.2.0
C      CALCULATES CONTACT PARAMETERS FOR SINGLE VALUE OF APPROACH
C*****************************************************************
C      SECTION IV D.2.1
C      DETERMINES POINTS IN CONTACT
       DO 400 L=1,NU
       K=MNL(L)
       J=MNU(L)
       SEPMIN(L) = SEPMIN(L) -DAPPR
       IF (F2 .LT. F2MAX) GO TO 715
       F2 = 0.
       IF (M .EQ. 13) GO TO 711
       IF ( M .EQ. 55) GO TO 712
       IF ( M.EQ. 56) GO TO 713
       GO TO 715
  711  WRITE (6,37)
       GO TO 714
  712  WRITE (6,38)
       GO TO 714
  713  WRITE (6,39)
  714  CONTINUE
       WRITE (6,30)
       WRITE (6,31)
       WRITE (6,29)
       WRITE (6,32)
  715  CONTINUE
       IF (SEPMIN(L)) 305,310,400
C      SECTION IV D.2.1  END
C*****************************************************************
C      SECTION IV D.2.2
```

```
C      CALCULATES CONTACT PARAMETERS AT POINTS WHICH SUPPORT PART OF THE
C      NORMAL LOAD
C      FOR  THE LARGEST LOAD DETERMINES MAXIMUM AND MINIMUM VALUES OF
C      THE SLOPE AND DIFFERENCE IN CALCULATED AND PROJECTED VALUES OF
C      INDIVIDUAL CONTACT AREAS
  305 CONTINUE
      DIST=SQRT((XSU(J)-XSL(K))**2+(YSU(J)-YSL(K))**2)
      Z = ZSU(J) - ZSL(K)
      SLOPE = DIST/Z
      W = RL + RU - SQRT (DIST**2 + Z**2)
      XCA = XSU(J) + Q*(XSL(K) - XSU(J))
      YCA = YSU(J) + Q*(YSL(K) - YSU(J))
      CAREA = 3.1416 *W * R
      CLOAD=(4./3.) * EP * SQRT(R) * W**1.5
      CTAVPR = CLOAD / CAREA
      CTMXPR = 1.5 * CTAVPR
      NCTPT = NCTPT + 1
      CF=1./SQRT(1.+SLOPE**2)
      CAREAP=CF*CAREA
      F1 = NO
      IF ( CLOAD .GE. WLIMIT ) F1=YES
      IF ( CLOAD .GE. WLIMIT ) FLAG = 1.0
      DUMA = APPR
      TAREA = TAREA + CAREA
      TAREAP = TAREAP + CAREAP
      TLOAD = TLOAD + CLOAD
      IF (M .EQ. 13) GO TO 720
      IF ( M .EQ. 55) GO TO 720
      IF ( M.EQ. 56) GO TO 720
      GO TO 721
  720 CONTINUE
      WRITE (6,13) DUMA,NCTPT,XCA,YCA,J,K,CAREA,CAREAP,SLOPE,CLOAD,
```

```
     1CTAVPR,CTMXPR,F1
  721 CONTINUE
      F2 = F2 + 1.
      IF (FLAG .EQ. 0.0) GO TO 400
      IF ( SLOPE .GT. SLOPMX) SLOPMX = SLOPE
      IF (SLOPE .LT. SLOPMN) SLOPMN = SLOPE
      DIFCA = 100. * (CAREA - CAREAP)/CAREA
      IF ( DIFCA .GT. DIFCMX) DIFCMX = DIFCA
      IF (DIFCA .LT. DIFCMN) DIFCMN = DIFCA
      SUMDFC = SUMDFC + DIFCA
      CP = CP + 1.
      SUMSLO = SUMSLO + SLOPE
      GO TO 400
C     SECTION IV D.2.2  END
C*****************************************************************
C     SECTION IV D.2.3
C     CALCULATES CONTACT PARAMETERS AT POINTS WHICH CONTACT WITHOUT
C     SUPPORTING A PART OF THE NORMAL LOAD
  310 CONTINUE
      NCTPT = NCTPT + 1
      CLOAD = 0.
      CAREA = 0.
      Z = ZSU(J) - ZSL(K)
      XCA = XSU(J) + Q*(XSL(K) - XSU(J))
      YCA = YSU(J) + Q*(YSL(K) - YSU(J))
      DIST=SQRT((XSU(J)-XSL(K))**2+(YSU(J)-YSL(K))**2)
      SLOPE = DIST/Z
      DUMA = APPR
      IF (M .EQ. 13) GO TO 730
      IF ( M .EQ. 55) GO TO 730
      IF ( M.EQ. 56) GO TO 730
      GO TO 731
```

```
  730 CONTINUE
      WRITE (6,12) DUMA,NCTPT,XCA,YCA,J,K,CAREA,SLOPE,CLOAD
  731 CONTINUE
      F2 = F2 + 1.
  400 CONTINUE
C     SECTION IV D.2.3  END
C*****************************************************************
C     SECTION IV D.3
C     WRITES TOTAL VALUES OF CONTACT PARAMETERS
C     DETERMINES NEXT INCREMENT OF APPROACH
      IF (M .EQ. 13) GO TO 740
      IF ( M .EQ. 55) GO TO 740
      IF ( M.EQ. 56) GO TO 740
      GO TO 741
  740 CONTINUE
      WRITE (6,14) TAREA,TAREAP,TLOAD
  741 CONTINUE
      F2 = F2 + 1.
      IF (SEPMIN(NCTPT + 1) -.0010)410,420,420
  410 CONTINUE
      DAPPR=SEPMIN(NCTPT+1)
      GO TO 430
  420 CONTINUE
      DAPPR = .001
  430 CONTINUE
C     SECTION IV D.3    END
C*****************************************************************
  500 CONTINUE
C     SECTION IV D.2.0  END
C*****************************************************************
  501 CONTINUE
C     SECTION IV D      END
```

```
C*************************************************************************
C      SECTION IV E
C      DETERMINES THE MAXIMUM,MINIMUM, AND CUMLATIVE SUM OF CONTACT
C      PARAMETERS FOR MAXIMUM LOAD AT GIVEN X-Y POSITIONS OF THE MODELS
       DIFA = 100. * (TAREA - TAREAP)/TAREA
       IF (TLOAD .GT. TLODMX) TLODMX = TLOAD
       IF ( TLOAD .LT. TLODMN) TLODMN =TLOAD
       IF (TAREA .GT. TARMX) TARMX = TAREA
       IF (TAREA .LT. TARMN) TARMN = TAREA
       IF ( NCTPT .GT. PTMX) PTMX = NCTPT
       IF ( NCTPT .LT. PTMN) PTMN = NCTPT
       IF ( DUMA .GT. APPRMX) APPRMX = DUMA
       IF ( DUMA .LT. APPRMN) APPRMN = DUMA
       IF ( DIFA .GT. DIFAMX) DIFAMX = DIFA
       IF ( DIFA .LT. DIFAMN) DIFAMN = DIFA
       SUMLOD = SUMLOD + TLOAD
       SUMAR = SUMAR + TAREA
       SUMAPP = SUMAPP + DUMA
       SUMPOS = SUMPOS + 1.
       SUMDFA = SUMDFA + DIFA
       ISUMPT = ISUMPT + NCTPT
C      SECTION IV E       END
  600 CONTINUE
C      SECTION IV         END
C*************************************************************************
C      SECTION V
C      CALCULATES AVERAGE AND PRINTS MAXIMIM, MINIMUM, AND AVERAGE VALUES
C      OF CONTACT PARAMETERS
       TARAV = SUMAR/SUMPOS
       TLODAV = SUMLOD/SUMPOS
       APPRAV = SUMAPP/SUMPOS
       PTAV = ISUMPT/SUMPOS
```

```
      DIFAAV =SUMDFA/CP
      SLOPAV = SUMSLO/CP
      DIFCAV = SUMDFC/CP
      WRITE (6,40)
      WRITE (6,44)
      WRITE (6,45)
      WRITE (6,41) TLODMX,TLODMN,TLODAV,TARMX,TARMN,TARAV
      WRITE (6,42) PTMX,PTMN,PTAV,APPRMX,APPRMN,APPRAV
      WRITE (6,43) SLOPMX,SLOPMN,SLOPAV
      WRITE (6,46) DIFAMX,DIFAMN,DIFAAV
      WRITE (6,48)
      WRITE (6,47) DIFCMX,DIFCMN,DIFCAV
      WRITE (6,49)
C     SECTION V          END
      STOP
       END
```

Appendix 5 Equations used in Computer Program

1. Determination of Maximum allowable misalignment of asperities for contact (CK or OFSTMX)

Figure 23 shows the most extreme case of asperity misalignment for which contact between the upper and lower asperities may take place. It can be shown that for asperities with equal summit radii the point of contact (P) will always occur halfway between their summits (or centers).

$$AK = \tfrac{1}{2}CK$$

It can also be shown that

$$EC = ND = \tfrac{1}{2}ZMAX$$

It follows that:

$$\overline{AK}^2 = \overline{RL}^2 - \overline{KD}^2$$

$$KD = RL - ND$$

$$= RL - \tfrac{1}{2}ZMAX$$

$$AK = RL - (\overline{RL}^2 - \tfrac{1}{2}ZMAX)^{2\,\frac{1}{2}}$$

if $ZMAX \ll RL$

$$AK = RL \cdot ZMAX^{\frac{1}{2}}$$

$$CK = 2\,RL \cdot ZMAX^{\frac{1}{2}}$$

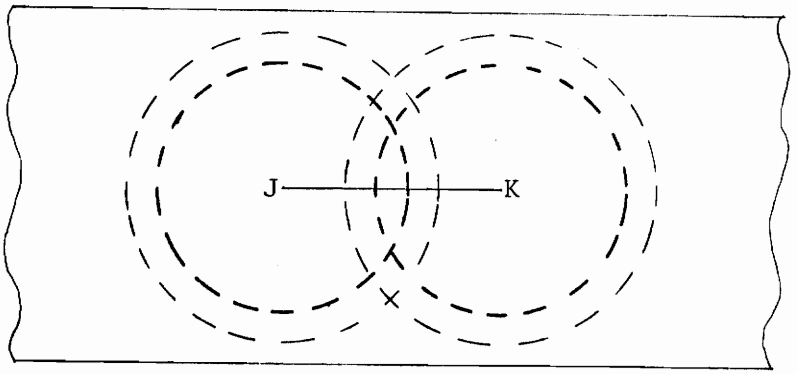

Top View

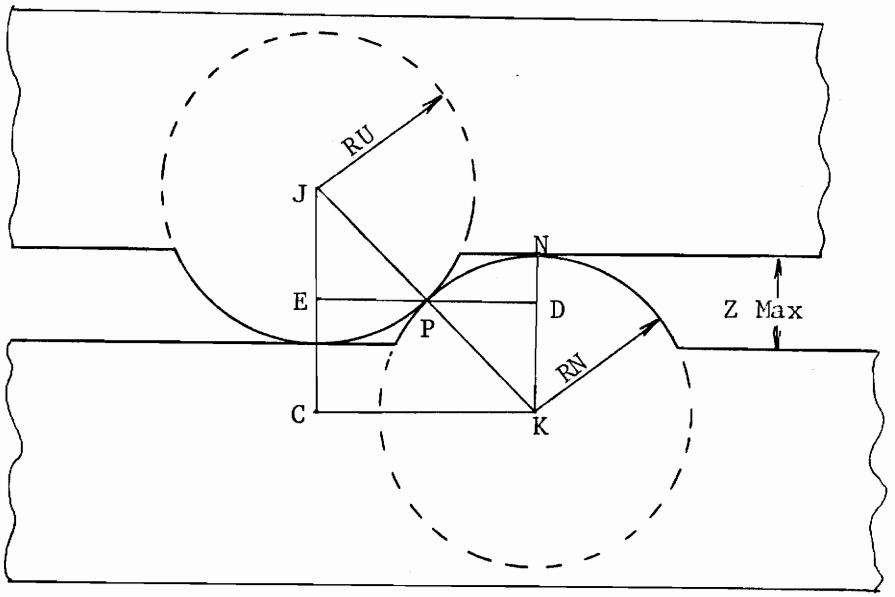

Side View

Figure 23. Determination of Maximum Asperity Misalignment for Contact

or with the symbols employed in the program:

$$OFSTMX = 2\ RL \cdot ZMAX^{\frac{1}{2}}$$

2. Minimum vertical separation between two asperities

Figure 24 shows two asperities which can come into contact as the separation between them is reduced. Contact will occur at point P which will be located halfway between the summits (or centers). The following derivation is obtained from simple geometric considerations.

$$DIST = (XSU(J) - XSL(K))^2 + (YSU(J) - YSL(K))^{2\ \frac{1}{2}}$$

$$DU = \overline{RU}^2 - \frac{DIST}{2}^{2\ \frac{1}{2}}$$

$$DL = \overline{RL}^2 - \frac{DIST}{2}^{2\ \frac{1}{2}}$$

$$ZL = ZSL(K) + DL$$

$$ZU = ZSU(J) - DU$$

Finally

$$SEP = XU - ZL$$

3. Effect of Misaligned Contact on Loading

As shown in Figure 25, when two misaligned asperities contact the force acting normal to the asperities (F_n) is not equal to the applied normal load (L). Furthermore there is also a tangential

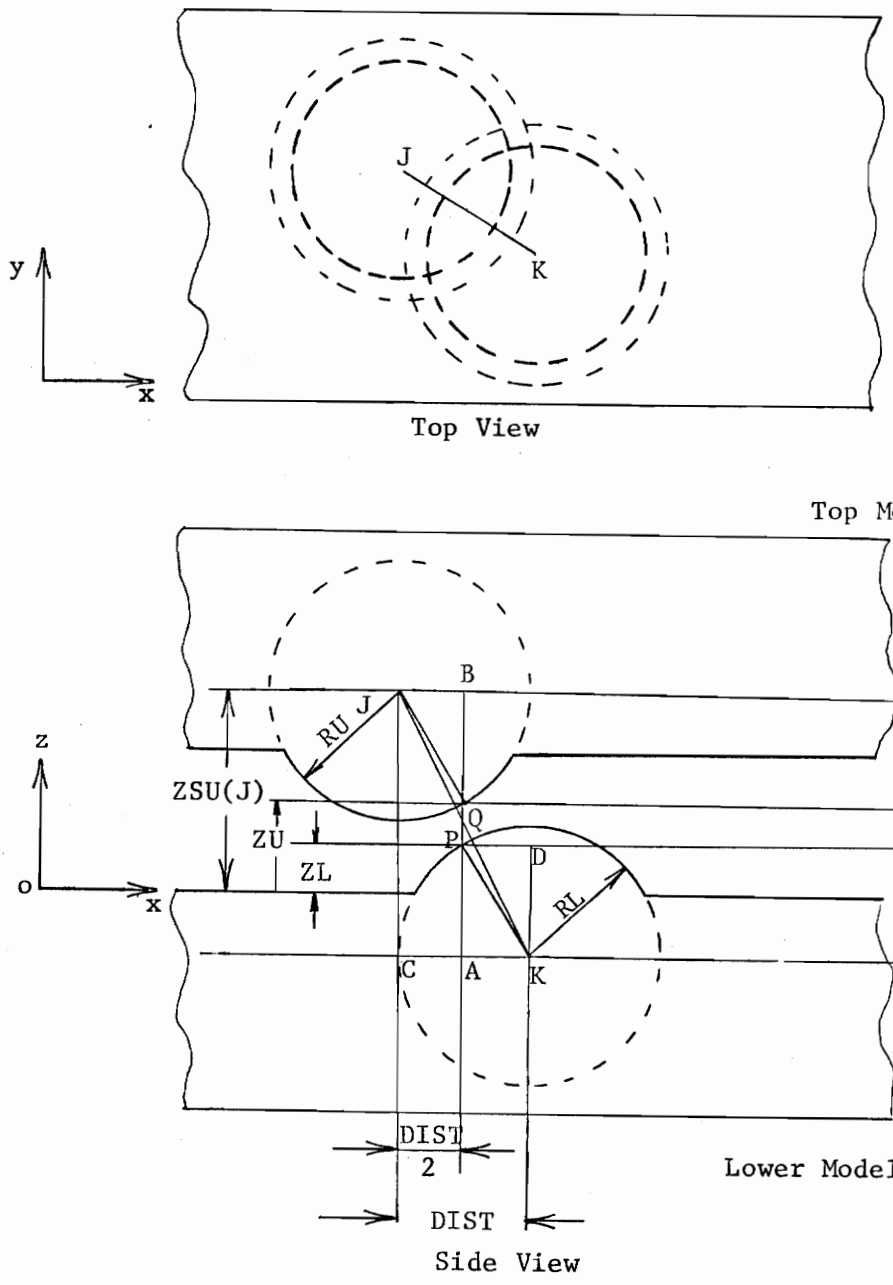

Figure 24. Determination of Vertical Separation

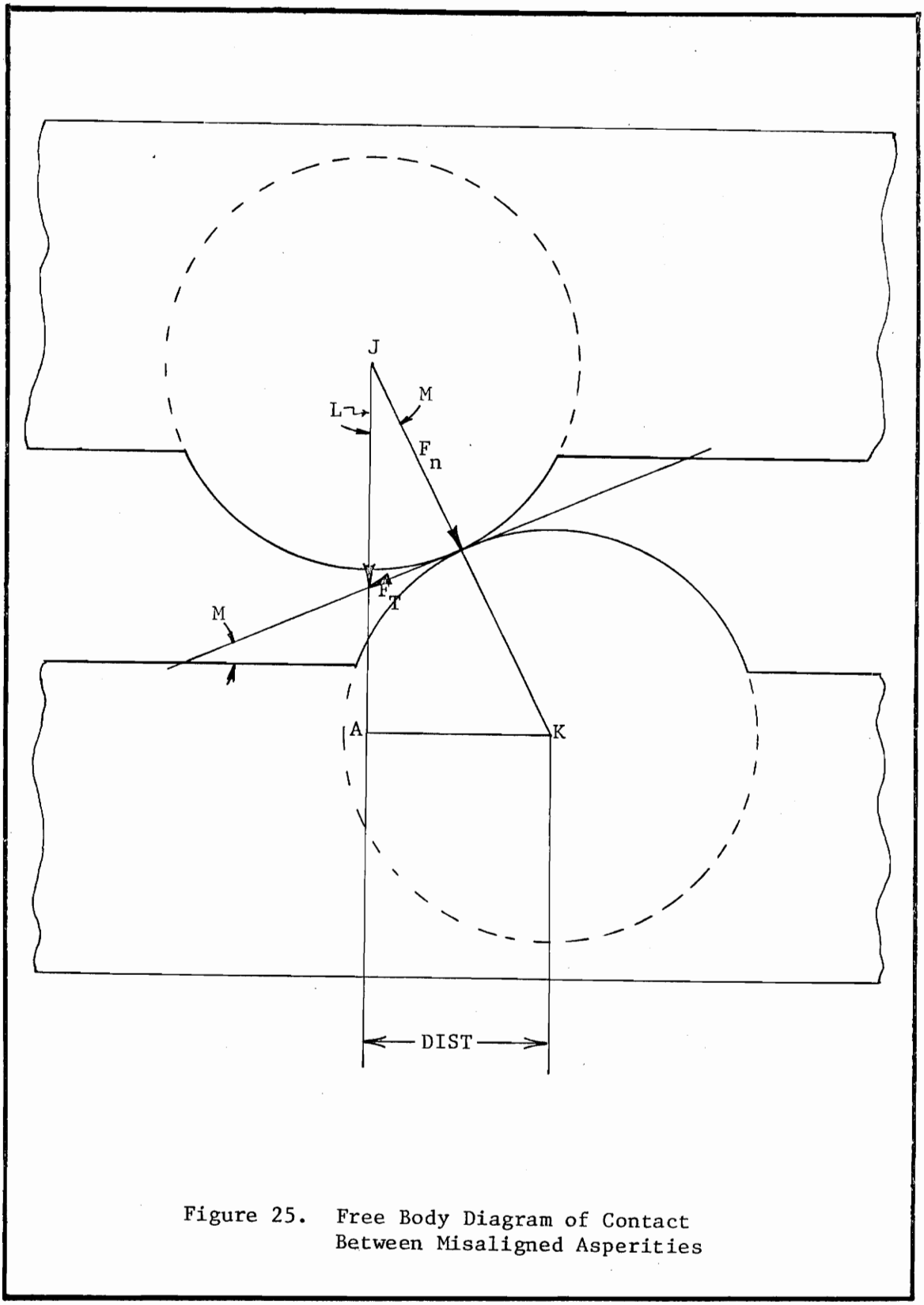

Figure 25. Free Body Diagram of Contact Between Misaligned Asperities

force (F_T) acting on the contact area.

$$L = F_n/\cos M$$

$$F_T = F_n \cdot \tan M$$

$$\text{SLOPE} = \tan M = \frac{\text{DIST}}{\text{ZSU(J)} - \text{ZSL(K)}}$$

$$\cos M = CF = \frac{1}{(1 + \tan^2 M)^{\frac{1}{2}}}$$

4. Effect of Misaligned Contact on the True Contact Area and the Observed Contact Area

It has been shown that as a consequence of contact between misaligned asperities, the normal load at the point of contact is less than the applied load. This of course results in a smaller contact area. Since the contact area is inclined with respect to the viewing plane (horizontal) the observed contact area will be smaller. Both of these effects may be corrected by geometric considerations.

As explained previously, the method selected for solving the multiple contact problem was that of calculating the contact parameters for various values of the approach. For the case of two perfectly aligned asperities, the decrease in the approach is equal to the decrease in the hypothetical center distance between the asperities, a parameter required for the use of the Hertz equations. However, as shown in Figure 26, for misaligned contact (which can be expected to occur most frequently), the decrease in the appraoch (PQ) is not the

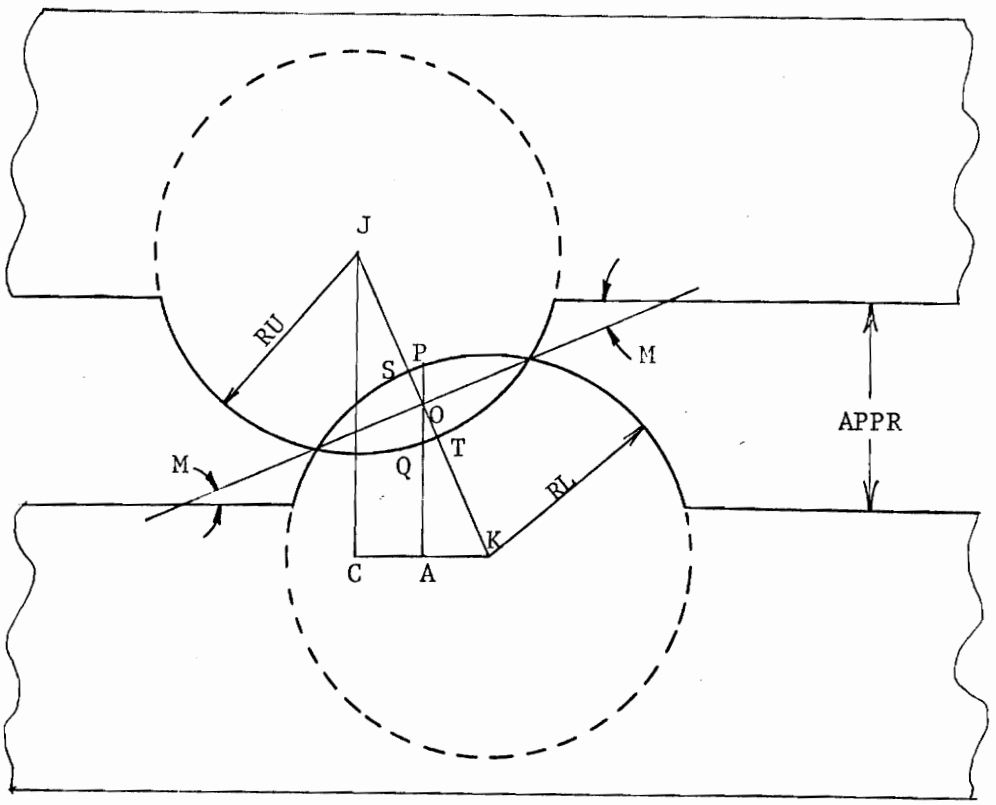

Figure 26. Enlarged View of Intersection of Asperities

same as the decrease in the center distance of the asperities (ST). The distance ST may be determined from the following equation:

$$ST = W = RU + RL - \overline{DIST}^2 + (ZSU(J) - ZSL(K))^2 \,^{\frac{1}{2}}$$

Substitution of W into the Hertz equation yields the normal load F_n.

Figure 27 shows that the contact area observed in the top view (CAREAP) is the projection of the calculated contact area (CAREA) onto the horizontal plane. Thus

$$CAREAP = CAREA \cdot \cos M$$

or

$$CAREAP = CAREA \cdot CF$$

It can be shown that the center of the contact area is located on the line joining the centers of the two asperities that the exact location is determined by the radii of curvature of the asperities. Thus the coordinates of the contact area are:

$$XCA = XSU(J) + \frac{XSL(K) - XSU(J)}{Q}$$

$$YCA = YSU(J) + \frac{YSL(K) - YSU(J)}{Q}$$

where:

$$Q = \frac{RU}{RU + RL}$$

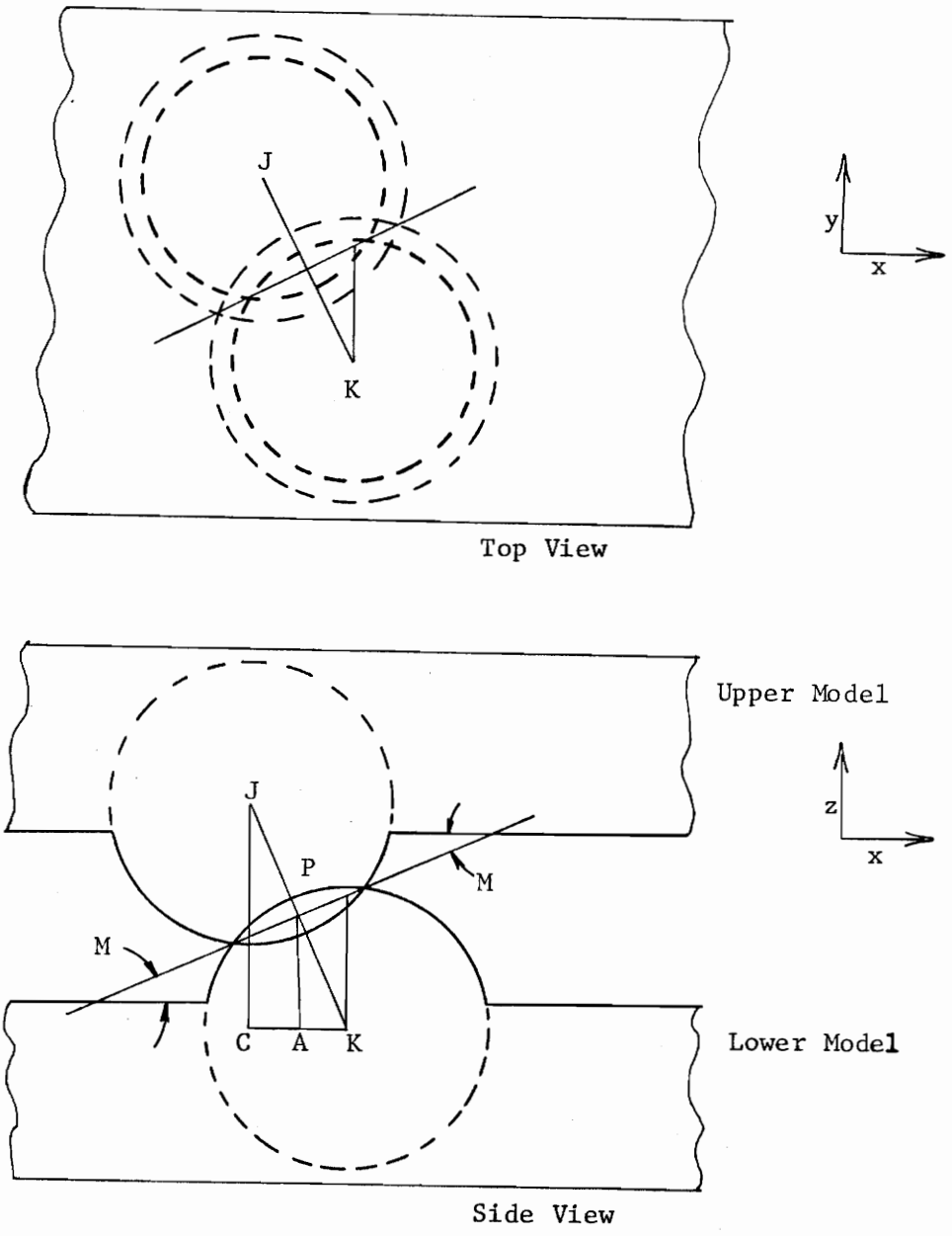

Figure 27. Determination of Projected Contact Area

TABLE VIIA

CONTACT PARAMETERS

RELATIVE DISPLACEMENT OF UPPER MODEL X 1.300 CM Y 0.0 CM

APPR (CM)	AREA NO.	CENTER COORD X (CM)	Y (CM)	ASPERITY INDEX U	I	CALC CONTACT AREA (CM2)	PROJ AREA (CM2)	SLOPE	LOAD (NT)	AVG PRESS (NT/CM2)	MAX PRESS (NT/CM2)	PLASTIC LIMIT EXCEEDED
0.3353	1	3.491	2.717	3	15	0.0		0.023	0.			
						0.0	0.0		0.	TOTAL		
0.3343	1	3.491	2.717	3	15	0.00200	0.00200	0.023	6.	2822.	4232.	NO
						0.00200	0.00200		6.	TOTAL		
0.3333	1	3.491	2.717	3	15	0.00399	0.00399	0.023	16.	3989.	5984.	NO
						0.00399	0.00399		16.	TOTAL		
0.3323	1	3.491	2.717	3	15	0.00599	0.00599	0.023	29.	4885.	7328.	NO
						0.00599	0.00599		29.	TOTAL		
0.3313	1	3.491	2.717	3	15	0.00798	0.00798	0.023	45.	5640.	8460.	NO
						0.00798	0.00798		45.	TOTAL		
0.3303	1	3.491	2.717	3	15	0.00998	0.00998	0.023	63.	6306.	9459.	NO
						0.00998	0.00998		63.	TOTAL		
0.3293	1	3.491	2.717	3	15	0.01197	0.01197	0.023	83.	6908.	10362.	NO
						0.01197	0.01197		83.	TOTAL		
0.3283	1	3.491	2.717	3	15	0.01397	0.01397	0.023	104.	7461.	11192.	NO
						0.01397	0.01397		104.	TOTAL		
0.3273	1	3.491	2.717	3	15	0.01596	0.01596	0.023	127.	7976.	11964.	NO
						0.01596	0.01596		127.	TOTAL		
0.3263	1	3.491	2.717	3	15	0.01796	0.01795	0.023	152.	8460.	12690.	NO
						0.01796	0.01795		152.	TOTAL		
0.3253	1	3.491	2.717	3	15	0.01996	0.01995	0.023	178.	8918.	13377.	NO

TABLE VIIA

CONTACT PARAMETERS

APPR (CM)	AREA NO.	CENTER X (CM)	COORD Y (CM)	ASPERITY INDEX U	ASPERITY INDEX L	CALC CONTACT AREA (CM2)	PROJ AREA (CM2)	SLOPE	LOAD (NT)	AVG PRESS (NT/CM2)	MAX PRESS (NT/CM2)	ELASTIC LIMIT EXCEEDED
						0.01996	0.01995		178.	TOTAL		
0.3243	1	3.491	2.717	3	15	0.02195	0.02194	0.023	205.	9353.	14029.	NO
						0.02195	0.02194		205.	TOTAL		
0.3233	1	3.491	2.717	3	15	0.02394	0.02394	0.023	234.	9769.	14653.	NO
						0.02394	0.02394		234.	TOTAL		
0.3223	1	3.491	2.717	3	15	0.02594	0.02593	0.023	264.	10167.	15251.	NO
						0.02594	0.02593		264.	TOTAL		
0.3213	1	3.491	2.717	3	15	0.02794	0.02793	0.023	295.	10551.	15827.	YES
						0.02794	0.02793		295.	TOTAL		

TABLE VIIB

CONTACT PARAMETERS

RELATIVE DISPLACEMENT OF UPPER MODEL X 5.500 CM Y 0.0 CM

APPR (CM)	AREA NO.	CENTER COORD X (CM)	Y (CM)	ASPERITY INDEX U	L	CALC CONTACT AREA (CM2)	PROJ AREA (CM2)	SLOPE	LOAD (NT)	AVG PRESS (NT/CM2)	MAX PRESS (NT/CM2)	ELASTIC LIMIT EXCEEDED
0.2909	1	9.546	5.787	8	9	0.0		0.131	0.			
						0.0	0.0		0.	TOTAL		
0.2899	1	9.546	5.787	8	9	0.00198	0.00196	0.131	6.	2809.	4214.	NO
						0.00198	0.00196		6.	TOTAL		
0.2889	1	9.546	5.787	8	9	0.00396	0.00393	0.131	16.	3972.	5958.	NO
						0.00396	0.00393		16.	TOTAL		
0.2888	1	9.546	5.787	8	9	0.00409	0.00405	0.131	16.	4036.	6053.	NO
0.2888	2	7.650	2.838	3	69	0.0		0.125	0.			
						0.00409	0.00405		16.	TOTAL		
0.2878	1	9.546	5.787	8	9	0.00607	0.00601	0.131	30.	4916.	7375.	NO
0.2878	2	7.650	2.838	3	69	0.00198	0.00197	0.125	6.	2811.	4216.	NO
						0.00805	0.00798		35.	TOTAL		
0.2868	1	9.546	5.787	8	9	0.00804	0.00798	0.131	46.	5662.	8493.	NO
0.2868	2	7.650	2.838	3	69	0.00396	0.00393	0.125	16.	3974.	5961.	NO
						0.01201	0.01191		61.	TOTAL		
0.2858	1	9.546	5.787	8	9	0.01002	0.00994	0.131	63.	6320.	9481.	NO
0.2858	2	7.650	2.838	3	69	0.00594	0.00590	0.125	29.	4867.	7300.	NO
						0.01597	0.01584		92.	TOTAL		
0.2848	1	9.546	5.787	8	9	0.01200	0.01190	0.131	83.	6916.	10374.	NO
0.2848	2	7.650	2.838	3	69	0.00792	0.00786	0.125	45.	5619.	8429.	NO
						0.01993	0.01976		128.	TOTAL		

TABLE VIIB

CONTACT PARAMETERS

APPR	AREA NO.	CENTER COORD X	Y	ASPERITY INDEX U	L	CALC CONTACT AREA	PROJ AREA	SLOPE	LOAD	AVG PRESS	MAX PRESS	ELASTIC LIMIT EXCEEDED
(CM)		(CM)	(CM)			(CM2)	(CM2)		(NT)	(NT/CM2)	(NT/CM2)	
0.2838	1	9.546	5.787	8	9	0.01398	0.01386	0.131	104.	7464.	11197.	NO
0.2838	2	7.650	2.838	3	69	0.00990	0.00983	0.125	62.	6283.	9424.	NO
						0.02389	0.02369		167.	TOTAL		
0.2828	1	9.546	5.787	8	9	0.01596	0.01582	0.131	127.	7975.	11963.	NO
0.2828	2	7.650	2.838	3	69	0.01188	0.01179	0.125	82.	6882.	10323.	NO
						0.02784	0.02762		209.	TOTAL		
0.2818	1	9.546	5.787	8	9	0.01794	0.01779	0.131	152.	8455.	12683.	NO
0.2818	2	7.650	2.838	3	69	0.01387	0.01376	0.125	103.	7433.	11150.	NO
						0.03180	0.03154		255.	TOTAL		
0.2808	1	9.546	5.787	8	9	0.01992	0.01975	0.132	177.	8909.	13364.	NO
0.2808	2	7.650	2.838	3	69	0.01584	0.01572	0.125	126.	7946.	11919.	NO
						0.03576	0.03547		303.	TOTAL		
0.2799	1	9.546	5.787	8	9	0.02172	0.02153	0.132	202.	9303.	13955.	NO
0.2799	2	7.650	2.838	3	69	0.01765	0.01751	0.126	148.	8386.	12579.	NO
0.2799	3	9.779	2.195	10	16	0.0		0.139	0.			
						0.03936	0.03904		350.	TOTAL		
0.2789	1	9.546	5.787	8	9	0.02370	0.02349	0.132	230.	9718.	14576.	NO
0.2789	2	7.650	2.838	3	69	0.01963	0.01947	0.126	174.	8844.	13266.	NO
0.2789	3	9.779	2.195	10	16	0.00199	0.00197	0.139	6.	2815.	4222.	NO
						0.04531	0.04494		409.	TOTAL		
0.2779	1	9.546	5.787	8	9	0.02567	0.02545	0.132	260.	10115.	15173.	NO

TABLE VIIB

CONTACT PARAMETERS

APPR (CM)	AREA NO.	CENTER COORD X (CM)	Y (CM)	ASPERITY INDEX U	L	CALC CONTACT AREA (CM2)	PROJ AREA (CM2)	SLOPE	LOAD (NT)	AVG PRESS (NT/CM2)	MAX PRESS (NT/CM2)	ELASTIC LIMIT EXCEEDED
0.2779	2	7.650	2.838	3	69	0.02161	0.02144	0.126	200.	9279.	13919.	NO
0.2779	3	9.779	2.195	10	16	0.00396	0.00393	0.140	16.	3975.	5962.	NO
						0.05125	0.05082		476.	TOTAL		
0.2769	1	9.546	5.787	8	9	0.02765	0.02742	0.132	290.	10498.	15747.	YES
0.2769	2	7.650	2.838	3	69	0.02359	0.02340	0.126	229.	9695.	14543.	NO
0.2769	3	9.779	2.195	10	16	0.00594	0.00588	0.140	29.	4866.	7299.	NO
						0.05718	0.05670		548.	TOTAL		

TABLE VIIC

CONTACT PARAMETERS

RELATIVE DISPLACEMENT OF UPPER MODEL X 5.600 CM Y 0.0 CM

APPR (CM)	AREA NO.	CENTER COORD X (CM)	Y (CM)	ASPERITY INDEX U	L	CALC CONTACT AREA (CM2)	PROJ AREA (CM2)	SLOPE	LOAD (NT)	AVG PRESS (NT/CM2)	MAX PRESS (NT/CM2)	ELASTIC LIMIT EXCEEDED
0.2852	1	9.974	2.126	10	2	0.0		0.162	0.			
						0.0	0.0		0.	TOTAL		
0.2851	1	9.974	2.126	10	2	0.00015	0.00014	0.162	0.	764.	1146.	NO
0.2851	2	9.829	2.195	10	16	0.0		0.123	0.			
						0.00015	0.00014		0.	TOTAL		
0.2841	1	9.974	2.126	10	2	0.00212	0.00209	0.162	6.	2905.	4357.	NO
0.2841	2	9.829	2.195	10	16	0.00198	0.00197	0.123	6.	2812.	4218.	NO
						0.00410	0.00406		12.	TOTAL		
0.2831	1	9.974	2.126	10	2	0.00409	0.00404	0.162	17.	4036.	6055.	NO
0.2831	2	9.829	2.195	10	16	0.00396	0.00393	0.123	16.	3975.	5962.	NO
						0.00805	0.00797		32.	TOTAL		
0.2828	1	9.974	2.126	10	2	0.00478	0.00472	0.162	21.	4366.	6549.	NO
0.2828	2	9.829	2.195	10	16	0.00466	0.00463	0.123	20.	4311.	6466.	NO
0.2828	3	9.596	5.787	8	9	0.0		0.154	0.			
						0.00945	0.00935		41.	TOTAL		
0.2826	1	9.974	2.126	10	2	0.00505	0.00499	0.162	23.	4488.	6732.	NO
0.2826	2	9.829	2.195	10	16	0.00494	0.00490	0.123	22.	4436.	6653.	NO
0.2826	3	9.596	5.787	8	9	0.00028	0.00027	0.154	0.	1052.	1578.	NO
0.2826	4	7.700	2.838	3	69	0.0		0.144	0.			
						0.01027	0.01016		45.	TOTAL		
0.2816	1	9.974	2.126	10	2	0.00702	0.00693	0.162	37.	5291.	7936.	NO

TABLE VIIC

CONTACT PARAMETERS

APPR (CM)	AREA NO.	CENTER COORD X (CM)	Y (CM)	ASPERITY INDEX U	L	CALC CONTACT AREA (CM2)	PROJ AREA (CM2)	SLOPE	LOAD (NT)	AVG PRESS (NT/CM2)	MAX PRESS (NT/CM2)	ELASTIC LIMIT EXCEEDED
0.2816	2	9.829	2.195	10	16	0.00692	0.00687	0.123	36.	5250.	7876.	NO
0.2816	3	9.596	5.787	8	9	0.00225	0.00222	0.154	7.	2995.	4492.	NO
0.2816	4	7.700	2.838	3	69	0.00198	0.00196	0.144	6.	2809.	4214.	NO
						0.01817	0.01798		86.	TOTAL		
0.2806	1	9.974	2.126	10	2	0.00900	0.00888	0.162	54.	5987.	8981.	NO
0.2806	2	9.829	2.195	10	16	0.00890	0.00883	0.123	53.	5955.	8933.	NO
0.2806	3	9.596	5.787	8	9	0.00422	0.00417	0.154	17.	4103.	6154.	NO
0.2806	4	7.700	2.838	3	69	0.00396	0.00392	0.144	16.	3970.	5955.	NO
						0.02607	0.02580		140.	TOTAL		
0.2799	1	9.974	2.126	10	2	0.01053	0.01039	0.162	68.	6477.	9716.	NO
0.2799	2	9.829	2.195	10	16	0.01044	0.01036	0.124	67.	6450.	9676.	NO
0.2799	3	9.596	5.787	8	9	0.00576	0.00569	0.154	28.	4791.	7186.	NO
0.2799	4	7.700	2.838	3	69	0.00549	0.00544	0.144	26.	4679.	7019.	NO
0.2799	5	7.510	7.492	12	6	0.0		0.169	0.			
						0.03222	0.03189		189.	TOTAL		
0.2789	1	9.974	2.126	10	2	0.01250	0.01234	0.162	88.	7058.	10587.	NO
0.2789	2	9.829	2.195	10	16	0.01242	0.01233	0.124	87.	7036.	10554.	NO
0.2789	3	9.596	5.787	8	9	0.00773	0.00764	0.154	43.	5551.	8326.	NO
0.2789	4	7.700	2.838	3	69	0.00747	0.00739	0.144	41.	5456.	8184.	NO
0.2789	5	7.510	7.492	12	6	0.00197	0.00194	0.169	6.	2803.	4204.	NO
						0.04209	0.04165		265.	TOTAL		

TABLE VIIC

CONTACT PARAMETERS

APPR	AREA NO.	CENTER X	COORD Y	ASPERITY INDEX U	ASPERITY INDEX L	CALC CONTACT AREA	PROJ AREA	SLOPE	LOAD	AVG PRESS	MAX PRESS	ELASTIC LIMIT EXCEEDED
(CM)		(CM)	(CM)			(CM2)	(CM2)		(NT)	(NT/CM2)	(NT/CM2)	
0.2787	1	9.974	2.126	10	2	0.01282	0.01265	0.162	92.	7146.	10720.	NO
0.2787	2	9.829	2.195	10	16	0.01274	0.01264	0.124	91.	7125.	10688.	NO
0.2787	3	9.596	5.787	8	9	0.00805	0.00795	0.154	46.	5663.	8495.	NO
0.2787	4	7.700	2.838	3	69	0.00779	0.00771	0.144	43.	5571.	3356.	NO
0.2787	5	7.510	7.492	12	6	0.00229	0.00225	0.169	7.	3019.	4528.	NO
0.2787	6	8.488	4.768	14	14	0.0		0.161	0.			
						0.04368	0.04321		278.	TOTAL		
0.2777	1	9.974	2.126	10	2	0.01478	0.01459	0.162	113.	7676.	11514.	NO
0.2777	2	9.829	2.195	10	16	0.01472	0.01461	0.124	113.	7659.	11489.	NO
0.2777	3	9.596	5.787	8	9	0.01002	0.00990	0.154	63.	6319.	9479.	NO
0.2777	4	7.700	2.838	3	69	0.00976	0.00966	0.144	61.	6237.	9356.	NO
0.2777	5	7.510	7.492	12	6	0.00425	0.00419	0.170	18.	4117.	6176.	NO
0.2777	6	8.488	4.768	14	14	0.00198	0.00195	0.161	6.	2808.	4212.	NO
						0.05552	0.05491		373.	TOTAL		
0.2774	1	9.974	2.126	10	2	0.01541	0.01521	0.162	121.	7836.	11754.	NO
0.2774	2	9.829	2.195	10	16	0.01535	0.01523	0.124	120.	7821.	11731.	NO
0.2774	3	9.596	5.787	8	9	0.01064	0.01052	0.154	69.	6513.	9770.	NO
0.2774	4	7.700	2.838	3	69	0.01039	0.01028	0.144	67.	6434.	9651.	NO
0.2774	5	7.510	7.492	12	6	0.00488	0.00481	0.170	22.	4409.	6614.	NO
0.2774	6	8.488	4.768	14	14	0.00260	0.00257	0.161	8.	3219.	4829.	NO
0.2774	7	7.527	7.654	12	36	0.0		0.101	0.			

TABLE VIIC

CONTACT PARAMETERS

APPR (CM)	AREA NO.	CENTER X (CM)	COORD Y (CM)	ASPERITY INDEX U	ASPERITY INDEX L	CALC CONTACT AREA (CM2)	PROJ AREA (CM2)	SLOPE	LOAD (NT)	AVG PRESS (NT/CM2)	MAX PRESS (NT/CM2)	ELASTIC LIMIT EXCEEDED
						0.05927	0.05862		407.	TOTAL		
0.2764	1	9.974	2.126	10	2	0.01738	0.01715	0.162	145.	8322.	12483.	NO
0.2764	2	9.829	2.195	10	16	0.01733	0.01720	0.124	144.	8310.	12465.	NO
0.2764	3	9.596	5.787	8	9	0.01262	0.01247	0.154	89.	7091.	10637.	NO
0.2764	4	7.700	2.838	3	69	0.01236	0.01224	0.144	87.	7019.	10529.	NO
0.2764	5	7.510	7.492	12	6	0.00685	0.00675	0.170	36.	5223.	7834.	NO
0.2764	6	8.488	4.768	14	14	0.00457	0.00451	0.161	20.	4268.	6403.	NO
0.2764	7	7.527	7.654	12	36	0.00199	0.00198	0.101	6.	2819.	4228.	NO
						0.07310	0.07230		526.	TOTAL		
0.2754	1	9.974	2.126	10	2	0.01935	0.01910	0.162	170.	8781.	13172.	NO
0.2754	2	9.829	2.195	10	16	0.01931	0.01916	0.124	169.	8772.	13158.	NO
0.2754	3	9.596	5.787	8	9	0.01459	0.01442	0.154	111.	7625.	11437.	NO
0.2754	4	7.700	2.838	3	69	0.01434	0.01419	0.144	108.	7559.	11338.	NO
0.2754	5	7.510	7.492	12	6	0.00881	0.00869	0.170	52.	5926.	8889.	NO
0.2754	6	8.488	4.768	14	14	0.00654	0.00646	0.161	33.	5106.	7659.	NO
0.2754	7	7.527	7.654	12	36	0.00398	0.00396	0.101	16.	3983.	5974.	NO
						0.08692	0.08598		660.	TOTAL		
0.2744	1	9.974	2.126	10	2	0.02132	0.02104	0.162	196.	9217.	13826.	NO
0.2744	2	9.829	2.195	10	16	0.02129	0.02113	0.124	196.	9211.	13816.	NO
0.2744	3	9.596	5.787	8	9	0.01656	0.01637	0.155	135.	8124.	12186.	NO
0.2744	4	7.700	2.838	3	69	0.01621	0.01615	0.144	132.	8063.	12094.	NO

TABLE VIIC

CONTACT PAPAMETERS

APPR	AREA NO.	CENTER COORD X	Y	ASPERITY INDEX U	L	CALC CONTACT AREA	PROJ AREA	SLOPE	LOAD	AVG PRESS	MAX PRESS	ELASTIC LIMIT EXCEEDED
(CM)		(CM)	(CM)			(CM2)	(CM2)		(NT)	(NT/CM2)	(NT/CM2)	
0.2744	5	7.510	7.492	12	6	0.01078	0.01063	0.170	71.	6554.	9831.	NO
0.2744	6	8.488	4.768	14	14	0.00851	0.00840	0.162	50.	5824.	8736.	NO
0.2744	7	7.527	7.654	12	36	0.00597	0.00594	0.101	29.	4876.	7314.	NO
						0.10074	0.09965		808.	TOTAL		
0.2739	1	9.974	2.126	10	2	0.02229	0.02200	0.162	210.	9425.	14137.	NO
0.2739	2	9.829	2.195	10	16	0.02227	0.02210	0.124	210.	9420.	14130.	NO
0.2739	3	9.596	5.787	8	9	0.01754	0.01733	0.155	147.	8360.	12539.	NO
0.2739	4	7.700	2.838	3	69	0.01729	0.01711	0.144	143.	8300.	12451.	NO
0.2739	5	7.510	7.492	12	6	0.01175	0.01159	0.170	80.	6843.	10265.	NO
0.2739	6	8.488	4.768	14	14	0.00948	0.00936	0.162	58.	6148.	9222.	NO
0.2739	7	7.527	7.654	12	36	0.00695	0.00691	0.101	37.	5261.	7892.	NO
0.2739	8	9.841	5.885	8	50	0.0		0.101	0.			
						0.10756	0.10640		885.	TOTAL		
0.2729	1	9.974	2.126	10	2	0.02426	0.02395	0.163	239.	9833.	14749.	NO
0.2729	2	9.829	2.195	10	16	0.02425	0.02406	0.124	238.	9830.	14745.	NO
0.2729	3	9.596	5.787	8	9	0.01951	0.01928	0.155	172.	8817.	13226.	NO
0.2729	4	7.700	2.838	3	69	0.01926	0.01907	0.144	169.	8762.	13142.	NO
0.2729	5	7.510	7.492	12	6	0.01372	0.01353	0.170	101.	7394.	11091.	NO
0.2729	6	8.488	4.768	14	14	0.01145	0.01131	0.162	77.	6756.	10135.	NO
0.2729	7	7.527	7.654	12	36	0.00893	0.00889	0.101	53.	5966.	8949.	NO
0.2729	8	9.841	5.885	8	50	0.00200	0.00199	0.101	6.	2823.	4234.	NO

TABLE VIIC

CONTACT PARAMETERS

APPR (CM)	AREA NO.	CENTER COORD X (CM)	Y (CM)	ASPERITY INDEX U	L	CALC CONTACT AREA (CM2)	PROJ AREA (CM2)	SLOPE	LOAD (NT)	AVG PRESS (NT/CM2)	MAX PRESS (NT/CM2)	ELASTIC LIMIT EXCEEDED
						0.12338	0.12206		1055.	TOTAL		
0.2719	1	9.974	2.126	10	2	0.02623	0.02589	0.163	268.	10224.	15336.	NO
0.2719	2	9.829	2.195	10	16	0.02623	0.02603	0.124	268.	10224.	15335.	NO
0.2719	3	9.596	5.787	8	9	0.02148	0.02123	0.155	199.	9252.	13878.	NO
0.2719	4	7.700	2.838	3	69	0.02124	0.02102	0.144	195.	9200.	13800.	NO
0.2719	5	7.510	7.492	12	6	0.01569	0.01546	0.170	124.	7906.	11860.	NO
0.2719	6	8.488	4.768	14	14	0.01343	0.01325	0.162	98.	7315.	10972.	NO
0.2719	7	7.527	7.654	12	36	0.01092	0.01086	0.101	72.	6596.	9895.	NO
0.2719	8	9.841	5.885	8	50	0.00399	0.00397	0.101	16.	3985.	5978.	NO
						0.13919	0.13771		1241.	TOTAL		
0.2709	1	9.974	2.126	10	2	0.02820	0.02783	0.163	299.	10601.	15902.	YES
0.2709	2	9.829	2.195	10	16	0.02821	0.02799	0.124	299.	10603.	15904.	YES
0.2709	3	9.596	5.787	8	9	0.02345	0.02318	0.155	227.	9668.	14501.	NO
0.2709	4	7.700	2.838	3	69	0.02321	0.02298	0.144	223.	9618.	14428.	NO
0.2709	5	7.510	7.492	12	6	0.01765	0.01740	0.170	148.	8388.	12581.	NO
0.2709	6	8.488	4.768	14	14	0.01540	0.01520	0.162	121.	7833.	11749.	NO
0.2709	7	7.527	7.654	12	36	0.01290	0.01284	0.101	93.	7171.	10756.	NO
0.2709	8	9.841	5.885	8	50	0.00597	0.00594	0.101	29.	4878.	7317.	NO
						0.15500	0.15336		1438.	TOTAL		

VIII. REFERENCES

1. Furey, M. J., "Tribology: A Study of the Sources of Friction and Wear Between Solids in Relative Motion," National Science Foundation Research Proposal, unpublished, Grant No. GK 31079.

2. Williamson, J. B. P., "Topography of Solid Surfaces" in Interdisciplinary Approach to Friction and Wear - NASA Symposium, San Antonio, Texas, NASA SP-181, pp. 85-142, Nov., 1967.

3. El-Refaie, M. and J. Halling, "Analysis of the Asperity Characteristics of Machined Surfaces Using A Statistical Mathematical Model," University of Salford, Salford, U.K., unpublished.

4. Williamson, J. B. P., J. Pullen, and R. T. Hunt, "The Shape of Solid Surfaces" reprint from Surface Mechanics, ASME.

5. Williamson, J. B. P. and R. T. Hunt, "The Microtopography of Solid Surfaces," Research Report No. 59, Burndy Research Division, Norwalk, Conn., Jan. 26, 1968.

6. Reason, R. E., "Significance and Measurement of Surface Finish," reprint from Grinding and Finishing Magazine.

7. Greenwood, J. A. and J. H. Tripp, "Contact of Nominally Flat Rough Surfaces," Burndy Research Report No. 66, Burndy Research Division, Norwalk, Conn., 1968.

8. D'yachenko, P. E., N. N. Tolkacheva, G. A. Andreev, and T. M. Karpova, "The Actual Contact Area Between Touching Surfaces," translated by Consultants Bureau, New York, 1964.

9. Selwood, A., "The Topography of Rough Surfaces," Wear, vol. 5, pp. 148-157, 1962.

10. Lubkin, J. L., "Contact Problems," reprint from unknown book.

11. Bowden, F. P. and D. Tabor, "The Area of Contact Between Stationary and Moving Surfaces," Proc. Roy. Soc., vol. 169A, pp. 391, 1939.

12. Rabinowicz, E., Friction and Wear of Materials, John Wiley and Sons, Inc., New York, 1965.

13. Newcomb, T. P., Communcation, Proc. Conf. Lubrication and Wear, London, Institution of Mechanical Engineers, pp. 837-838, 1957.

14. Gregory, B., "Intermetallic Diffusion and Contact Areas," Wear, vol. 21, pp. 361-365, Sept. 1972.

15. Williamson, J. B. P. and R. T. Hunt, "Relocation Profilometry," Journal of Scientific Instruments (Journal of Physics E), series 2, vol. 1, pp. 749-752, 1968.

16. Tsukisoe, T. and T. Hisakado, "On the Mechanism of Contact Between Metal Surfaces--The Penetrating Depth and Average Clearance," Journal of Basic Engineering, vol. 87, pp. 666, 1965.

17. Jones, M. H., R. I. L. Howells, and S. D. Probert, "Solids in Static Contact," Wear, vol. 2, pp. 225-240, 1968.

18. Parker, R. C. and D. Hatch, "The Static Coefficient of Friction and the Area of Contact," Proc. Phys. Soc. (London), vol. 3B, pp. 185-197, 1950.

19. Dyson, J. and W. Hirst, "The True Contact Area Between Solids," Proc. Phys. Soc. (London), vol. 67B, pp. 309-312, 1953.

20. Archard, J. F., "Elastic Deformation and the Laws of Friction," Proc. Roy. Soc. (London), vol. 243A, pp. 190-205, 1951.

21. Kragelskii, I. V., Friction and Wear, English translation by L. Ronson in collaboration with J. K. Lancaster, Butterworths, Washington, 1965.

22. Kragelskii, I. V. and V. P. Sabelnikov, "Experimental Check of the Elementary Laws of Friction," Proc. Conf. on Lubrication and Wear, London, Instn. of Mechanical Engineers, pp. 246-251, 1957.

23. Furey, M. J., "The Solid-Solid Interface and Real Area of Contact," Conf. on Physico-Chemical Mechanics of Friction and Wear (Contact Interaction and Fretting Corrosion), Kiev, U.S.S.R., June 1973.

24. Janka, M. J., "Tribology: The Real Area of Contact Between Macroscopic Model Surfaces," unpublished thesis, Virginia Polytechnic Institute and State University, Blacksburg, Va., Sept. 1973.

25. Bartenev, G. M., V. V. Lavrentjev, and N. A. Konstantinova, "The Actual Contact Area and Friction Properties of Elastomers Under Frictional Contact with Solid Surfaces," Wear, vol. 18, pp. 439-448, 1971.

26. Bowden, F. P. and D. Tabor, The Friction and Lubrication of Solids, Part II, Oxford University Press, Oxford, U.K., 1968.

27. Uppal, A. H., S. D. Probert, and T. R. Thomas, "The Real Area of Contact Between a Rough Surface and a Flat," Wear, vol. 22, pp. 163-184, Nov. 1972.

28. Uppal, A. H. and S. D. Probert, "Deformation of Single and Multiple Asperity Models of Modeling Clay," Wear, vol. 23, pp. 367-375, Mar. 1973.

29. Uppal, A. H. and S. D. Probert, "Deformation of Single and Multiple Asperities on Metal Surfaces," Wear, vol. 20, pp. 381-400, Nov. 1972.

30. Williamson, J. B. P., J. Pullen, and R. T. Hunt, "Plastic Contact of Surfaces," Burndy Research Reports, No. 78 and 79, Burndy Research Division, Norwalk, Conn., 1970.

31. Timoshenko, S. and J. N. Goodier, Theory of Elasticity, 2nd. ed., McGraw-Hill, New York, 1951.

32. Greenwood, J. A. and J. H. Tripp, "The Elastic Contact of Rough Spheres," ASME Paper No. 66-WA/APM-28, May 1966.

33. Blok, H., "Comments on Paper by R. Wilson," Proc. Roy. Soc. (London), vol. 212A, pp. 480-482, 1952.

34. Halliday, J. S., "Application of Reflection Electron Microscopy to the Study of Wear," Proc. Conf. on Lubrication and Wear, London, Instn. of Mechanical Engineers, pp. 647-651, 1957.

35. Greenwood, J. A. and J. B. P. Williamson, "Contact of Nominally Flat Surfaces," Proc. Roy. Soc. (London), vol. 295A, pp. 300-319, 1966.

36. Courntney-Pratt, J. S. and E. Eisner, "The Effect of a Tangential Force on the Contact of Metallic Bodies," Proc. Roy. Soc. (London), vol. 238A, pp. 529-550, 29 Jan. 1957.

37. Mindlin, R. D., "Compliance of Elastic Bodies in Contact," J. Appl. Mech., vol. 71, pp. 259, 1949.

38. O'Connor, J. J. and K. L. Johnson, "the Role of Surface Asperities in Transmitting Tangential Forces Between Metals," Wear, vol. 6, pp. 118-139, 1963.

39. Furey, M. J., "Friction, Wear, and Lubrication," Industrial and Engineering Chemistry, vol. 61, pp. 12-29, Mar. 1969.

40. Furey, M. J., "The Solid-Solid Interface and Real Area of Contact," Ph.D. Thesis, Rensselaer Polytechnic Institute, Troy, N.Y., Sept. 1967.

41. Brownlee, K. H., Statistical Theory and Methodology in Science and Engineering, 2nd ed., John Wiley and Sons, Inc., New York, 1965.

42. Dalley, J. W. and W. F. Riley, Experimental Stress Analysis, McGraw-Hill, New York, 1965.

43. Hardy, C., C. N. Baronet, and G. V. Tordion, "The Elasto-Plastic Indentation of a Half-Space by a Rigid Sphere," International Journal for Numerical Methods in Engineering, vol. 3, pp. 451-462, 1971.

44. Tabor, D., The Hardness of Metals, Clarendon Press, Oxford, 1951.

45. Johnson, K. L., "An Experimental Determination of the Contact Stresses Between Plastically Deformed Cylinders and Spheres," in Engineering Plasticity, edited by J. Heyman, F. A. Leckie, University Press, Cambridge, 1968.

46. Chou, S. C., K. D. Robertson, and J. H. Rainey, "The Effect of Strain Rate and Heat Developed During Deformation on the Stress-Strain Curve of Plastics," Experimental Mechanics, vol. 13, pp. 422, Oct. 1973.

47. "Plexiglas Design and Fabrication Data," Rohm and Haas Company, Philadelphia, Sept. 1964.

48. Nuri, K. A., "The Contact of Rough Flat Surfaces," University of Salford, Salford, U.K., unpublished.

IX. VITA

The author was born in Saltville, Virginia on September 21, 1948. He attended public schools there and graduated from R. B. Worthy High School in June 1966. In September of that year he entered Virginia Polytechnic Institute and State University and graduated in June 1971 with a Bachelor of Science Degree in Mechanical Engineering. During his undergraduate study, the author participated in the Co-operative Education Program and received two years of industrial experience with Tennessee Eastman Company. While an undergraduate he became a member of Pi Tau Sigma and Tau Beta Pi national honorary fraternities.

During the Summer of 1971, the author participated in a training program at N. V. Philips' Gloeilampenfabrieken in Eindhoven, the Netherlands, under the auspices of the International Association for the Exchange of Students for Technical Experience. In the Fall of that year he returned to VPI & SU as a Graduate Research Assistant and began work toward a Master's Degree in Mechanical Engineering. In July 1972, the author returned to the Netherlands as a Rotary Fellow and pursued a course of study in automatic control engineering at the Eindhoven University of Technology. In September 1973, he returned to VPI & SU to complete requirements for the M.S. degree.

Wesley O. McCready

CONTACT BETWEEN MODELS OF ROUGH SURFACES CONTAINING SPHERICAL ASPERITIES

by

Wesley O. McCready

(ABSTRACT)

A brief introduction to the problem and importance of solid-solid contact as well as to the nature of surface topography is given. A number of experimental techniques, both direct and indirect, for determining the true area of contact between surfaces as well as a number of theories for predicting contact areas in the case of elastic, plastic, and elasto-plastic deformation of contacting surface asperities are reviewed. The effect of tangential loading upon the area of contact is also reviewed.

In order to implement a previously established goal of observing the nature of contact between transparent models of scaled-up surfaces, a procedure for three-dimensional model design, a technique for model fabrication, and an experimental apparatus have been developed. A computer program to predict points of contact and elastic contact parameters between macroscopic surface models is presented. Determining the range of application of the Hertz equations is discussed.

The computer program is used to predict the contact parameters between the three-dimensional surface models developed. For this situation the nature of contact was found to vary from the case of a single pair of asperities dominating elastic contact to the case

of multiple asperity contact between several pairs of contacting asperities.